Near-Wellbore Salinity Effect on Sand Control Plugging by Fines Migration in Steam-Assisted Gravity Drainage Producer Wells

by

Hoda Dadjou

A THESIS SUBMITTED IN PARTIAL FULFILLMENT OF
THE REQUIREMENTS FOR THE DEGREE OF

MASTER OF SCIENCE

in

Petroleum Engineering

Department of Civil and Environmental Engineering

UNIVERSITY OF ALBERTA

Abstract

Sand control screens are necessary for steam-assisted gravity drainage (SAGD) wells drilled into oil sands to prevent sand production. However, the accumulation of mobilized fine particles near the wellbore can result in screen plugging, adversely affecting the well's flow performance. This research assesses the effects of formation water salinity on fines migration and the flow performance of sand control screens in SAGD wells. The study primarily examines these effects through sand retention testing (SRT) conducted under representative rock and multi-phase flow conditions.

This research developed a novel SRT methodology, which implemented the salinity effect in multi-phase flow through sand pack and sand control screen. Two sand retention tests were designed using identical procedures in two-phase fluid flow (oil and brine), flow rate, and water cut. The first test used constant salinity, emulating existing SRT procedures in the literature. The second test, however, used gradually reducing salinity levels to emulate declining salinities around SAGD production wells caused by the flow of condensed steam.

The results indicated a significant decrease in the retained permeability of the screen coupon due to fines migration triggered by the reduction of salinity. Single-phase oil flow stages did not show noticeable produced fine particles at the outlet. In two-phase flow conditions, high flow rate and water cut stages induced higher produced fine particles under constant salinity, reflecting the hydrodynamic effects in fines migration. However, observations confirmed that a substantial mass concentration of fine particles was mobilized, retained, and produced by reducing salinity.

The findings of this study reveal the importance of the salinity effect on fines migration and the flow performance of SAGD wells where high saline formation water is diluted by low saline

condensate steam. Testing results indicate the necessity of incorporating the chemical effects in sand retention tests. Further research considering high-pressure and high-temperature conditions around SAGD wells and interactions with other formation damage mechanisms would extend this research.

Dedication

I dedicate this thesis to the following individuals whose unwavering support and encouragement have been pivotal in my academic journey:

To my loving parents, Mom and Dad, your constant belief in my abilities and unwavering love has been my greatest inspiration. Your sacrifices and unwavering encouragement have fueled my determination.

To my fantastic son, your kind, cheerful, and loving words in blues moments have always pushed me forward and helped me face my fears. Your support has meant the world to me. Thank you for your empathy and understanding.

To my supportive husband, thank you for standing by my side and empowering me to pursue my education and dreams. Your unwavering belief in me has been a driving force behind my success.

To my brothers, Hadi and Ali, your advice and support through video and phone calls have been invaluable. Your love and encouragement have been instrumental in my achievements.

Lastly, to all the friends, teachers and professors who have guided me, I am deeply grateful for imparting your knowledge and inspiring my passion for learning. Your dedication to education has been transformative in shaping my academic journey.

This thesis is dedicated to every one of you. Your unwavering support, encouragement, and belief in me have been the driving force behind this accomplishment. Thank you for being an integral part of my journey.

Acknowledgments

I want to express my gratitude and respect to my supervisor, Dr. Alireza Nouri, who has provided the knowledge growth opportunity for me.

My gratitude extends to Dr. Rahman Miri, who helped me through this journey. With him, this research was successful. I appreciate Dr. Salimi's insight and help during the study and the tests.

I also would like to thank my family and friends for their valuable support and kindness.

I would like to acknowledge NSERC Discovery Grant RGPIN-2017-06257 and the Canada First Research Excellence fund through the Future Energy Systems (Thermal Well Design and Testing) for the financial support of the research in this work.

Table of Contents

List of Tables

List of Figures

Nomenclature

CSS	Cyclic Steam Stimulation
D_{10}	Sieve size retains 10% of the sand
D_{50}	Sieve size retains 50% of the sand
DCI	Class I oilsand for Devon Pike I
DCII	Class II oilsand for Devon Pike I
DCIII	Class III oilsand for Devon Pike I
DCIV	Class IV oilsand for Devon Pike I
DP	Differential Pressure
FCT	Full-scaled Completion Testing
P	Pressure
ppm	Part Per Million
PS	Punch-Screen
PSD	Particle Size Distribution
SC	Screen Coupon
SAGD	Steam-Assisted Gravity Drainage
SCD	Sand Control Device
SCT	Scaled Completion Testing
SL	Slotted Liner
SOP	Standardized Operating Procedure
SPC	Slot Per Column
SRT	Sand Retention Testing
Swirr	irreducible water Saturation
WWS	Wire Wrapped Screen
F_a	The adhesive force
h_r	Roughness Height
F_d	Drag Forces
F_l	Lift Forces
F_b	Resultant Force of Buoyancy and Gravity
l_d	Lever Arm of Drag Force
l_a	Lever Arm of Lift Force
cp	centipoise
T_H	Hydrodynamic Torque
T_A	Adhesive Torque

Chapter 1: Introduction

1.1 Overview

In Northern Alberta, vast oil sand deposits are found beneath an area of 140,000 km², encompassing the Athabasca, Cold Lake, and Peace River regions (**Figure 1.1**). These deposits hold approximately 168 billion barrels of bitumen, ranking as the third-largest oil sand reserves globally.

Figure 1.1 Alberta Oil Sands Map (Patchett & Lozowy, 2012).

Oil sands are a composition of sand, clay, water, and bitumen. Since bitumen is extra viscose crude oil, it cannot be produced using conventional oil-producing methods. Two effective ways exist to produce unconventional oil deposits: 1) Surface mining and 2) In-situ oil recovery.

The in-situ oil recovery method is applicable for up to 80% of recoverable bitumen in Alberta, where oil deposits are deep that are not accessible by surface mining (Nasr & Ayodele, 2005). Various techniques are utilized for in-situ bitumen recovery, with thermal in-situ recovery being the predominant method. This approach involves the application of steam to heat the reservoir,

effectively reducing the bitumen's viscosity for extraction purposes. Steam-Assisted-Gravity-Drainage (SAGD) and Cyclic Steam Stimulation (CSS) account for two primary technologies for extracting high viscose bitumen (AER, 2022), out of which SAGD is the most popular in-situ oil recovery method (Bennion, 2009).

The SAGD method consists of two horizontal wells about 5 meters vertically apart. Steam is injected from the upper well, forming a steam chamber growing vertically and laterally. At the edge of the steam chamber, the latent heat of steam transfers to the cold adjacent bitumen, lowering its viscosity and increasing the bitumen mobility. The melted bitumen and condensed steam concurrently move toward the lower well (producer well) and pump to the surface (Butler et al., 1981).

SAGD operation is often associated with sand production and fines migration in naturally unconsolidated oil sand reservoirs (Haftani et al., 2020a; Montero, 2016). Sand production is detrimental to downhole and surface equipment (damaged by erosion) and deliverability, and in the worst-case scenario, excessive sand production results in formation collapse and economic loss. Fines migration and retention can adversely affect the near wellbore permeability by plugging the thin pore throat (Russell et al., 2018). The sand control technology is employed to maintain the integrity of the formation and prevent the uncontrolled amount of sand or other solid particles into the wellbore, thereby avoiding any undesirable consequences. Therefore, Sand control devices (SCDs) are needed to prevent sand production while offering the least resistance to flow and passing fine particles through to minimize screen and pore plugging (Anderson, 2017).

Different sand control methods include using mechanical screens, lowering the production rate, injecting resin-coated gravel, and consolidating the near wellbore formation using chemicals. The gravel packing and mechanical screens are the most suitable for SAGD wells (Roostaei et al., 2021). A stand-alone screen such as Slotted Liner (SL) and Wire Wrapped Screen (WWS) is widely used in SAGD wells as they are affordable and less complicated. The SL is the best choice among other SCDs for the SAGD wells if the slots are not plugged (Montero et al., 2018a). The SCDs type, slot size, and slot density are selected based on the dominant factor of the formation's particle size distribution, which sand control retention tests can further evaluate.

Sand control tests for evaluating the performance and design criteria of the sand control screens are categorized as slurry sand retention testing (SRT) and pre-packed SRT. The linear tests are

designed to represent near-wellbore conditions in a relatively small, simple setup providing an affordable test to investigate physical phenomena and measure SCD's performance. The full-scale test is somewhat complex and accounts for the natural radial flow toward the screen.

Pre-packed sand retention tests, including conventional SRTs and triaxial stress SRTs, represent the SAGD conditions around the wellbore. Conventional SRT mimics the initial stage of a SAGD process when unconsolidated and high porosity sand collapse on the SCD, while other shows the effect of stress build-up around the borehole during a SAGD life cycle (Montero et al., 2018a).

Several researchers have contributed to the sand control testing for the SAGD wells by implementing various experimental and numerical work. The test methods including SRT (Montero et al., 2018b; Wang et al., 2020), Full-scaled Completion Testing (FCT) (Haftani et al., 2020b), Scaled Completion Testing (SCT) (Fattahpour et al., 2016) and large-scale sand control tests (Anderson, 2017) have investigated the design criteria for SCDs, radial flow effect, stress effect and the effect of a large sand pack size on results, respectively. The test results suggest a suitable slot size and density range for the sand control screens. The upper bond limits sand production, while the lower bond limits the plugging by retention of fine particles.

Migratory fines are referred to as loose particles with sizes smaller than 37 μm (Muecke, 1979) or 44 μm (Abram & Cain, 2014; Kaminsky, 2009). The most common fine minerals in the reservoirs are kaolinite, chlorite, and illite (Russell et al., 2018). In addition, movable fines can come from non-clay minerals such as quartz, silica, feldspar, dolomite, and calcite (Muecke, 1979). The most common fine mineral in the Alberta oil sand deposits is kaolinite (Gunter et al., 1994).

Yang et al. (2022) explained straining and bridging as possible retention mechanisms in a porous medium by fines migration. The release of fines from grain surfaces enhances the permeability by providing a sizeable accessible pore surface area. On the other hand, detachment or discharge of many fine particles may cause blockage of the pore throats and adversely affect permeability.

Many researchers have experimentally studied the fines migration process through consolidated sand core floods. They mentioned that particle and pore size distributions, the concentration of fine particles, the ionic activity of fluids, and the type and saturation of fluids affect the process (Egbogah, 1984; Gabriel & Inamdar, 1983; Gruesbeck & Collins, 1982; Muecke 1979; Sarkar & Sharma, 1990). Rahman et al. (1994) mentioned several factors affecting fines migration and precipitation, including 1) formation characteristics, 2) fluid flow rate and 3) Particle

electrophysical properties, 3) wettability, 4) relative permeability, and 5) chemical interaction of particles and formation fluid. The last three factors are only present while immiscible fluid exists in the reservoir (Rahman et al., 1994).

A limited study has been done on the effect of fines migration on SCD performance in a near SAGD producer well. Miri et al. (2022) proposed a long-term SRT method to consider the impact of fines migration on SCD performance represented by the near producer well in a SAGD process. He then studied the effect of salinity change during several single-phase brine injections to an SRT. He reported the salinity reduction as a leading cause of fines migration and plugging (Miri et al., 2023).

This research aims to provide a condition like the near screen zone in a SAGD producer well. Therefore, two SRTs are conducted with identical flow stages, water cut, synthetic oil, and sand. However, in the second SRT, the brine salinity experiences a gradual decrease in salinity from formation water salinity to the lowest amount of produced water salinity reported for SAGD wells. The effect of flow rate, single/two-phase flow, water cut, and specifically the brine salinity reduction on fines migration, screen, and pore plugging are revealed by analyzing and comparing the results. Understanding the mechanisms and fundamentals in a SAGD provides insight into preventing and mitigating the issue if it is likely to happen.

1.2 Research Objectives

The key objectives of this research are as follows:

- Investigate the effect of salinity reduction, water cut, and flow rate in a multi-phase SRT on the fines migration and the retained permeability in near SAGD producer well zone.
- Determine the parameters that have the most significant impact on the results of the multi-phase SRT experiment by conducting several multi-phase conventional SRT screening tests and analyses.

1.3 Research Hypothesis

Fines migration can be beneficial to increasing the wellbore productivity unless it is too much and causes pore plugging. In a SAGD process, the high saline formation water is mixed with low saline steam condensate at the edge of the steam chamber, flowing toward the production well. The produced water salinity near the wellbore in a SAGD process is much lower than the initial salinity

of the formation water, which provides favorable conditions to release fine particles under a chemical shock effect. Previous research shows that significant fines migration, production, and even pore plugging can occur while the high-salinity brine is flushed out using low-salinity brine injection (Miri et al., 2023).

Similar results are expected in multi-phase flow with more severity. Because multi-phase flow experiences more resistance passing through the formation than each phase alone.

Water-wet fines can become mobile by an increase in water saturation (water cut percentage). They can further plug the pore throat of the porous medium and cause a rise in pressure drawdown.

Figure 1.2 shows schematically sand bridging around a perforation because of a balance between fluid and resistant forces. Formation compressive strength, friction between grains (overburden or confining stress), and capillary and pore pressure are resistant forces. Mechanical stress, including overburden stress and the drag force of flowing fluid through a porous medium, can cause rock failure. Sand arch (**Figure 1.2**) provides natural resistance against sand production, even though they are unstable. A suitable size of the sand control device is chosen based on particle size distribution to ensure this kind of bridge is formed during the process. Therefore, it is expected to produce sand within the acceptable range if the proper SCD is selected.

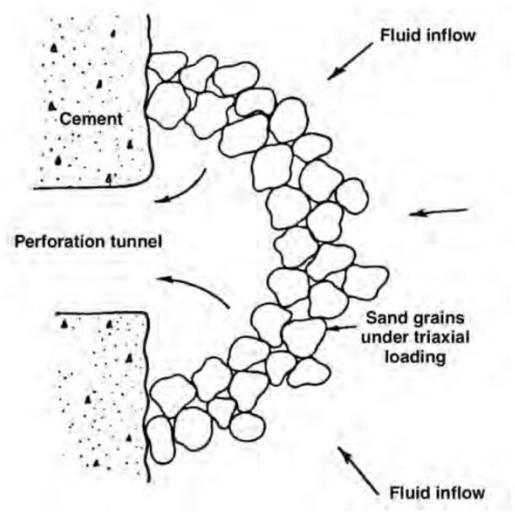

Figure 1.2 Sand bridging formed around the perforation (Junmano1 et al., 2016).

1.4 Research Methodology

The subsequent actions are taken to fulfill the objectives: (1) Conduct multiple conventional SRT tests under ambient temperature and atmospheric pressure conditions to gain insights into the underlying phenomena and identify critical factors influencing the test results. (2) Analyze the collected data to identify core issues and develop practical solutions. (3) Develop a standardized operating procedure (SOP) to mitigate the identified problems and prevent test failures. This new methodology leads to slot size and density optimization by capturing the salinity reduction impact on fines migration and plugging.

Additionally, an SRT is operated based on the modified SOP, consisting of eleven stages. The applied flow rate, water cut, sand pack, and oil are identical to the conventional SRT except for the varying and decreasing brine salinity. This variation allows for the investigation of the effects of salinity on fines migration.

1.5 Significance of the Work

Around 134 billion barrels of oilsands are available in northern Alberta, which are extractable using in situ conventional oil recovery methods (Alberta.ca, 2023). SAGD is one of the most popular techniques to produce oil from these oil sands.

Formation damage (pore plugging) and sand production are two common issues impacting the economics of a steam-assisted gravity drainage (SAGD) production well. Formation damage leads to clogging the pore spaces, reducing the permeability of the reservoir. At the same time, sand production can also reduce the well's productivity by clogging up the production tubing and equipment, leading to increased downtime and maintenance costs. Both issues can result in reduced production rates, increased operating costs, and decreased profitability. Experimental work should be done to investigate and mitigate the root cause of these challenges.

Previous works have yet to explore the problem entirely. The effect of salinity changes and reduction in multi-phase flow has been overlooked. This research's results significantly contribute to investigating the sanding and flow performance of sand control devices used in SAGD wells under more realistic field conditions.

This thesis is structured into seven chapters:

Chapter 1 (the current chapter) provides this research's background, scope and organization.

Chapter 2 contains a literature review of the conventional SRT tests, sand production and fines migration mechnisms.

Chapter 3 shows the SRT setup, material, and equipment with the applied test procedure for the last two tests.

Chapter 4 integrates the six unsuccessful tests and lessons learned from each failure.

Chapter 5 explains the calibrations and the improvements applied to the accuracy of the tests.

Chapter 6 represents the last two test's results and discussion.

Chapter 7 summarizes the significant findings of this research and presents suggestions for future research on this topic.

Chapter 2: Literature Review

2.1 Background

Canada, Alberta, is known for one of the largest oil sand deposits worldwide. Athabasca, Wabasca, Peace River, and Cold Lake deposits hold most of the bitumen in northern Alberta (Gunter et al., 1994).

Steam-Assisted Gravity Drainage (SAGD) is widely regarded as one of the most influential and profitable thermal methods for extracting oil sands and heavy oil, introduced by Butler et al. (1981). **Figure 2.1** depicts the schematic of a Steam-Assisted-Gravity- Drainage process. The process involves placing an injector well near the bottom of the reservoir and a producer well close to it at a lower depth. The steam is injected from the upper well, creating a steam chamber with elevated temperature. The latent heat of the steam transfers to the adjacent cold oil sand at the edge of the steam chamber, reducing its viscosity and enabling it to move. At the same time, hot oil, and condensate flow towards the production well by the gravity force parallel to the steam interface. This process creates more area for the chamber to grow vertically and laterally, increasing oil production (Butler et al., 1981).

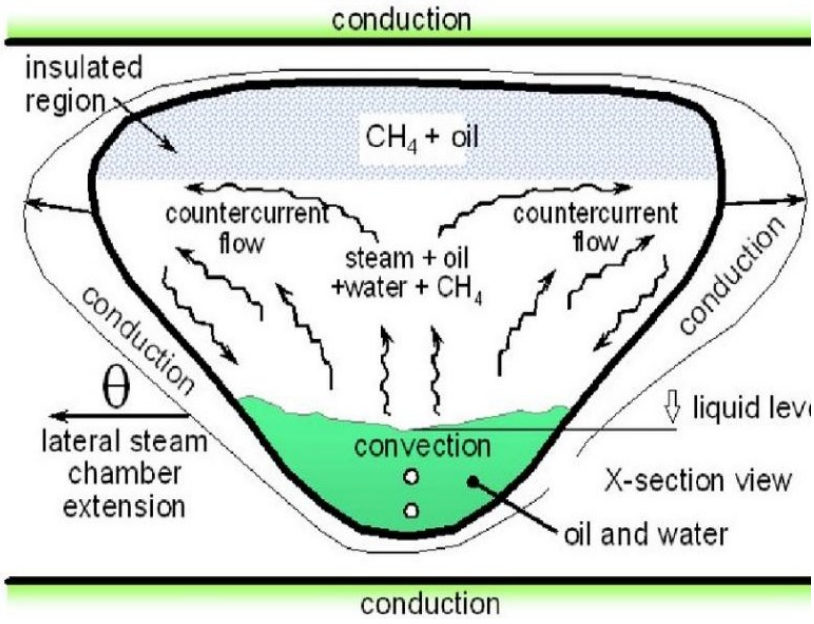

Figure 2.1 Steam-Assisted-Gravity-Drainage mechanisms schematic (Shafiei et al., 2007).

Oil sands are characterized by poorly consolidated or unconsolidated nature, often leading to sand production. This issue can be effectively addressed by implementing various methods, including installing sand control devices during completion.

A variety of stand-alone screens such as Slotted-Liner (SL), Wire-Wrapped Screen (WWS), and Punch-Screen (PS) are commonly employed as Sand Control Devices (SCDs) in SAGD well completion. **Figure 2.2** shows three different SCDs in actual and coupon sizes. These SCDs function as a sieve, preventing sand from entering the wellbore while reserving wellbore integrity and improving the production of liquid and oil (Wang et al., 2005).

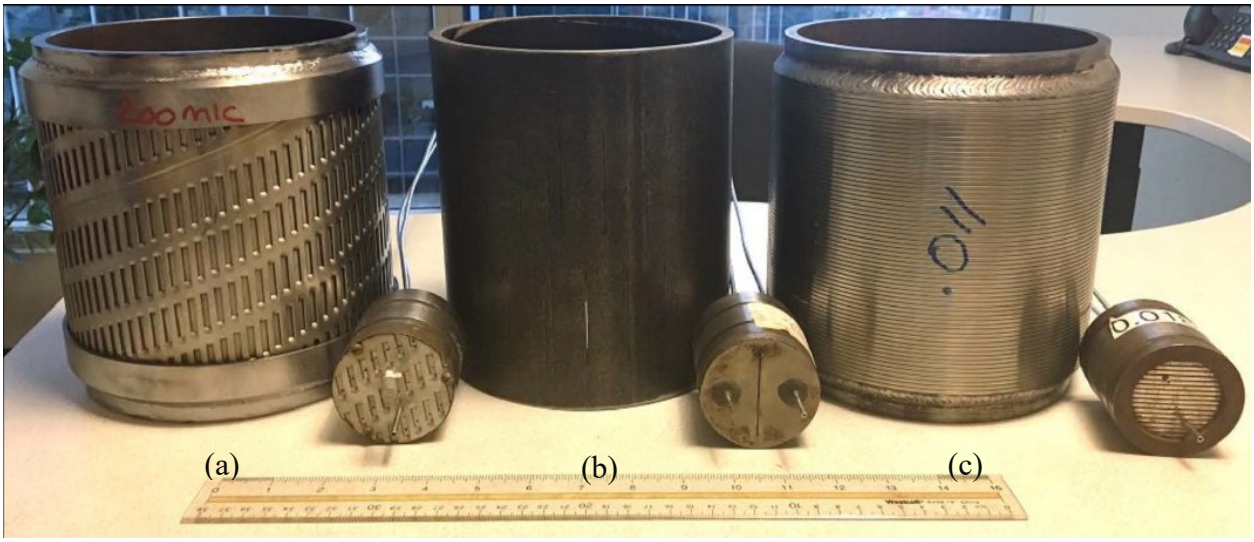

Figure 2.2 Mechanical sand control devices, (a) Punch screen, (b) Slotted liner, and (c) Wire-wrap screen (Anderson, 2017).

Fines production is another characteristic of an unconsolidated oil reservoir which can damage formation near the wellbore, decrease production, or completely plug the sand control device (Ansari et al., 2018; Miri, 2022.). Fines are small particles <44μm (Abram & Cain, 2014), including rock flour, metal oxide, or clay (2-4 μm) (Kaminsky, 2009). A suitable SCD design allows the fines particle to produce alongside the produced liquids and limits sand production.

Sand control evaluation tests are implemented experimentally to assess the sand retention and flow performance of the SCDs. According to a study by Montero (2018), a pre-packaged Sand Retention Testing (SRT) facility mimics the initial stage of a SAGD lifecycle wherein loose sand accumulates near the SCD and fluid flows through it. Many researchers adopted this test to evaluate the sand control devices regarding slot width and density, open flow area, sand, and fines

production (Mahmoudi, 2017; Wang, 2019). Bennion (2009) conducted more than two hundred tests to investigate the effect of single/multi-phase flow, pH, the impact of the sand control device's geometry, and the formation wettability on sand production and SCD's performance. He concluded that more plugging would occur when the wetting phase is mobile. Mahmoudi (2017) performed several experiments with brines of different pH and concluded higher brine pH leads to more plugging (Mahmoudi, 2017). Anderson (2017) performed large-scale liner testing to provide the WWS selection guide based on the McMurray formation sand mixture in Pike 1 SAGD project and confirmed the large-scale liner test results supported the small-scale results. Wang et al. (2020) performed several SRTs by incorporating the effect of slot density, Particle Size Distribution (PSD), and steam breakthrough. Montero Pallares et al. (2019) used SRT to evaluate the current design criteria for WWS in thermal wells. Kotb et al. (2021) modified the SRT setup and workflow, and the fluid flow rate is mentioned as the most influential factor in sanding from thermal wells.

The effect of salinity on the screen performance and in a SAGD context is investigated in multiple SRT research works. By injecting single-phase brine with three different salinities (0, 4000, and 7000), it is concluded that the fines migration intensifies at lower brine salinity levels (Mahmoudi et al., 2016). Later, Haftani et al. (2019) conducted several pre-packed SRT and studied the effect of salinity on fines migration and retained permeability. Sodium Chloride brine (NaCl) brine with constant pH and different salinities (7000, 2600, 400, 100, 50, and 0 ppm) was injected to obtain the critical salt concentration for fines migration. It was concluded that the fines migration was the highest at the 50-ppm brine salinity, and the fines migration was insignificant for salinities beyond 400 ppm.

Miri et al. (2022) proposed an SRT procedure as a reliable test method representing the fines migration and plugging in SAGD wells. Later, they extended their research by conducting a set of single-phase flow SRTs. Miri et al. (2023) reported that reducing the salinity in single-phase brine flow caused near-screen damage and permeability reduction.

To the author's knowledge, no research has been done on the effect of salinity decrease in a multi-phase flow SRT to investigate the impact on near-screen damage and plugging. This research investigates fines migration and formation damage influenced by varying brine salinity in a multi-phase flow that passes through a slotted liner placed on a sand retention test (SRT) setup.

2.2 Sand Production Mechanisms

Sand production can increase the inflow performance or reduce well productivity (Wang et al., 2005). Produced sand can be less than a few grams per cubic meter of reservoir fluid or tons of sand during a small-time span. Therefore, the problem may be manageable or cause a catastrophic situation by erosion, plugging, or complete well blockage and impose high maintenance and workover (Rahmati et al., 2013).

Various failure mechanisms for the unconsolidated formations can occur in oil and gas reservoirs and lead to stable, unstable, or catastrophic sand production. Shear, tensile, and compression are three common failure mechanisms during petroleum production. Shear failure is induced by stress concentration around the wellbore and fluid pressure drawdown and reservoir pressure depletion; while tensile failure is caused by high pressure gradients at excessive hydrocarbon production rates or quick ramp-ups (Morita et al., 1987). Additionally, fluid viscous drag forces can transport failed materials from perforation tunnels into the wellbore. The failure mechanisms can lead to changes in the mechanical properties of the reservoir material, affecting oil and gas production (Wang et al., 2005; Fjaer, 2008). **Figure 2.3** shows the sand production during multi-phase flow production.

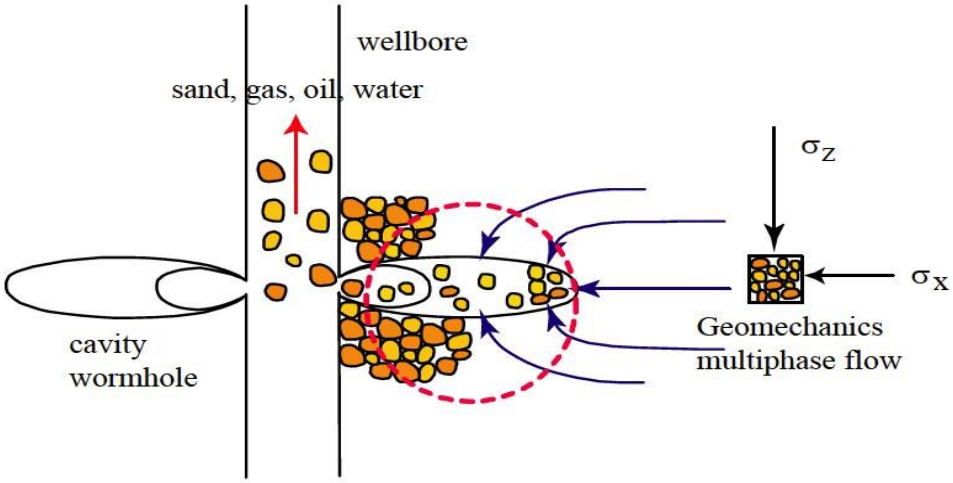

Figure 2.3 Sand production mechanisms (Wang et al., 2005).

Wormholes cavity and sand arches are formed during fluid production. The stability of the arc depends on fluid pressure, fluid flow rate, arch geometry, principal stresses, and the relations to the material strain and completion type (Bratli, 1981; Rahmati et al., 2013). Larger arches are more

stable than smaller ones if the flow per cavity stays constant (Fjaer, 2008). **Figure 2.4** depicts the growth of the wormhole occurring during production around slots.

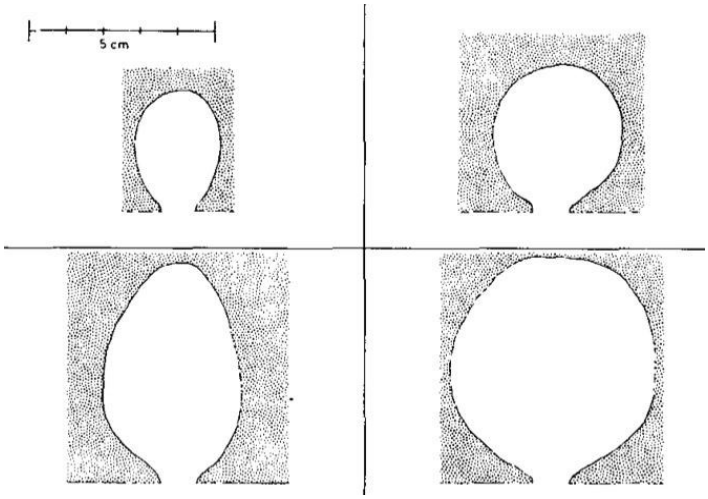

Figure 2.4 Sand cavities profile (Bratli, 1981).

According to Hall (1970), rock shearing leads to dilation and higher porosity in consolidated sands, as opposed to contraction in high-porosity unconsolidated sands. Reservoir pressure depletion increases effective stresses in the reservoir, increasing the sand production due to more favorable conditions for shear failure (Morita et al., 1987). Cyclic load, which relates to the number of times a well has undergone "shut-in," sometimes results in more sand production rate (Fjaer, 2008). Further, higher water cuts lead to capillary reduction, thus a weaker formation structure which often is observed to initiate sand production in the field (Hall et al., 1970; Fjaer, 2008).

2.2.1 Evaluation Tests on Sand Control Devices

Montero et al. (2018) critically reviewed the testing methods of sand control devices. They pointed out that there is no standard technique for this test. They mentioned the SRT as the best method to emulate the near SCD conditions in thermal wells. However, these tests use different size samples and SCD coupon's diameter. The SRT setup develops linear flow through the sand control device (SCD).

Besides the SRT, two more pre-packed sets are used to examine the performance of the sand control device. The Full-scale Completion Testing (FCT) setup is designed to emulate the radial flow near the screen coupon (Haftani et al., 2020a), and the Scaled Completion Testing (SCT)

setup is built to provide the vertical and lateral stress like the SAGD near producer well zone (Fattahpour et al., 2016).

2.3 Fines Migration and Production Mechanisms

The process of fines migration and, eventually, pore and screen plugging is recognized as a significant contributor to formation damage and reduced well performance (Bennion, 2009). Fines migration can be responsible for the onset of sand production due to the permeability reduction around the borehole, increasing the drag force (Santarelli & Brown, 1989; Fjaer, 2008).

Fines migration is characterized by the movement of particles attached to rock surfaces, which become detached and mobilized within the porous media. Subsequently, these particles may be entrapped within narrow pore throats through straining or bridging mechanisms, leading to a reduction in pore space availability and permeability reduction. The effects of fines migration are significant in hydrocarbon and geothermal reservoirs, where the accumulation of fine particles can significantly impact well performance and productivity (Muecke, 1979; Khilar et al., 1990; Huang et al., 2021).

Before delving into the study of fines migration, it is essential to understand the size and type of particles that are considered as fine. The most common fine particles in the reservoirs are clays like kaolinite, chlorite, and illite (Russell et al., 2018). In addition, movable fines can come from non-clay minerals such as quartz, silica, feldspar, dolomite, and calcite (Muecke, 1979). The most common fine mineral in the Alberta oil sand deposits is kaolinite (Gunter et al., 1994). There exist various definitions for fine particle sizes in the literature. Migratory fine particles are usually considered loose particles with sizes smaller than 37 μm (Muecke, 1979) or 44 μm (Kaminsky, 2009; Abram & Cain, 2014).

Core flooding experiments were conducted on core samples from the Cold Lake oil sands in Alberta to investigate fines migration. By examining the flow of single-phase bitumen, the researchers observed the permeability reduction because of pore throat blockage near the core outlet by detached fine particles (Lin, 1985). Kwan et al. (1989) conducted various experiments on core samples from the Cold Lake oil sands. They confirmed that fines migration caused permeability impairment. The tests were conducted under varying salinity, flow velocity, and flow reversal conditions. The reduction in permeability was due to the migration of fines, which led to the blockage of pore throats in the direction of flow. However, it was also observed that reversing

the flow direction and injecting Methylene Chloride could partially restore the impaired permeability. Numerous laboratory studies have observed permeability decline during core floods with piecewise increasing velocity, a decrease in salinity, or an increase in pH (Lever & Dawe, 1984; Khilar & Fogler, 1987; Kia et al., 1987).

2.3.1 Clay-Water and Clay-Clay Interactions

Clay minerals can be set apart from other colloidal substances due to their markedly anisometric and frequently irregular particle shape, wide-ranging particle-size distribution, diverse charge types (including permanent charges on surfaces and pH-dependent charges at edges), varied layer charge heterogeneity, notable cation exchange capacity (CEC), layer flexibility, and diverse aggregation mechanisms. The chemical mechanisms involved in clay mineral interactions with water include hydrogen bonding, attraction between charges and dipoles, as well as van der Waals forces (Bergaya & Lagaly 2013). Additionally, electrostatic forces (attraction between positively and negatively charged particles) can also contribute to clay-clay interactions.

Adsorbed cations are strongly bound to the surfaces of negatively charged dry clay particles. Excess cations, beyond what is required to neutralize the clay particle's negative charge, tend to diffuse away to establish uniform concentrations within the surrounding pore fluid. The interplay between this diffusion-driven tendency to escape and the opposing electrostatic attraction results in ion distributions near a single suspended clay particle, which are commonly represented as depicted in **Figure 2.5** (Mitchell & Soga, 2005). Collectively, the charged surface and the distributed charge in the adjacent phase are termed the "diffuse double layer." The most frequently referenced theory explaining the distribution of ions in this context was initially formulated by Gouy (1910) and further developed by Chapman (1913). Subsequently, Derjaguin and Landau (1941), and Verwey and Overbeek (1948), expanded upon the Gouy-Chapman theory to describe the repulsive energies and interaction forces between colloidal particles, as well as to predict the stability of colloidal suspensions. This extended theory is commonly referred to as the DLVO theory.

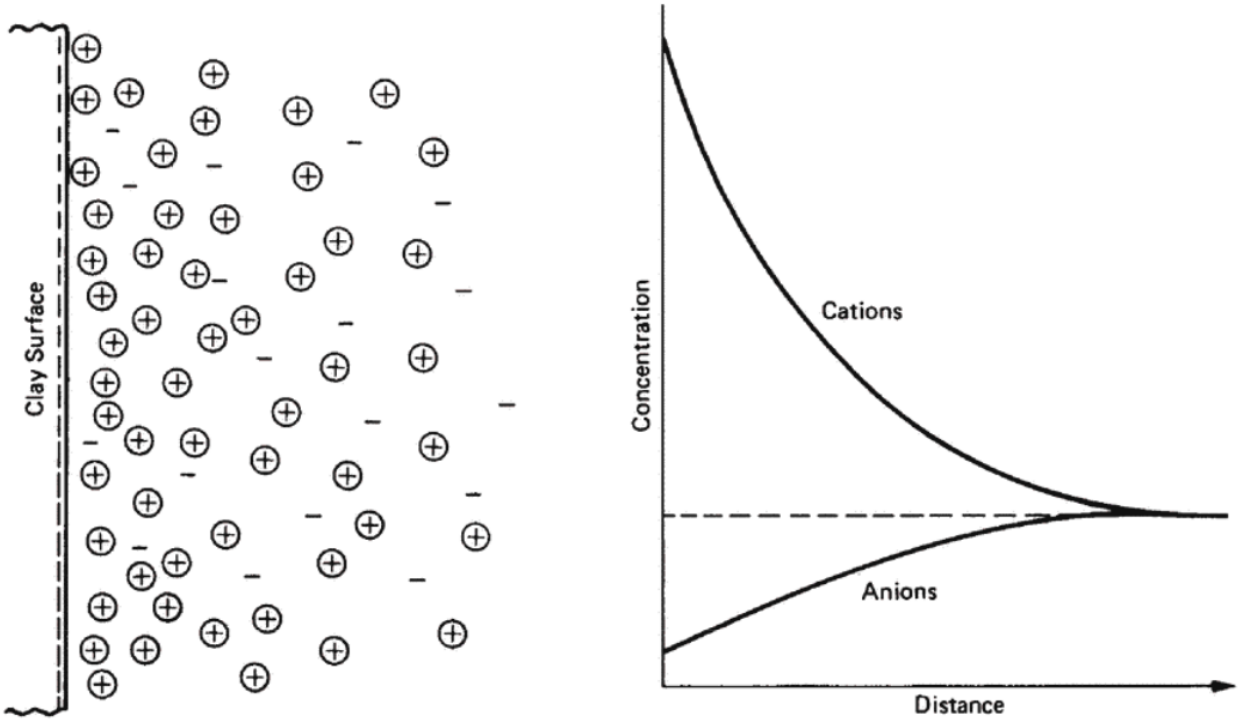

Figure 2.5 Distributions of ions adjacent to a clay surface according to the concept of the diffuse double layer (Mitchell & Soga, 2005).

The thickness of double layer can be estimated using Gouy-Chapman model as shown in Eq (1).

$$Thickness = \left(\frac{\varepsilon_0 DkT}{2ne^2v^2}\right)^{1/2} \quad (1)$$

Where,

ε_0 is permittivity.

D is dielectric constant.

k is Boltzmann constant.

T is temperature.

n is concentration.

e is electron charge.

v is ionic valance.

This correlation demonstrates that the thickness of the diffuse layer is inversely proportional to the valence of ions and the square root of their concentration, while it is directly proportional to the square root of the dielectric constant and temperature. In a broader context, a thicker diffuse layer generally corresponds to a reduced tendency for suspended particles to undergo flocculation (Mitchell & Soga, 2005).

2.3.1.1 Effect of pH

Hydroxyls $(OH)^-$ are exposed on the surfaces and edges of clay particles. The tendency for hydroxyls to dissociate in water,

$$SiOH \rightarrow SiO^- + H^+ \quad (2)$$

is significantly influenced by the pH level. pH is defined as the negative logarithm (base 10) of the H^+ concentration: pH values below 7 indicate an acidic environment (characterized by a high H^+ concentration), while pH values above 7 indicate alkaline conditions (with a low H^+ concentration). As the pH increases, there is a greater tendency for H^+ ions from the hydroxyl groups to dissolve into the solution, resulting in an increased effective negative charge on the clay particle. Conversely, a lower pH promotes interactions between positive charges at the edges and negative charges on the surface, often leading to flocculation and settling of the particles from suspension. To maintain stable suspensions or dispersions of clay particles, it is often necessary to maintain a high pH environment (Mitchell & Soga, 2005).

2.3.1.2 Energy and Force of Repulsion

The DLVO theory (Derjaguin & Landau, 1941; Verwey & Overbeek, 1948) is employed for calculating the potential and charge distribution within interacting diffuse double layers and quantifying the electrostatic repulsion force. Van der Waals forces, on the other hand, manifest between all matter entities and foster attraction among colloidal particles. By combining the equations governing the repulsion energies of diffuse layers with those dictating van der Waals attraction, we can generate curves depicting the net energy of interaction as a function of distance, as illustrated in **Figure 2.6**. The repulsive energy is notably sensitive to variations in electrolyte concentration, cation valence, dielectric constant, and pH, while, theoretically, the attractive energy primarily responds to changes in the dielectric constant and temperature. When the net interaction curve exhibits a substantial repulsive energy barrier, it impedes the close approach of

suspended particles, rendering the suspension stable. Conversely, in scenarios where this repulsive energy barrier is absent, particles can easily come into close proximity, leading to flocculation, as indicated by the minimum in the energy curves.

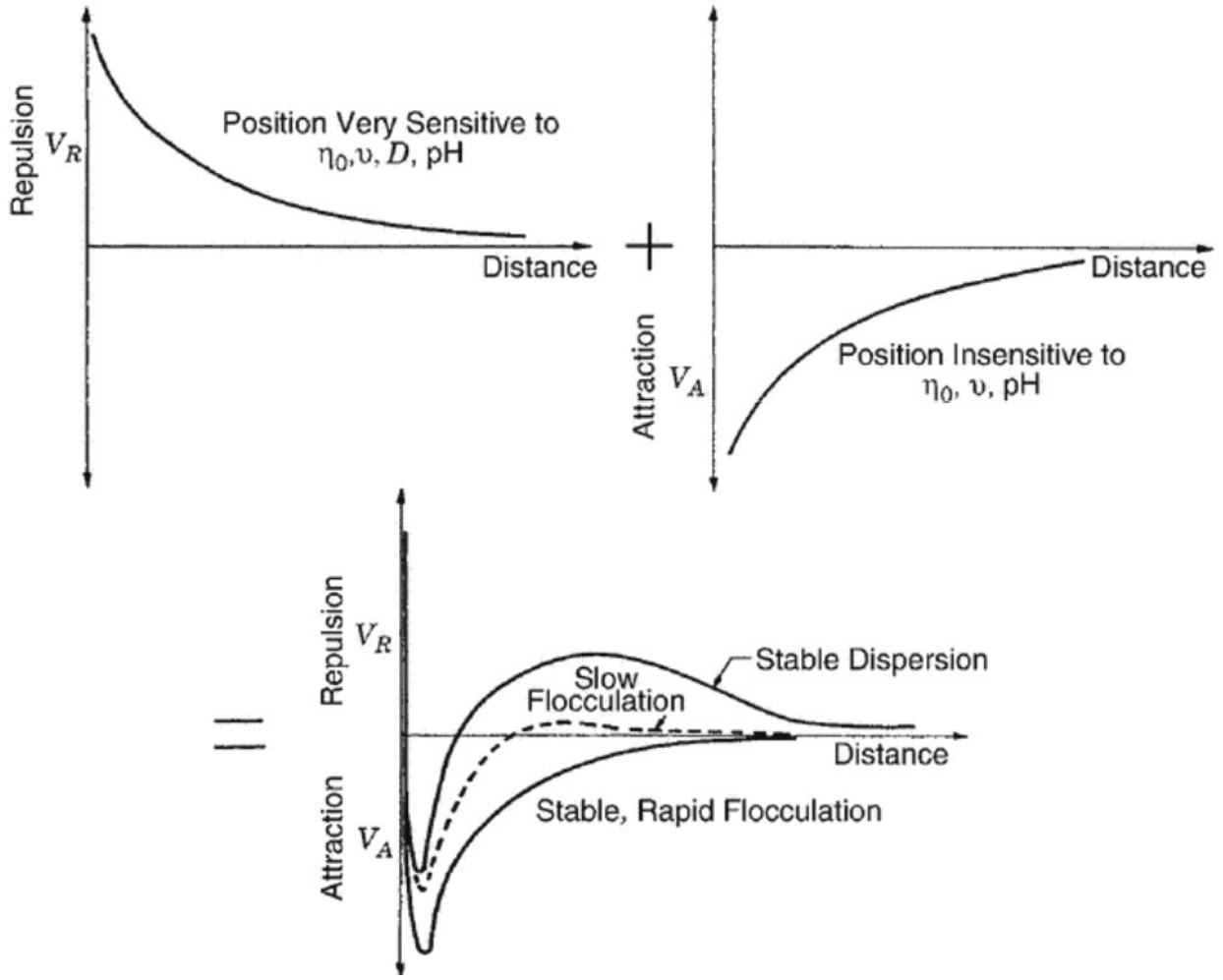

Figure 2.6 Energies of repulsion, attraction, and net curves of interaction for parallel flat plates of clay (Mitchell & Soga, 2005).

2.3.2 Clay to Sand Surfaces Interactions

Figure 2.7 demonstrates different statuses of fine particles inside a porous medium. Initially, fine particles are assumed to be attached to the rock's surface. When changes in hydrodynamic and electrical forces disrupt the resultant force exerted on fine particles, fine particles may detach from the rock surface. Detaching fine particles from the rock surface may initially increase the rock's permeability due to widening the pore radius open to flow. Depending on the fine particles' size,

number, and mineralogy, they may deposit, form a bridge against pore throats, or block more petite pore throats (straining), reducing permeability (Yang et al., 2022).

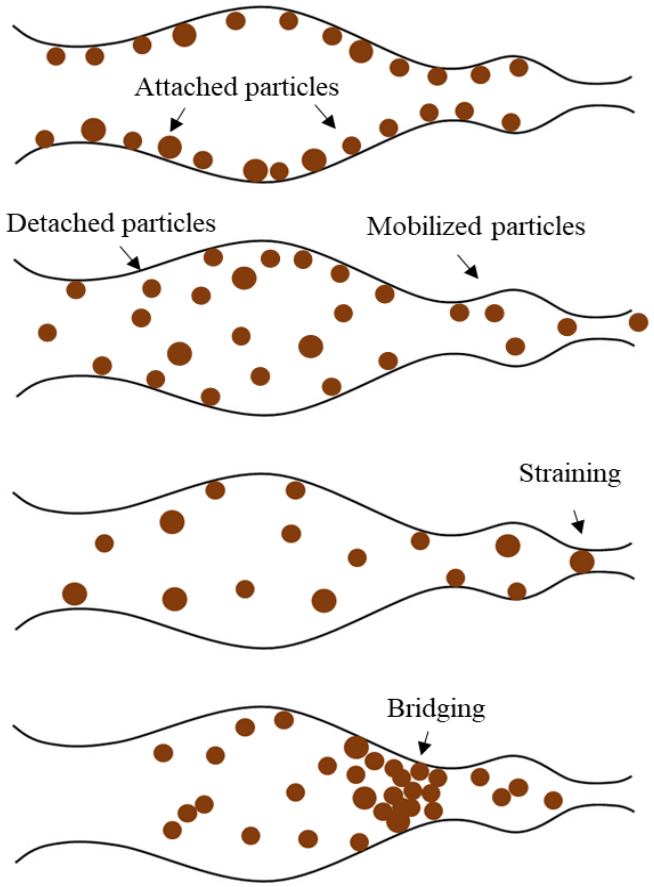

Figure 2.7 Four stages of fines migration: attached, detached, mobilized, and plugged (Russell et al., 2018).

The balance of hydrodynamic forces generated by fluid flow and the adhesive interactions between fine particles and rock surface governs fine particles attachment and detachment in porous media (Sharma & Yortsos, 1987; Torkzaban et al., 2007; Vanness et al., 2019). Sharma et al. (1992) proposed three conceptual fines displacement modes in porous media: rolling, sliding, and lifting. Lifting is not a primary mechanism for particle detachment and can be neglected at flow rates that fluids flow through the reservoir rock (Bergendahl & Grasso, 2000; Freitas & Sharma, 2001; Yang et al., 2022). For near-spherical fine particles, the detachment is more likely to be initiated by rolling rather than sliding (Sharma et al., 1992).

Figure 2.8 depicts the forces and torques exerted on a fine particle positioned on a solid surface with a roughness height of h_r. F_d and F_l are drag and lift forces generated by the flow velocity

profile. F_b is the resultant force of buoyancy and gravity forces which becomes essential only for large particles. F_a is the adhesive force between the fine particle and the rock surface. The hydrodynamic torque (T_H) at a given separation distance h, which tends to roll the fine particle and detach it from the rock surface, can be written as:

$$T_H = l_d F_d + l_a F_l \tag{3}$$

where l_d and l_a are the lever arms of drag and lift forces, respectively.

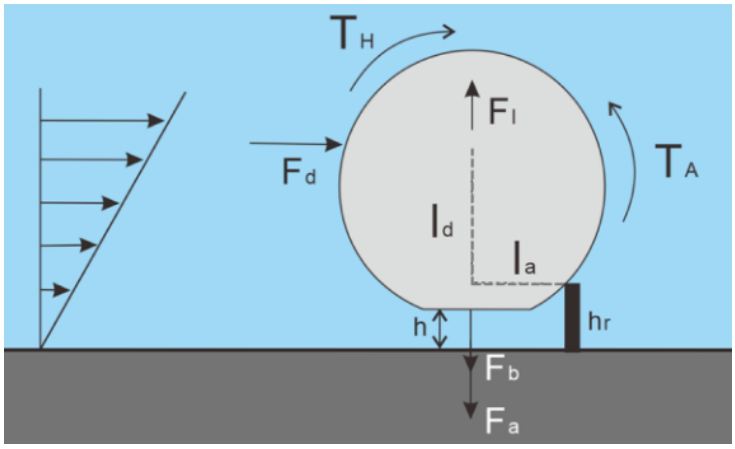

Figure 2.8 Schematic of forces and torques acting on a fine particle on a rock surface with a roughness of h_r (Yang et al., 2022).

The resisting adhesive torque, which tends to keep the fine particle attached to the rock surface, can be determined by:

$$T_A = l_a(F_a + F_b) \tag{4}$$

The resultant of hydrodynamic and adhesive torques determines whether the fine particle rolls or stays attached to the rock surface. Since adhesive force is considered negative, if $T_A + T_H > 0$, the fine particle will roll and detach from the rock surface. If $T_A + T_H < 0$, the fine particle will stay immobile. Determination of F_d, F_l, and F_b can be easily carried out using commonly recognized equations found in literature, while calculating $F_a$is relatively more complicated and requires estimating interaction energy using DLVO (Derjaguin–Landau–Verwey–Overbeek) theory (Bradford & Torkzaban, 2013; Derksen & Larsen, 2011; Yang et al., 2022).

Based on DLVO theory, the total interaction energy (V) is the summation of three components: London-van-der-Waals (LVW) attraction V_{LW}, the electrical double-layer repulsion V_{EDL}, and the Born repulsion V_B (Elimelech et al., 2013). The adhesive force (Fa) can be understood as keeping the particle and surface together, opposing their separation. It can be approximated as the negative derivative of the total interaction energy to the fine particle-grain separation distance (h) (Russel et al., 2017).

$$V = V_{LW} + V_{EDL} + V_B \quad (5)$$

$$F_a = -\frac{\partial V}{\partial h} \quad (6)$$

$where\ V_{LW}$ represents the intermolecular attraction between polarized molecules of fine particles and the rock surface, which depends on the size of the fine particles and the distance between the particle and the rock surface. V_B, the Born repulsion force is a short-range force originating from the overlap of electron clouds of atoms when two particles become too close. V_{EDL}, is the repulsion force between two similarly charged surfaces in a fluid. The electric double layer is a structure around a charged particle inside an electrolyte solution.

Surface charge balancing of fine particles results in forming a fixed Stern layer. In contrast, an overlapping diffuse layer creates a repulsive electrical double-layer force between the particles and rock surfaces. The detachment of fine particles from rock surfaces is influenced by flow rate, while their adhesion is affected by salinity and pH. Lower salinity expands the diffuse layer, leading to a repulsion force that can detach particles, and high pH can result in the flocculation of clay particles and decrease permeability (Vaidya & Fogler, 1992).

The hydrodynamic torque tends to detach the fine particles from the rock surface and depends on the flow rate. The adhesion torque, which tends to keep the fine particles in place, is affected by salinity and pH. In multi-phase flow, interfacial tension and wettability can also play a role (Huang et al., 2021; Ge et al., 2022). **Figure 2.9** compares the position and stability of the fines particle in high and low-salinity brine. Fluid salinity can alter the double layer and hence change the adhesive force. As salinity decreases, the diffuse layer expands to balance the surface charge of the fine particle and rock surface. The grown double layers will overlap at further distances and cause a repulsion force that may detach the fine particle from the rock surface.

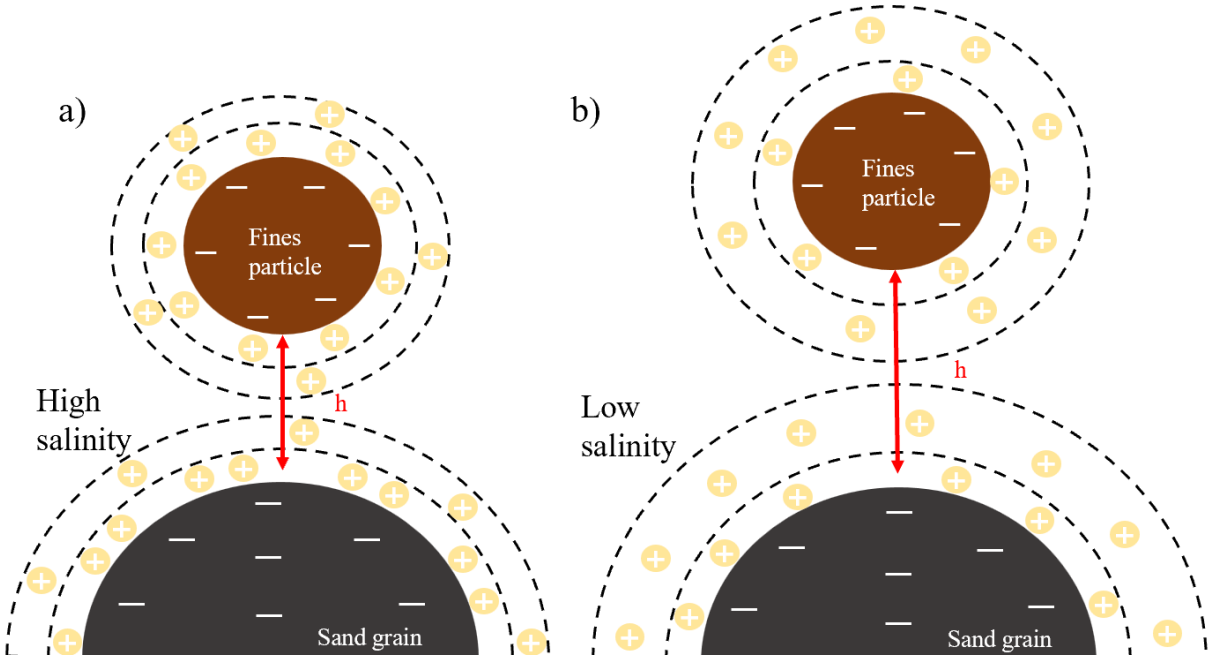

Figure 2.9 Schematic of fines particle-sand grain electrostatic attraction at a) high and b) low salinities. (h: particle-grain separation distance) (Adapted from Cardellini et al., 2016; Russel et al., 2017).

2.3.3 Fine Particles and Plugging

Unconsolidated sandstone reservoirs hold a wide variety of small, loose, solid particles of diverse sizes and chemical compositions (Muecke, 1979).

In a SAGD well pair, the sand control screen may become plugged with debris, and the steam flow into the reservoir or oil into the producer may be restricted. Two main types of plugging can occur in a slotted liner: pore plugging and screen plugging.

Pore plugging occurs when small particles of sand, clay, or other minerals accumulate in the pores of porous media near the sand screen, reducing the medium's effective porosity and limiting the fluid flow. Pore plugging is typically managed through regular well maintenance, including periodic cleaning or stimulation of the wells.

Screen plugging occurs when larger particles, such as pieces of gravel or rock combined with the fines and scaling and corrosion materials, become lodged in the liner slots, which could completely block the flow of fluids (Ramonava et al., 2013), requiring more extensive maintenance or replacement of the liner. Screen plugging is less common than pore plugging, but it can be more challenging to manage because the larger particles can be harder to remove.

Overall, both pore plugging and screen plugging can reduce the effectiveness of a sand screen in a SAGD well pair. Regular maintenance and monitoring can help identify and address these issues before they become more severe and require more extensive interventions.

2.3.3.1. Screen plugging

To thoroughly comprehend the plugging mechanism within the slots, it is imperative to analyze the deposited mineral layer on the stand-alone screens, considering both field observations (Ramonava & Ma, 2013) and laboratory experiments (Bennion et al., 2008). Bennion et al. (2008) noted severe plugging caused by clay particles, with their test results indicating the formation and thickening of a bank of clay particles over time inside the slot and on the coupon surface.

Romanava et al. (2013) conducted a series of tests on extracted slotted liners from the McMurray formation and found that the materials causing slot plugging were clay and corrosion byproducts. The plugging observed in the slotted liner appears to be influenced by the clay adsorption to the carbon steel, as highlighted by both Benion et al. (2008) and Ramonava and Ma (2013). Adhesive forces within the clay mixture are due to the electrostatic forces between the clay minerals and screen materials. The structure of the clay film formed on the liner's surface depends on the porous medium's pH level. Van Olphen (1965) explained that the Point Zero Charge (PZC) for kaolinite is at a neutral pH value of 7, while chlorite and bentonite are lower than the neutral pH. When the pH exceeds the PZC, charges with opposite signs form on the faces and edges of the clay particles.

In 1954, Fountaine designed a vertical adhesion test, which indicated that the adhesion was due to the water film between the contact surfaces. Later, Fukagawa et al. (2002) found that the adhesive stress decreased with increased porosity (compaction reduction). Satomi et al. (2012) discovered that the metal surface's roughness affects the adhesion between clay and metal. Kooistra et al. (1998) emphasized the impact of ionic conditions on the adhesion of clay minerals to metal. Romanova et al. (2013) discussed how the coexistence of corrosion materials and clay deposits in the slots leads to slot plugging.

According to several studies, corrosion products can penetrate the deposited clay. Jeannin et al. (2010) explained that the deposition of kaolinite in a compact film on the metal surface leads to a local increase of Fe^{2+} at the clay-steel interface. In some situations, the clay film breaks due to the growth of corrosion, enabling the corrosion byproducts to infiltrate the deposited film. The clay

mineralogy significantly influences these processes. For example, chlorite has a higher shield tendency than kaolinite (Jeannin et al., 2010).

Foct et al. (2004) observed that fluid flow increases the adherence of clay particles. They performed in-situ tests to study carbon steel corrosion from exposure to illite/smectite-rich formations. They measured an average corrosion rate of 5.2-17 μm/year, which can increase to 39 μm/year in the presence of fluid flow. The primary corrosion product was FeO (OH), consistent with the observations of Romanova et al. (2013). Urios et al. (2011) observed that steel corrosion produces mineralogical dissolutions (Ca phases) and precipitations (iron oxides and hydroxides), resulting in a partial mixture of the clay film and corrosion products in the vicinity of the test coupon. They observed five distinct zones: (1) partially corroded steel, (2) corroded steel, (3) Fe-enriched layer in the formation, (4) Ca-enriched layer in the formation, and (5) unaltered formation. The thickness of the altered zone was approximately 4 mm.

Foct et al. (2004) observed two distinguished layers on top of the steel coupon: (1) the first layer (nearly 40 μm thick) was located at the interface with steel and did not contain any Si or Al (clay free), and (2) the second layer (also around 40 μm thick) was located at the interface with clay and had a high Si and Al content (mixed iron oxide and clay zone). These zones were distinguishable from the energy-dispersive spectrometry image reported by Romanova et al. (2013).

2.3.3.2. Pore plugging

Sand particles form the load-bearing skeleton in oil sands, whereas fines are not part of this skeleton and can be transported by fluid flow under certain conditions. As fines collide with pore walls, they may become trapped, reducing pore throat sizes and lower permeability. When particles are smaller than ten μm, their interaction with pore fluids becomes more significant, as electrical attraction/repulsion is as crucial as gravitational and hydrodynamic forces (Wakeman, 2007).

Clay minerals in oil sands serve as a binding agent, holding particles together at particle contacts. Clay minerals' content and distribution dictate permeability and sensitivity to oil sand ionic conditions (Gaida et al., 1985; Khilar & Fogler, 1998). The relevant particle dimension in fines migration is perpendicular to the longest dimension, as suspended particles tend to orient their largest dimension along the flow direction (Khilar & Fogler, 1998).

Experimental observations by Barkman and Davidson (1972) and Abrams (1977) have shown that particles equal to or larger than one-third of the average pore throat size bridge at the pore throat. Particles smaller than one-third but larger than one-seventh of the average pore throat size deposit in the pore spaces, reducing effective pore/pore throat size. Particles smaller than one-seventh of the pore throat size pass through the pores with little or no impediment. At meager flow rates, particles larger than one-fourteenth but smaller than one-seventh of the average pore throat can still deposit in the pore spaces (van Oort et al., 1993).

2.3.4 Physical and Chemical Factors Affecting Fines Migration

Wettability, surface/interfacial forces, and mechanical bridging at pore restriction in multi-phase flow contribute to particle movements through porous media. However, fines move with the wetting phase (Muecke, 1979). Muecke, (1979) noted that backflow and pressure disturbances in single-phase flow may cause a bridge to be broken.

Rahman et al. (1994) stated several factors affecting fines migration and precipitation, including 1) formation characteristics, 2) fluid flow rate and 3) Particle electrophysical properties, 3) wettability, 4) relative permeability, and 5) chemical interaction of particles and formation fluid. The last three factors are only present while immiscible fluid exists in the reservoir.

2.3.4.1 Critical conditions

Critical conditions are avoided to keep the fines migration and deposition within the acceptable range, ensuring fluid flow through porous media. (Rahman et al., 1994). Critical conditions show that fines migration and deposition are threshold processes (Khilar et al., 1990).

2.3.4.2 Critical fluid velocity

A state of equilibrium is attained when the velocity is below the critical threshold, resulting in a constant pressure drop over time. Conversely, when the velocity is above the critical threshold, the pressure drop exhibits a linear increase followed by a sharp increase over time. This critical velocity is the defining point between these two behaviors (Arshad et al., 1993).

2.3.4.3 Critical Particle Size and Concentrations & Salinity Reduction

The term "critical size" pertains to the size at which larger particles detach while smaller ones remain attached. It was observed that the reduction in brine salinity led to a decrease in the critical

size, indicating that the size range of detached particles expanded by salinity reduction (Russell et al., 2017).

2.3.4.4 Kaolinite content & Salinity reduction

The experimental findings reveal that sand packs with 0 to 10 weight percent Kaolinite exhibit a decrease in permeability ranging from a factor of 9 to 54 when exposed to brine injection with salinity levels ranging from seawater to de-ionized water. However, injecting high salinity brine in a low Kaolinite sand pack results in an increase in permeability. Additionally, the study reported a 0.2-1.6% recovery of the initial fine content (Russell et al., 2017).

2.4 Two-phase Flow

The effect of two-phase flow and pattern on fines production and migration in a SAGD well can be complex and multifaceted. Understanding these factors and their interactions is essential for optimizing the performance of the SAGD process and minimizing the potential for fines-related issues such as plugging and decreased productivity. The selection of operating parameters, such as injection rates, well spacing, and well completion design, can also impact fines production and migration and should be carefully considered to optimize the performance of the SAGD process.

Typically, when the pH of injected water increases and the salinity decreases, it reduces water relative permeability and residual oil saturation (Zeinijahromi et al., 2016).

The existence of oil as a residual oil saturation reduces the formation damage by fines migration because the accessible surface area for the brine is less, and particle straining is less likely to happen(Sarkar & Sharma, 1990; Sharma & Filoco, 2000).

Moreover, (Yuan & Shapiro, 2011) related the maximum retention function to saturation due to the water velocity dependence on saturation. After that, Zeinijahromi et al. (2016) reported that the full retention function, which is related to the attached particle (either by electrostatic force or straining), is water saturation dependent, as the accessible surface of rock for brine increases, the formation damage worsens.

$$\sigma_{cr} = \sigma_{cr}(\gamma,\ PH,\ T,\ U,\ S_w) \tag{7}$$

γ is brine ionic strength, and PH shows brine PH, T, U, and Sw, respectively, for temperature, superficial velocity, and brine saturation. Equation (7), modified after Zeinijahromi et al. (2016),

mathematically showed the maximum retention function, defined by the excess concentration of the attached particle over the current value of σ_{cr} is detached, mobilized, and migrated.

2.5 Summary

In conclusion, this chapter provides a comprehensive literature review on sand control devices and fines migration in the context of Steam-Assisted Gravity Drainage (SAGD) operations in the Alberta oil sands. The chapter begins by introducing the background of oil sand deposits in northern Alberta and the significance of SAGD as a thermal extraction method. The Steam-Assisted-Gravity-Drainage mechanism is explained, highlighting the role of low-pressure steam injection in reducing oil viscosity and increasing production.

The chapter then discusses the various sand control devices used in SAGD well completions, including Slotted-Liner, Wire-Wrapped Screen, and Punch Screen. The purpose of these devices is to prevent sand production while improving liquid and oil production rates. The issue of fines production and its detrimental effects on formation near the wellbore is addressed. Fines, which include small particles such as rock flour, metal oxide, and clay, can lead to formation damage, decreased production, and screen plugging.

The literature review further explores the evaluation tests used to assess the performance of sand control devices, particularly the Sand Retention Testing (SRT) method. Several researchers have conducted SRTs investigating slot width, density, open flow area, and sand and fines production. The influence of salinity on sand control device performance is also studied through single-phase SRT tests, with findings indicating that fines migration is most significant at lower brine salinities.

Sand production mechanisms are discussed in detail, including shear failure, tensile failure, and the formation of sand arches and cavities. The factors affecting sand production, such as fluid pressure drawdown, high hydrocarbon production rates, completion stresses, and fluid viscous drag forces, are highlighted. The chapter also addresses the evaluation tests used for sand control devices, including SRT, Full-scale Completion Testing (FCT), and Scaled Completion Testing (SCT).

Finally, the chapter delves into fines migration and its impact on formation damage and well performance. The size and types of fine particles, such as clays and non-clay minerals, are examined. Core flooding experiments have been conducted to investigate fines migration and

permeability reduction. The triggers for fines mobilization, including hydrodynamic forces and adhesive interactions between fine particles and rock surfaces, are discussed. The literature review provides a comprehensive understanding of sand control devices, fines migration, and sand and fines production mechanisms, setting the stage for the research conducted in the thesis. This study investigates the effect of varying and reducing brine salinity through two-phase SRT. The research focuses on the prementioned parameter's impact on screen and pore plugging, particularly in the near-screen zone in SRT. This test methodology introduces similar conditions to the actual SAGD conditions. In actual SAGD conditions, the formation water salinity is diluted while producing and mixing with steam condensate and melted bitumen.

Overall, a thorough literature review is provided encompassing background information, sand control devices, fines migration, sand production mechanisms, evaluation tests, and influential factors. It lays the foundation for the subsequent research conducted in the thesis and contributes to the existing knowledge of SAGD operations in the Alberta oil sands.

3 SRT Experiment Facility, Test Design, and Procedure

3.2 Introduction

This chapter integrates the materials, the SRT setup, the testing facility, the experiment design, and the procedure. A small-scale SRT setup holding a screen coupon is used to evaluate the effect of flow rate, water cut, single/two-phase flow, and salinity reduction on fines migration and its influence on-screen performance. The testing is performed at room temperature and ambient pressure; the other test parameters represent the actual SAGD conditions. The following sections detail the materials, SRT facility, testing design, and procedures.

3.3 Materials

The primary fluids used in the tests were distilled water and synthetic oil. The viscosity of the oil was 8 cp with a density of 0.8. Sodium Chloride with 99.9% purity was used to mix with distilled water and made 7000, 4000, 1000, and 400 ppm salinity brine.

3.4 Sand Retention Testing Facility

This setup was designed to evaluate a sand control screen performance. This is a scaled-down of a large SRT setup consisting of a cell body, a metal plate, a metal frame, an axial load, a sand control screen, an upper platen, pressure transducer, accumulators, pump, mesh, pressure line, fluid line, oil accumulator, brine accumulator, scales, the bottom part of SRT, sand trap, butterfly valve, check valve, sampling tab, and turbidimeter.

Figure 3.1 shows the entire sand retention testing facility used for this research, composed of five different sections, including:

- A cylindrical metal cell with a diameter of 6.3 cm and a height of 30.5 cm housing the sand pack. The sand is packed in four layers over a multi-slot coupon of a slotted liner screen placed at the bottom of the cell. Two pressure transducers measure the differential pressure of the top and bottom intervals. The differential pressure along the top and bottom intervals are measured using pressure transducers 1 and 2, respectively.

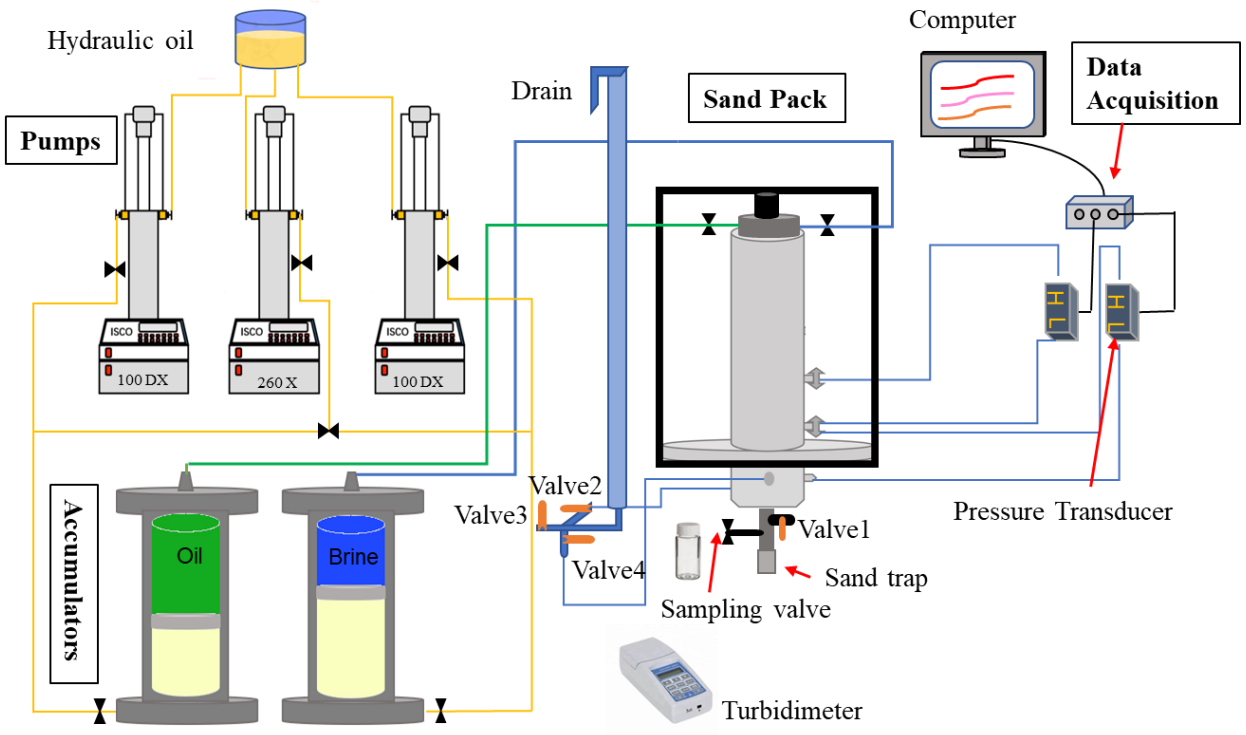

Figure 3.1 Schematic of the Sand Retention Testing facility.

Figure 3.2 shows the sand pack, pressure transducers, coupon, and four sand pack layers. Layers 1 and 2 comprise the bottom interval, whereas Layers 3 and 4 cover the top interval. The differential pressure along the top and bottom intervals are measured using pressure transducers 1 and 2, respectively.

- The injection unit consists of two ISCO pumps,100 DX (∓0.3% accuracy), with two accumulators filled with water and synthetic oil. In addition, an ISCO pump, 260 D (∓ 0.5% accuracy), serves as a backup.
- The data acquisition section includes two calibrated YOKOGAWA differential pressure transducers with an accuracy of 0.25% of their full range of 15 psi. The LabVIEW data acquisition program depicts the recorded data.
- The backpressure column applies a 3-psi pressure at the bottom of the sand pack during the tests.
- The sampling unit includes a cylindrical container at the bottom of the cell for taking accumulated fines or sand after each flow stage. Also, a sampling valve enables taking

regular samples of discharge fluids right underneath the screen coupon for produced fines concentration measurements by a turbidity meter.

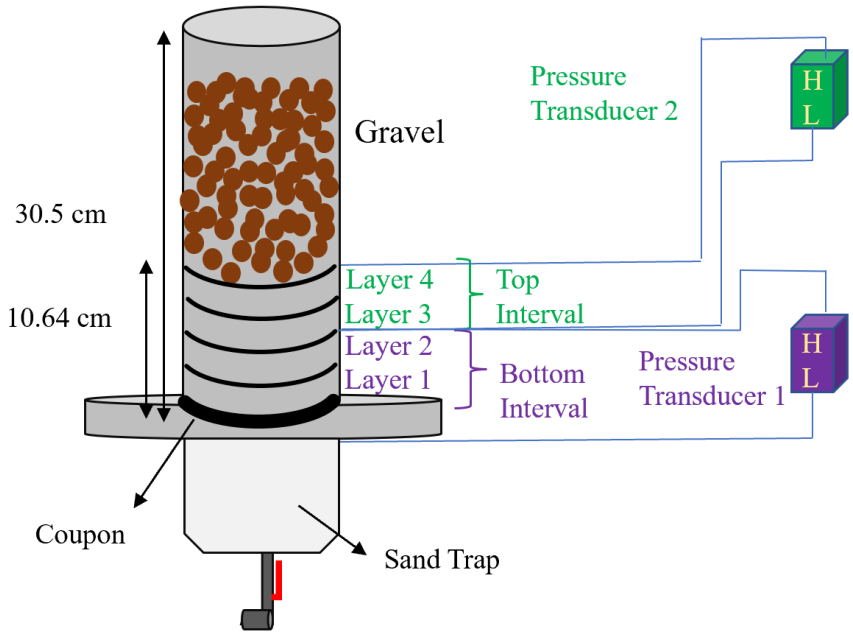

Figure 3.2 Schematic of the metal cell, including four sand pack layers topped with gravel.

3.5 Test Design

In this study, Test #1, which served as the baseline test, the brine salinity remained constant at 7000 ppm for the duration of the test. On the other hand, Test #2 examined the salinity reduction effect by exposing the system to different NaCl brine salinity levels of 7000, 4000, 1000, and 400 ppm.

3.5.1 Sand pack (sand mixture, PSD)

Abram and Cain (2014) proposed four typical PSD classes for McMurray formation. **Figure 3.3** shows the (particle size distribution) PSD of DCI, DCII, DCIII, and DCIV sand classes. The DCI and DCIV classes are the finest and coarsest sands, respectively.

This study considered the DCII class to compare the test results with previous works (Wang et al., 2020). **Figure 3.3** illustrates a good agreement between the PSD of the constructed sand sample and the DCII sand.

Kaolinite clay is chosen to add to the mixture representing the dominant fine particles in McMurray formation (Romanova et al., 2015). After mixing the dry prepared sands, 10 wt% brine (7000

ppm), representing formation brine, was added to moist the mixture for a wet packing procedure. The sand was packed in four layers targeting a 42% porosity for each layer.

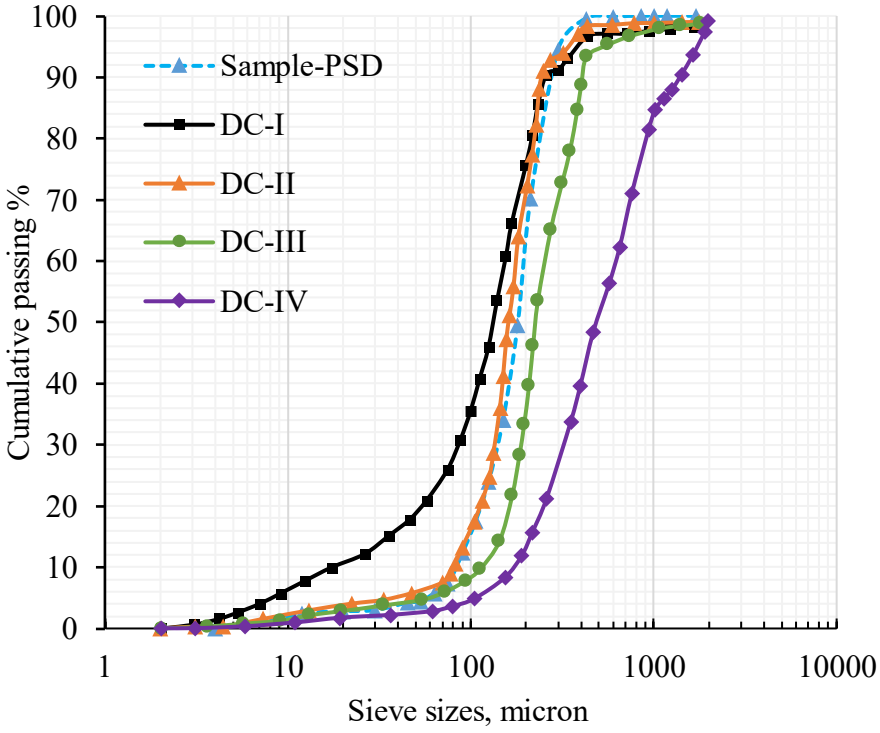

Figure 3.3 Particle Size Distribution (PSD) of the four categories of McMurray formation sands compared to the PSD of the replicated sand mixture used in the SRTs.

3.5.2 Sand Screen

Coberly (1937) proposed a range for slot width that prevents massive sand production while the grains form a stable arch on pore openings (< $2D_{10}$ or D_{10}). Later, Fermaniuk (2013) modified the range to $2D_{50}$ < slot width < $3.5D_{50}$. Wang et al. (2020) conducted multiple three-phase single rate tests (SRT) experiments. The objective of these experiments was to enhance the criteria for selecting slot sizes in slotted liners installed within wells drilled in the McMurray formation. They reported a safe range of slot widths of 0.010 to 0.016 inches with SPC (slot per column) of 54 for DC-II sand. The SPC is the number of slots in each column on the liner with a 7-inch diameter. However, trial tests with the slot sizes of 0.014 and 0.010 inches resulted either unacceptable sand production or excessive plugging, respectively. Therefore, this study chose a screen size of 0.013 inches with SPC of 54 to minimize sand production and prevent screen plugging.

3.5.3 Flow Test Design

The real SAGD flow rates were scaled down to obtain the flow rate design. AER, 2018 reported that a typical SAGD well produces 800-7000 bbl/day. Considering a 600 m horizontal well completed with a 7 inches diameter slotted liner, the average flow rate per unit length surface area of the slotted liner is 7400 cc/hr/ft^2 (Wang et al., 2020). The surface area of the screen coupon was 0.03 ft^2. Therefore, the base flow rate is 4 cc/min.

Romanova & Ma, 2013 mentioned that the slotted liner is prone to plugging due to corrosion, fines migration, scaling, and asphaltene deposition. In the worst-case scenario, the screen can produce through 10% of its surface area. Thus, the fluid velocity increases in the openings. This research assumed that the slotted liner produces through 20%, 30%, and 50% of the total surface area, resulting in the corresponding flow rates of 8, 13, and 21 cc/min.

McMurray formation water has a wide salinity range from 240 to 279000 ppm (Cowie et al., 2015). Haftani, 2019 reviewed the hydro-chemical analyses of the produced water of the SAGD wells. He reported a salinity within 1000 to 7000 ppm for the produced water, with Na and Cl as the dominant ions. The concentration of NaCl salt ranged from 400 to 3400 ppm (Haftani et al., 2019). In contrast to the formation water, the lower concentrations observed in the produced water can be attributed to the combination of low saline condensed steam with formation water at the edge of the steam chamber during the SAGD process.

As mentioned above, two tests were designed. The first reflected the effect of increasing flow rates, varying water cuts, and two-phase flow conditions on the pre-packed sand pack's fines migration and permeability changes. The second test, with a similar procedure to the first one, investigated mainly the effect of varying and reducing the salinity.

Figure 3.4 shows the testing procedures for the two tests. As depicted, each test started with Stage A (saturation), where 7000 ppm brine was injected from the bottom of the sand pack. It was followed by Stage B (initial absolute permeability measurement of the sand pack). In Stage C (displacement), oil was injected into the sand pack to displace water and reached the irreducible water saturation (S_{wirr}) when no more water came out of the sand pack. Stages 1, 2, and 3 were designed to show the effect of increased flow rate in single oil phase flow, considering flow rates of 8, 13, and 21 cc/min. Stages 4, 5, and 6 were designed to show the impact of flow rates in two-phase flow conditions. Stages 7 and 8 reflected the effect of varying water cuts. In the end, Stage

D represented the final permeability of the sand pack as a measure to show the salinity change effect on near-screen flow performance.

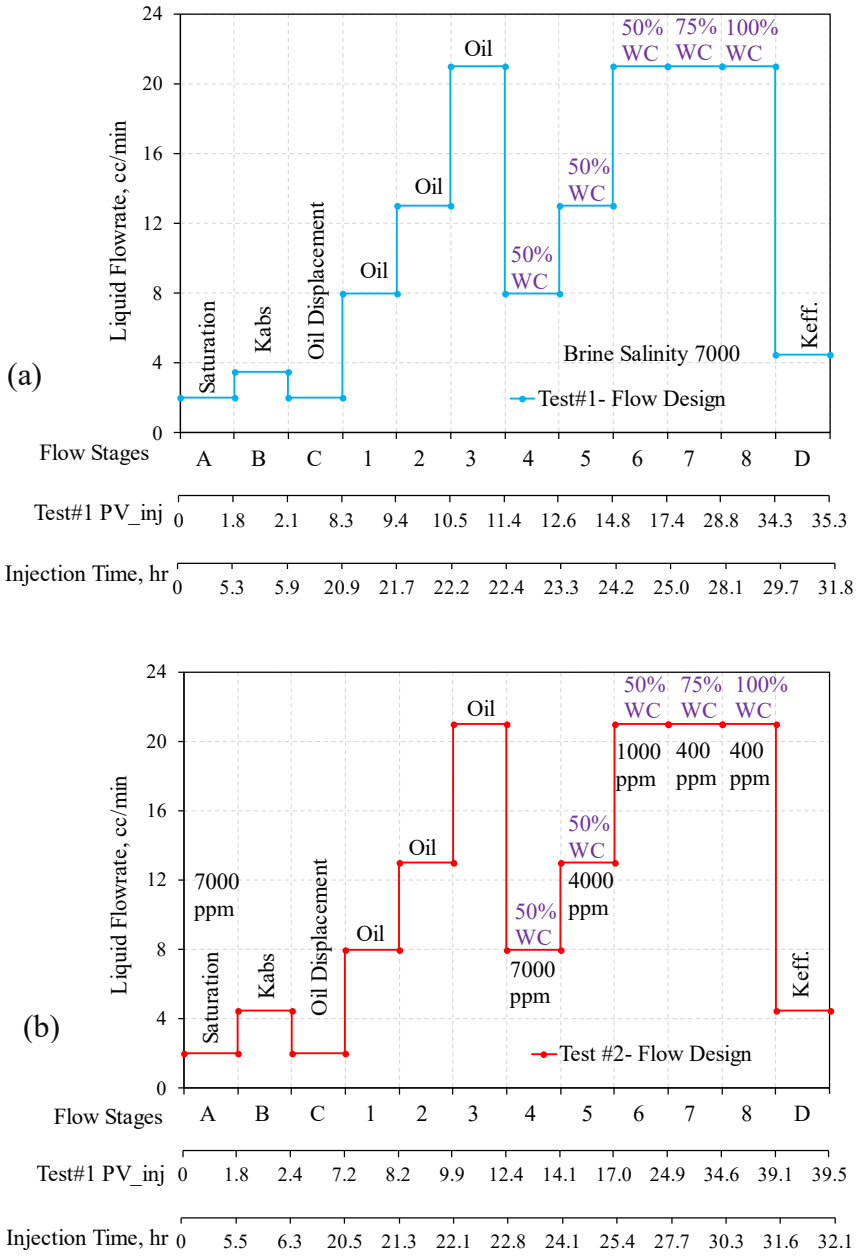

Figure 3.4 Applied flow rates, water cuts, and salinity of a) Test#1 and b) Test#2.

3.6 Test Procedure

A 7000-ppm brine was made by mixing 70 grams of NaCl salt in 10 L of distilled water. It was then poured into the accumulator. Synthetic oil was also fed to another 10-L capacity accumulator.

After de-airing the area under the piston, the connections of the accumulator to the ISCO pump were placed, and the output pipes connected to the accumulators were de-aired by injecting oil and water to the line until all the bubble came out of the pipe, and the fluid became continuous. Then these two pipes were placed upward to avoid air entering them.

The sand mixture was formulated by blending various commercial sands, namely Sil-1, LM 70, and Helmer. Helmer, characterized by its fine-grained nature, predominantly consisted of kaolinite. Meanwhile, LM 70 and Sil-1 contributed particles of medium and large sizes, respectively. The particle size distribution of each constituent is illustrated in **Figure 3.5**. In the preparation of the DC-II sand mixture, a combination of 145 grams of Sil-1, 873 grams of LM 70, and 82 grams of Helmer was utilized. For a reliable replication of the laboratory's DCII sand mixture, **Table 3.1** provides the requisite weight percentages for each component.

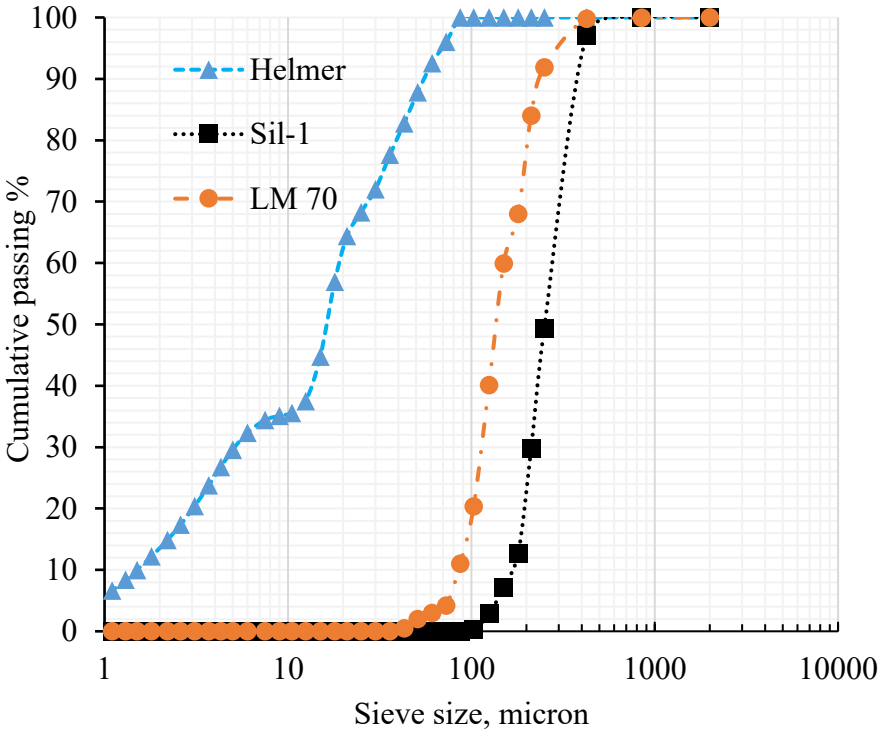

Figure 3.5 Particle size distribution of Sil-1, LM 70 and Helmer.

Helmer was sieved using a shaker with a sieve of 120 for 10 minutes. In the sieving process, materials were collected from sieves number 140, 170, 200, 230, 270, and 325 and the tray. After weighing the materials, they were mixed and placed in the oven at 120 C for 24 hours to dry.

After removing the sand mixture from the oven, it was spread on a plate and was allowed to cool. After reaching room temperature, it was evenly mixed with a spatula to separate the particles and remove the clamps of attached fines. Then 110 cc 7000 ppm brine equal to 10 %wt of the sand mixture was added to the sand mixture and mixed well manually.

Table 3.1: Sand mixture type and composition.

Sand Type	Sil-1	LM 70	Helmer
DC-II	13.2%	79.4%	7.4%

3.6.1 Setup Assembly

A stainless-steel size 0.013” and SPC 54 was chosen for the target test. After plugging the holes at the back of the screen coupon (SC) with fitting and the holes on the front using mesh, the SC was put on the base plate on a rubber O-ring, and a gasket was placed afterward to support the sealing. Next, the sand pack cell was placed on top, while the sand trap was kept under the screen coupon. Two nuts and bolts across from each other were placed to connect the upper and lower part of the setup; this then continued for the other six. After finishing, they were again fastened in a diagonal sequence to ensure the sealing. There were three pressure ports on the cell wall, and a small mesh was placed in each port to prevent sand from transferring to the pressure lines. Two junctions were placed on the cell’s lower and medium pressure ports, 2 and 4 inches above the SC, respectively.

3.6.2 Packing

The packing was performed in a way to achieve 42% porosity. The first layer was 43%, and the others were 42%. The height correction incorporated the compaction effect on the first layer while the other layers were compacted. The first layer height was assumed to be decreased by 4 mm and matched the 42% target porosity after compacting the second layer.

A mesh was put on top of the fourth layer, followed by a circular porous distributer before adding the gravel up to 5.5 cm to the top of the cell. Gravels were washed carefully before use. Another mesh then topped up the gravel before putting the upper platen. The inlet oil and brine valves were connected to the upper platen. The sand weight, height, and porosity of each layer of the sand pack are reported in **Table 3.2**.

Table 3.2: Sand pack layers specifications.

Sand pack	Wet sand weight, gm	Height, cm	Porosity
Layer1	154	3.00	0.430
Layer2	136	2.60	0.420
Layer3	136	2.60	0.420
Layer4	130.8	2.50	0.419

For this test, three YOKOGAWA differential pressure transducers with 15 ± 0.04 psi were used to record the DP data. Six plastic tubes were used to connect them to the cell. The upper point in the cell was connected to the high section, while the lower point was connected to the low part of each transducer. Moreover, two more tubes connected the sand trap to the back column.

3.6.3 Axial Load

A 60-psi axial load was applied to the sand pack to support the sand pack integrity. It prevented the sand pack fluidization during the tests.

3.6.4 Saturation

To boost the speed of the test, the sand trap was filled using a high flow rate. When brine came out of the ports, the tube to that port was connected, and when the brine came out of the valve connected to its body, the valve was closed. It was then followed by filling the back column while the connections to the sand trap were closed (yellow and blue valves).

After filling the injection line with the brine, the tube was connected to the sand trap, and the flow rate was set at 2 cc/min. Each valve that let the water out remained close, then all the pressure transducer valves were checked to ensure they were filled with brine (from the bottom to the top).

After all the valves and outlet were closed, the pump was set at 15 psi constant pressure, and the sand pack was exposed to brine flow overnight to ensure full saturation. **Table 3.3** presents the pore/ bulk volume of sand and gravel in the cell.

Table 3.3: Sand pack and gravel specifications.

Sand pack and Gravel Specifications	
Sand Specific gravity	2.65 gr/cc
Sand Bulk volume	328.9 cc
Sand pore volume	137.9 cc
Gravels Bulk volume	443.8 cc
Gravel Pore Volume	221.9 cc

3.6.5 Pump

There were three ISCO pumps; two were 100 DX with 100-cc tank capacity, one for the oil injection and the other for brine injection. A 260 D pump with 260-cc tank capacity also worked as a backup pump to ensure a continuous flow rate during the test. After the sand pack was fully saturated, the pump was stopped and the valves on the upper platen were slowly opened to release the bubbles. During the entire process, the axial load was checked to ensure it stayed at 60 psi and the pressure transducer lines were checked to ensure there were no bubbles in them.

3.6.6 Brine Injection

The brine injection procedure is listed as followed: (1) Close the inlet of the saturation valve and connect the line to the top. (2) Let some brine come out of the line, pump the liquid in the line to release all the bubbles, and then connect the line to the valve while the pump is set at 2.5 cc/min as the first flow rate. (3) Open the back column to the sand pack. The other two rates are 3.5 and

4.5 cc/hr. (4) Using Darcy's equation, three different rates and differential pressure (DP), calculate the absolute permeability for the top and the bottom part of the sand pack.

3.6.7 Oil Displacement

The oil displacement phase is described as follows: (1) Close the inlet valve of the brine, fill the oil line, open the oil inlet line, and connect them. (2) Set the pump at 3 cc/min constant flow rate and record the pressure data.

There was a sharp pressure increase first in the top, then in the bottom transducer, followed by a gradual decrease. This point might show when the oil front reached the sand pack and pushed and displaced the brine.

3.6.8 Single-phase Oil Injection

The single-phase oil flow stage is performed as follows:

- Start injection (top to bottom of the sand pack) with single phase oil at 8 cc/min rate. Flow until stable ΔP is reached. Afterward, record pressure drops through the entire sand pack, over the top of the slots, and at the base of the slot for 30 mins.
- Stop the fluid injection.
- Close the butterfly valve after 30mins flows and open the sand trap. Collect the produced sand in a sand trap. Fill the sand trap with brine, connect it to the butterfly valve, and open it for the following stage. This step should be repeated after each stage to collect the produced sand.
- Take samples in each flow stage to measure fines concentration in outlet liquid. Open the valve slowly to take the sample every 5 minutes. Moreover, after using a turbidity meter to measure the concentration of the fine, record the value in an Excel sheet.
- Start injection (top to bottom of the sand pack) with single phase oil at a rate of 13 cc/min. Flow until stable ΔP is reached. Record pressure drops through the entire sand pack, on top of the slot, and at the base of the slot. Inject the oil for 30 mins at this flow rate, and then stop the injection. Then, take the samples as mentioned above.
- Start injection (top to bottom of the sand pack and out through slot) with single phase oil at a rate of 21 cc/min. Flow until stable ΔP is reached. Record pressure drops through the

entire sand pack, on top of the slot, and at the base of the slot. Inject the oil for 30 mins at this flow rate, and then stop the injection. Then, take the samples as mentioned above.

3.6.8.1 Instantaneous Fines Concentration Measurement

A turbidimeter is a device that can quickly measure the cloudiness, or the turbidity of water caused by solid particles. The sampling began as each major stage was started (Stage 1 through 8). The sampling valve was a needle valve located at the bottom of the cell and was used to take the sample from right below the screen coupon. The sampling valve should be opened slowly enough to decrease the impact on the pressure drop. Sampling was repeated every 5 minutes until the end of each stage when the pressure dropped, and the turbidity reached stability.

The Turbidity device shows the number of solid particles with the unit of NTU (3 mg/l), which can then be converted to the particle's concentration in mg/l.

3.6.9 Fifty Percent Water Cut Fluid Injection with an Increasing Flow Rate

Stage 4 incorporated a 50% water cut and 8 cc/min fluid flow rates. The procedure to conduct Stage 4 is as follows:

1. Set the brine and oil pump at 4 cc/min.
2. Check the brine inlet valve to the sand pack, the outlet valve from the accumulator, and the outlet valve of the pump.
3. Start data recording.
4. Start both pumps simultaneously.
5. Open the back-column valve slowly to the sand pack.
6. Take the first sample and write its information on the excel sheet for further analysis.
7. After reaching the plateau, stop recording.
8. Stop the pump.
9. Close the back-column valve.
10. Close the butterfly valve, remove the sand trap, transfer the produced particles to a measured cup, and label it Stage 4.
11. Fill up the sand trap from the brine with the same salinity and return it.
12. Gently open the butterfly valve.
13. Stage 5 incorporates %50 WC and 14 cc/min flow rate. Set the brine and oil pump at 8 cc/min. Repeat the procedure number 2 to 12.

14. Stage 6 incorporates %50 WC and 22 cc/min flow rate. Set the brine and oil pump on 11 cc/min. Repeat the procedure number 2 to 12.

3.6.10 Increasing Water Cut

Stage 7 incorporated 75% water cut and 22 cc/min fluid flow rates. The following steps were taken to conduct Stage 7.

1. Set the brine pump to 16.5 cc/sec and the oil pump to 5.5 cc/min.
2. Start data recording.
3. Start both pumps simultaneously.
4. Open the back-column valve slowly to the sand pack.
5. Take the first sample and write it on the excel sheet for further analysis.
6. After reaching the plateau, stop recording.
7. Stop the pump.
8. Close the back-column valve.
9. Close the butterfly valve, remove the sand trap, transfer the produced particles to a measured cup, and label it Stage 7.
10. Fill up the sand trap from the brine with the same salinity and return it.
11. Gently open the butterfly valve.
12. Set the brine pump on the 22 cc/min.
13. Close the inlet valve of oil to the sand pack.
14. Repeat the Stage 7's procedure from step 2 to 11 to conduct Stage 8.

3.6.11 Brine Injection and Retained Permeability Measurement

At this stage, 100% brine was injected with three different flow rates to obtain the retained permeability of the sand pack. The flow rates were chosen the same as Stage B to make the permeabilities comparable.

For Test #1, brine was injected at 3.5, 4.5, and 5.5 cc/min. Each flowrate continued for nearly 15 minutes until it reached stability. For Test #2, the pressure drops were low, and the 2.5 cc/min did not generate high enough pressures in the specified range of pressure transducers. Therefore, 3.5, 4.5, and 5.5 cc/min brine were injected to achieve effective permeability for the top and bottom layers.

3.6.12 Dis-assembly of the Setup

The setup was dis-assembled following each test using the following steps:

1. Disconnect the line from the upper platen to have air on top of the platen.

2. Open the valves on top of the upper platen to the air.

3. Slowly open the valve between the sand trap and the back column, then open the lower valve of the sand trap to discharge the liquid from both the back column and the sand trap.

4. Disconnect the lines of the back column to the sand trap using a 9/16 wrench.

5. Disconnect the valves from the upper platen.

6. Remove the axial load.

7. Remove the pressure lines from the cell.

8. Loosen the valves attached to the sides of each pressure transducer to release the liquid.

9. Screw the hook-on top of the upper platen and push it upward to open that.

3.6.13 Post-mortem Test Analysis

Post-mortem analysis was meticulously performed to measure the retained fines content in four different samples taken from the sand pack after the test and the four samples initially taken from each layer of the sand pack during the packing phase. The goal was to obtain the initial fines content of each layer, ensure the homogeneity of the sand pack, measure the final fines content of each layer, and compare those with the initial amount.

These analyses support the differential pressure changes and give insight into the produced fines' origin. The sequence for fines content measurement is categorized below:

1) After disassembly, put the metal cell on a table. There are four layers of the sand pack, each with a length of 2 inches. Gently take 2 inches of the sand pack from the bottom of the cell using a trowel and then measure the depth using a ruler to ensure all the layer one is out.
2) Label and weigh a plate. Then weigh the layer one sand mixture and spread that on the labeled plate.
3) Return to step 1 and step 2 for the rest of the layers (layer 2, 3, and 4).

4) Set the oven temperature to 120°C and put all the plates in the oven for 24 hours.

5) Take out all the plates and let them cool down for 10 mins and weigh them again, again return them to the oven.

6) Continue step 5 until the weight of the plates and sand on them stays unchanged, indicating all the fluids are vaporized.

7) Take out plate one, weigh the sand mixture for the last time, and crush the dried mixture using a mortar and pastel.

8) Then transfer the dry mixture to a 500-cc beaker, pour 300 cc distilled water, and mix for 5 minutes.

9) Transfer the wet mixture to sieve #325 and wash away all the mixture using distilled water for 10 minutes. The particles with a size of less than 44 microns are washed away.

10) After ten minutes, take a sample from the discharge water that passed through the sieve. Put the sample in a turbidimeter. If the NTU is 10, stop washing. If not, continue washing and taking samples until the discharge water becomes 10 NTU, like pure water. It means that no more fines exist in the wet mixture.

11) Transfer the sand mixture to plate 1 and put it back in the oven at 120℃.

12) Repeat step 7 to 11 for plate 2, 3 and 4.

13) After 24 hours, remove all the plates from the oven. Let them cool down for 10 minutes, then weigh the dried sand mixture.

14) Calculate the retained fines content for each layer using the following formula:

$$\%Fine\ Content = \frac{Dry\ Sand\ before\ Wash - Dry\ Sand\ after\ Wash}{Dry\ Sand\ before\ Wash} \quad (3)$$

15) Calculate the initial fines content similarly and then compare the results of fines content after the test with the initial amount.

3.7 Summary

This chapter introduces synthetic oil and brine as the primary fluids injected into the sand pack. It then describes the testing facility, including the SRT cell, accumulators, pumps, pressure

transducers, and the fines collection unit. The 0.013” and 54 SPC screen coupon selection and details of the sands used to make the DC-II sand mixture in the laboratory are explained. These tests are composed of thirteen stages, Stage A (saturation), Stage B (brine injection and absolute permeability measurement), Stage C (oil displacement), Stage 1-3 (single-phase oil flow with increasing flow rate), Stage 4-6 (50% WC and increasing flow rate), Stage 6-8 (constant flow rate and rising water cut from 50% to 100%), Stage D (brine injection and retained permeability measurement).

This chapter then further explains the details of the test procedure, including but not limited to sand mixture preparation, cell assembly, packing methods, each stage parameter, and at the end, the applied post-mortem analysis is well described.

4 Trial Tests and Lessons Learned

4.2 Introduction

Bitumen extraction from poorly consolidated reservoirs predominantly relies on the Steam-Assisted Gravity Drainage (SAGD) technique. However, sand production has emerged as a recurring issue associated with this method. To mitigate the challenges posed by sand production, mechanical screens, such as slotted liners, are deployed in production wells to prevent sand influx while inducing minimal restrictions for fine particle production.

The present study employs the Sand Retention Test (SRT) to assess the performance of these mechanical screens and aid in selecting the optimal size for practical thermal/SAGD wells. The determination of the optimum size involves striking a delicate balance between acceptable sand production, well deliverability or flow performance, fines production, and minimal pore plugging.

This chapter outlines the comprehensive analysis of six SRT tests conducted, laying the groundwork for the last two tests that form the central focus of this thesis. Four of the six tests were conducted with the large SRT cell, while the remaining two utilized the smaller cell. Following each test, meticulous examination and deliberation on the outcomes led to the identification of potential reasons for unfavorable results. Subsequently, the lessons gleaned from each test were applied to refine the subsequent trials, thereby yielding more reliable and informative outcomes. A detailed explanation of the objectives pursued in each test is provided, and the results are concisely discussed to provide a glimpse into the study's findings.

4.3 Large Cell SRT (Hydrodynamic Effect, Multi-Phase Flow, Water Cut)

The schematic of the SRT facility is illustrated in **Figure 4.1**. The SRT facility has five major sections: fluid injection unit, pressure transducers, sand, fines measurement, data acquisition system, and back pressure unit. Three pressure transducers record the pressure changes over the sand pack's top, middle, and bottom intervals. A sand mixture of known composition is packed inside the Aluminum cell (18.5 inches high and 6.75 inches wide) on top of the installed slotted liner screen.

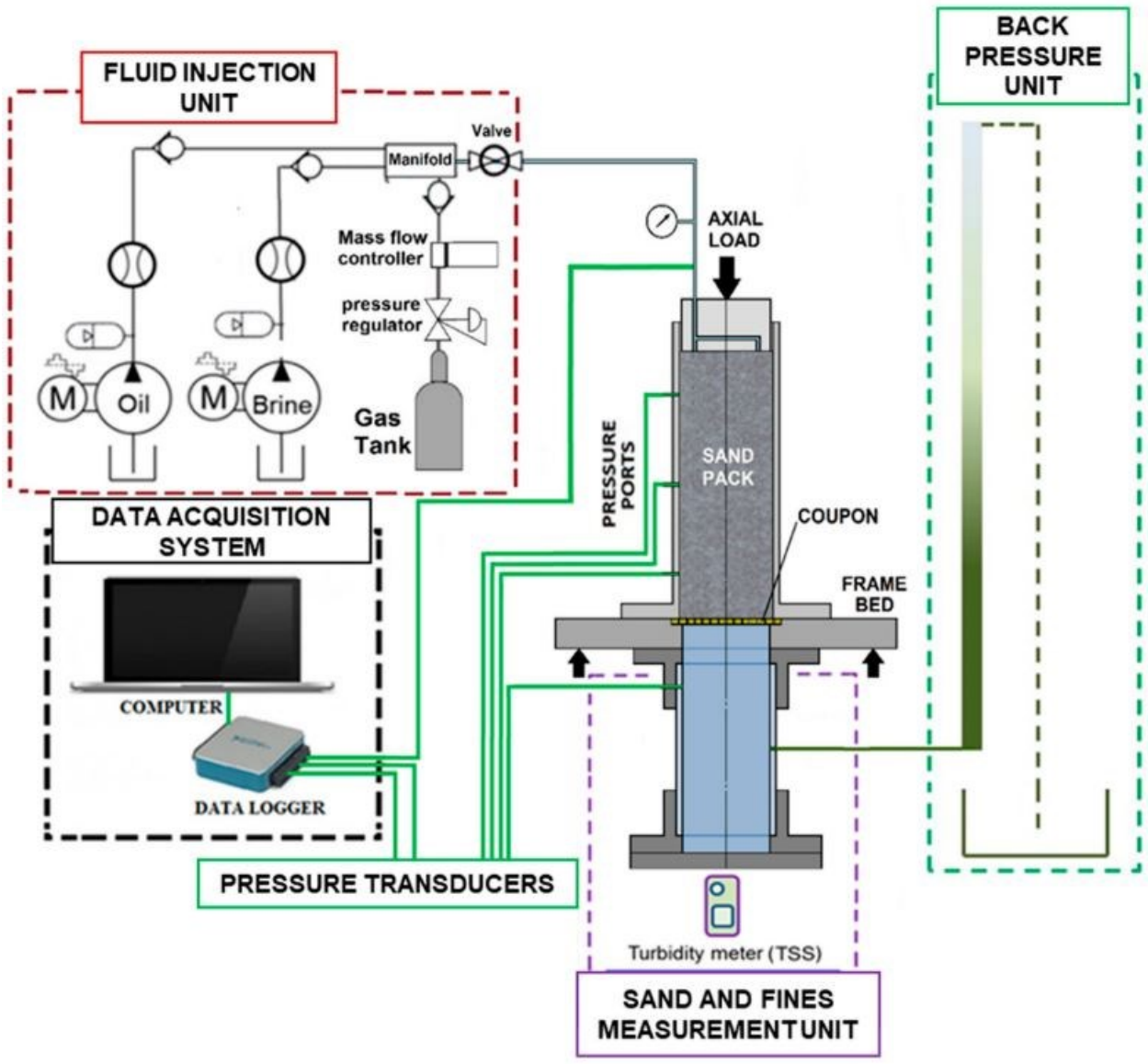

Figure 4.1 Sand Retention Testing Facility (Wang et al., 2020).

Wang et al. (2020) conducted several SRTs to introduce design criteria for three PSDs of the McMurray formation incorporating three slot densities of 30, 42, and 54 SPC (slot per column). The following flow test design **Figure 4.2** was applied to the SRT tests.

Figure 4.2 illustrates the sequential phases of the conducted test, which commence with saturation, followed by the brine's absolute permeability measurement. The subsequent Stages, namely 1, 2, and 3, involve oil injection with a stepwise increment in flow rate, replicating the pre-heat phase of the Steam-Assisted Gravity Drainage (SAGD) process wherein melted bitumen is produced. Subsequently, Stages 4, 5, and 6 simulate a typical SAGD production scenario, wherein condensed

steam is produced alongside the melted bitumen. However, it should be noted that at higher flow rates, certain slots may become plugged, leading to increased liquid velocity in the unplugged slots.

To study the impact of different water cuts, Stages 6, 7, and 8 maintain the same flow rate while varying the water cut. In Stage 8, the retained permeability is measured when 100% brine is injected at the maximum flow rate. This stage provides valuable insights into the influence of water cuts on the overall permeability retention behavior.

In the event of a steam breakthrough, a three-phase condition may arise during the SAGD life cycle. Consequently, Stages 9 and 10 encompass injections of oil, brine, and nitrogen, specifically designed to represent the steam breakthrough scenario. These stages enable the investigation of the system's response under such conditions and offer critical observations regarding its behavior during this phase of the SAGD process.

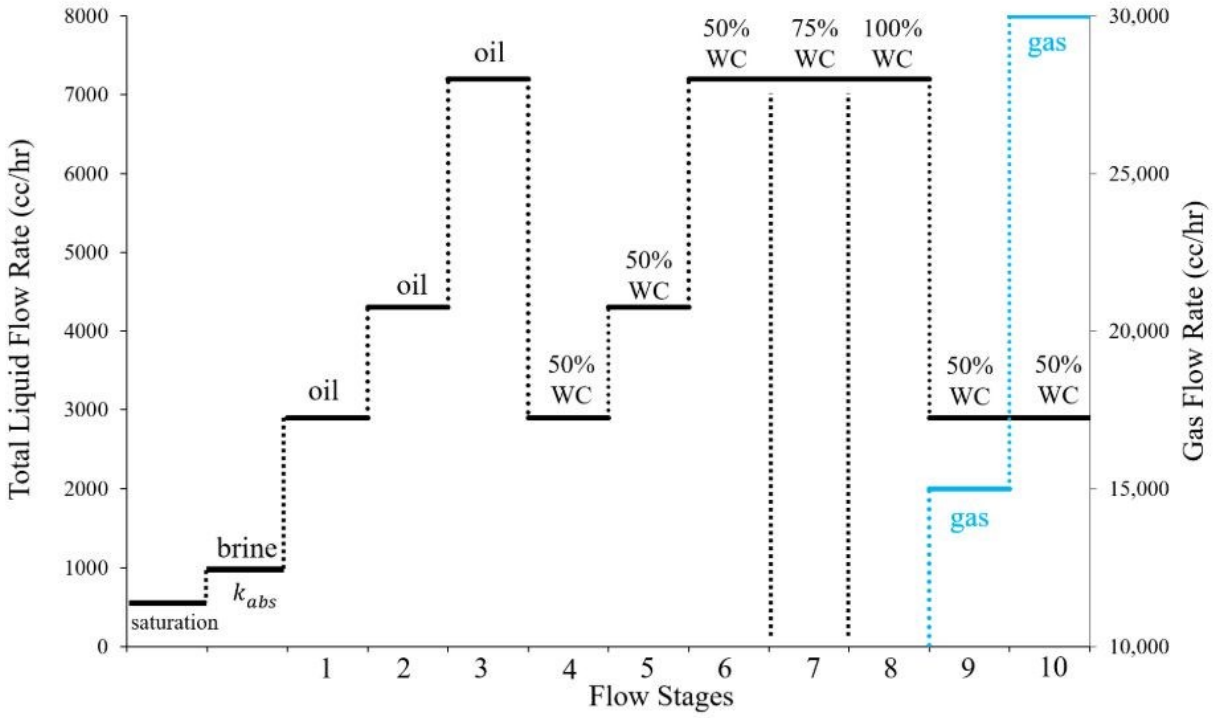

Figure 4.2 The target flow test design (Wang et al., 2020).

4.3.1 Test #1

Test #1 is undertaken to replicate the study conducted by Wang et al. (2020) using the same Sand Retention Test (SRT) facility as depicted in **Figure 4.1**. Additionally, the flow test design, as illustrated in **Figure 4.2**, is adopted, and the focus is on the DC-II PSD of the McMurray formation.

For this experiment, specific aperture size is chosen, amounting to 0.014 inches in slot width with a Slot Perforation Density (SPC) of 42. The selection of this slot size is driven by the objective of achieving a satisfactory range of sand production, namely, less than 0.15 lb/ft^2, while concurrently aiming for a retained permeability of approximately 60%—as derived from comparing the absolute permeability at Stage 8 with the initial absolute permeability. These criteria have been carefully considered to ensure the viability of the experiment and to align with the desired outcomes of the SRT investigation.

4.3.1.1 Test #1 Methodology

The preparation of the sand pack is accomplished through the recommended layer-by-layer wet packing method, comprising thirteen layers, with each layer achieving a targeted porosity of 41%. To facilitate the injection process, a designated flow pattern is utilized as depicted in **Figure 4.2**. However, a significant concern arises due to substantial flow rate fluctuations encountered during each stage, leading to unintended flow velocities within the sample. This issue stems from the sensitivity of the reciprocal pumps to the head and discharge pressure. Despite setting the flow rate at the onset of each stage, it undergoes variations because of fluctuations in the fluid level within the tank and changes in pore pressure within the sand pack.

Throughout the course of the test, it is noted that the axial load experiences fluctuations and fails to maintain a constant value as per the set point of 60 psi. This variation in axial load introduces an element of uncertainty during the testing process, potentially impacting the reliability and consistency of the results obtained. Consequently, these observations warrant careful consideration and necessitate strategies to address the flow rate and axial load fluctuations, ensuring their stability and adherence to the prescribed set points for the successful execution of the experimental procedure.

4.3.1.2 Discrepancies with the Expected Results

In Test #1, it was observed that the quantity of sand production surpassed the targeted test initially conducted by Wang et al. (2020). **Figure 4.3** illustrates the quantity of sand production per surface area for Test #1 across Stages 1 to 10. The red and orange lines represent the acceptable sand production range of 0.11- 0.15 lb/ft^2 for this test. Notably, this range is surpassed during Stages 9 and 10 due to the injection of gas at high flow rates.

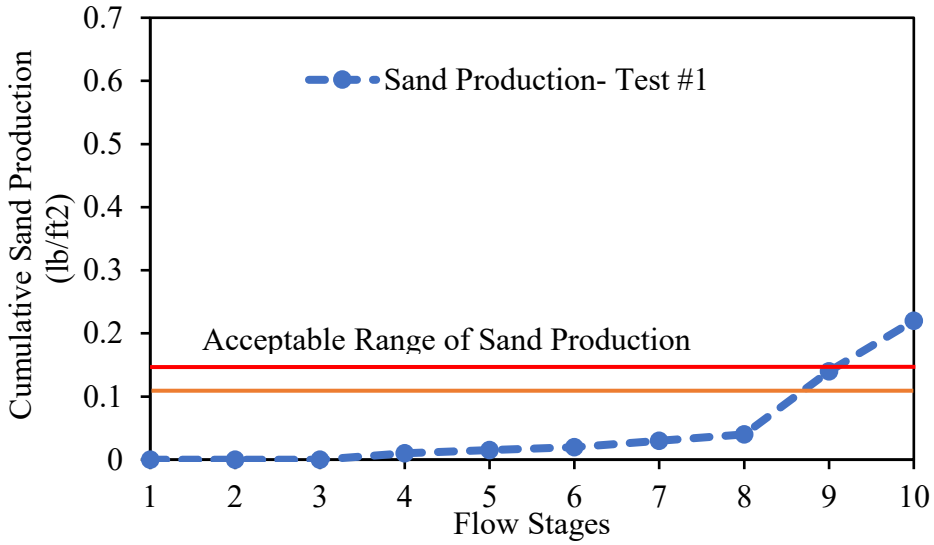

Figure 4.3 Cumulative sand production and the comparison to the acceptable range of sand production- Test #1, large cell SRT.

Moreover, the initial permeabilities measured for different intervals exhibit values lower than anticipated, displaying a variation of more than 100 mD. Surprisingly, the calculation of retained permeability unveils a permeability improvement near the screen zone, contrary to the expected 40% permeability impairment in the near-screen area. Specifically, the permeabilities for the top, middle, and bottom intervals stand at 521, 496, and 245 mD, respectively, as opposed to the target permeability of approximately 2000 mD.

These findings highlight the need for careful examination and assessment of sand production levels and permeability measurements. The observed deviations from expected values call for further investigation and analysis to ascertain the underlying factors influencing the test outcomes and to identify potential measures to address these discrepancies.

4.3.1.3 Lessons Learned from Test #1

Discrepancies in the permeability of each interval within the sand pack raise concerns and prompt consideration of potential contributing factors to these undesirable outcomes. Several plausible reasons are postulated as follows:

- A malfunction or non-calibrated pressure transducer could lead to inaccurate differential pressure measurements, consequently affecting permeability calculations.
- The fluctuating flow rate during the test may result in unintended shocks to the sand pack. A comparison between the targeted flow rate and water cuts, represented by a solid black line in **Figure 4.4**, and the actual values applied in Test #1, depicted by a solid red line, reveals discrepancies in their alignment.

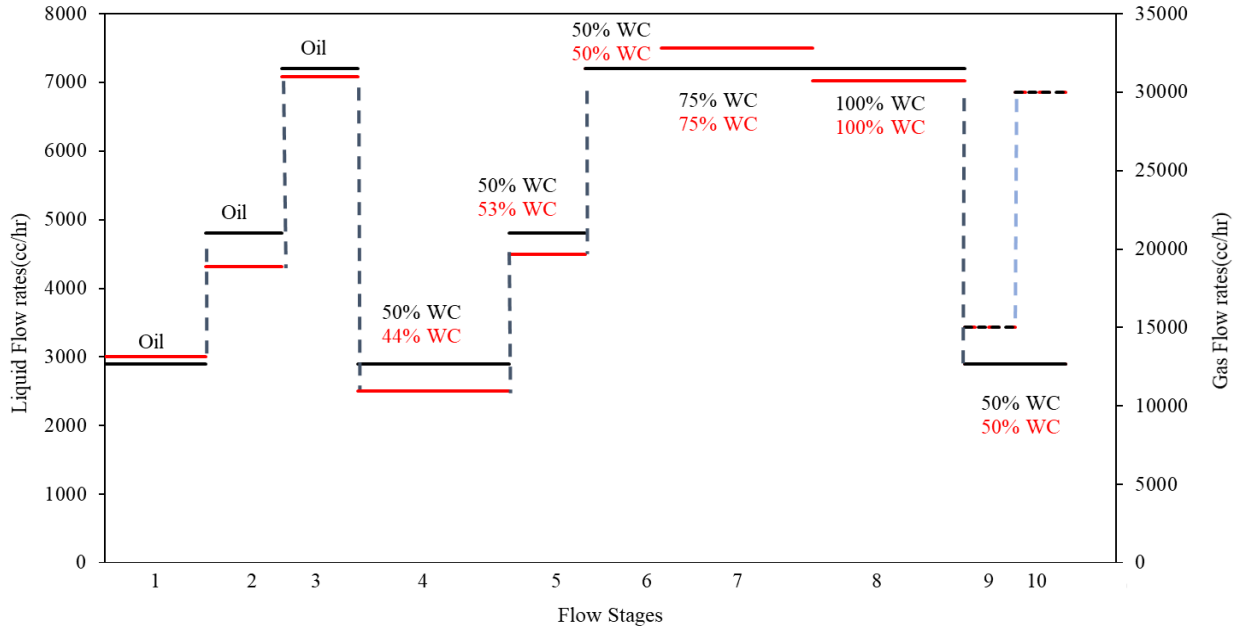

Figure 4.4 Liquid flow injection rate, water cut, flow stages- Test #1, large cell SRT.

- The varying axial load applied during the experiment could impart shocks to the sand pack, potentially influencing the permeability results.
- The employed packing method, designed to achieve uniform porosity for each layer, may inadvertently cause greater compaction in the lower layers, resulting in lower permeabilities compared to the upper layers.

- Notably, the observed rate dependency of permeability suggests that measurements should be conducted at multiple flow rates instead of relying solely on one flow rate for accurate assessments.

Given these potential contributing factors, careful examination and rigorous analysis are essential to elucidate the root causes of the permeability discrepancies. Addressing and rectifying these issues will enhance the reliability and credibility of the test results and facilitate a more comprehensive understanding of the sand pack's behavior under varying conditions.

4.3.2 Test #2

Test #2 introduces several notable modifications compared to the initial test, targeting improvements in various aspects of the experimental setup. Notably, alterations are made to the packing method, with a focus on aligning permeability rather than porosity. Additionally, attention is given to calibrating pressure transducers accurately and maintaining a fixed axial load during the test to enhance precision and reliability.

For Test #2, the sand mixture is meticulously prepared to match the exact composition of Test #1. However, a novel approach is implemented in the packing process, involving the utilization of twelve layers. This adjustment is intended to address potential over-packing effects on the lower layers, to achieve distinct porosities that align with the desired permeability distribution throughout the sand pack.

To enhance the accuracy of permeability measurements, a calculated approach is adopted in Test #2. The initial absolute permeability is determined using data from three distinct points, thereby mitigating errors arising from pressure and flow rate measurements. These refinements enable a more comprehensive assessment of the permeability characteristics within the sand pack. **Table 4.1** presents the initial absolute permeabilities for the top, middle, and bottom sections of the sand pack, along with the corresponding retained permeability, assuming a relative permeability of 0.50 for the brine.

The comprehensive adjustments made in Test #2 signify a concerted effort to address shortcomings identified in the initial test and promote a more robust experimental framework. By placing emphasis on matching permeability, calibrating equipment meticulously, and maintaining stability

in axial load, the study endeavors to enrich the reliability and accuracy of the results, fostering deeper insights into the behavior of the sand pack and its implications for practical applications.

The packing procedure involves specific porosity targets for each layer within the sand pack. The first two layers, located near the screen coupon, are meticulously packed to achieve a porosity of 47%. This porosity value slightly decreases to 46% for the subsequent three intermediate layers. Finally, the uppermost seven layers are set to a porosity of 44%. By adopting this approach, an average porosity of 45% is assumed for the entire sand pack.

Table 4.1 Initial Absolute Permeabilities for Test #2 for the sand pack's top, middle, and bottom intervals.

Sand pack Sections	Top	Middle	Bottom
Initial Absolute Permeabilities (mD)	1960	2387	2771
Retained Permeabilities (mD)	3850	2308	3133

In Test #1, the extent of sand production throughout Stages 1 to 10 is presented in **Figure 4.5**. Observably, the undesired range of sand production is conspicuously evident during Stages 9 and 10. These findings raise concerns about the adequacy of the experimental approach and highlight the need for further investigation and potential refinements to address the observed sand production issues.

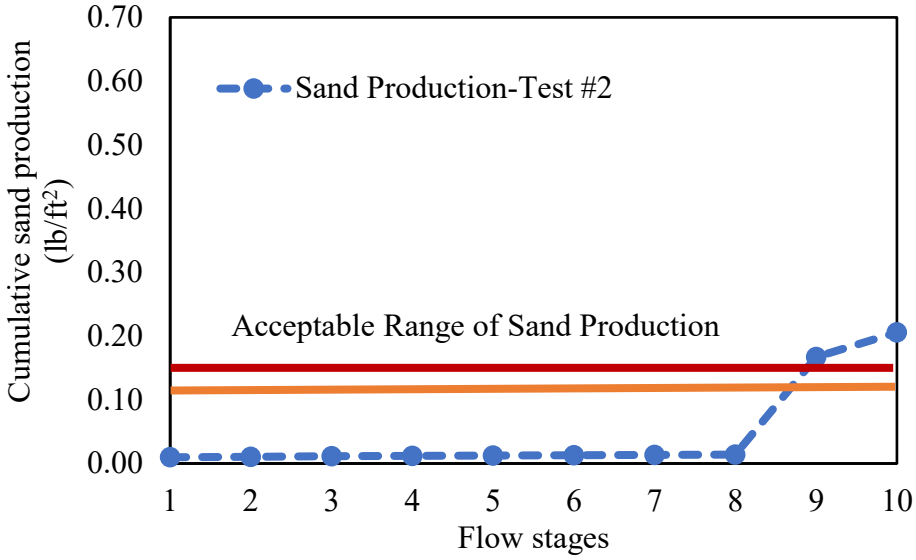

Figure 4.5 Cumulative sand production and the comparison to the acceptable range of sand production- Test #2, large cell SRT.

4.3.3 Test #3

To ensure the credibility and validity of the SRT findings, Test #3 is meticulously undertaken with identical packing, sand mixture, and porosity as Test #2. The same packing method as in Tests #2 is employed in Test #3 results in a homogenous sand pack. Despite both tests exhibiting initial absolute permeabilities of approximately 2000 mD, the outcomes reveal notable disparities in average sand and fines production between the two tests. Consequently, Test #3 fails to replicate the findings of Test #2.

Figure 4.6 portrays the cumulative sand production observed during Stages 1 to 10 in Test #3. Sand production commences from the initial stages and exacerbates during Stages 9 and 10. These observations underscore the significance of identifying and rectifying factors contributing to the undesired sand production phenomenon.

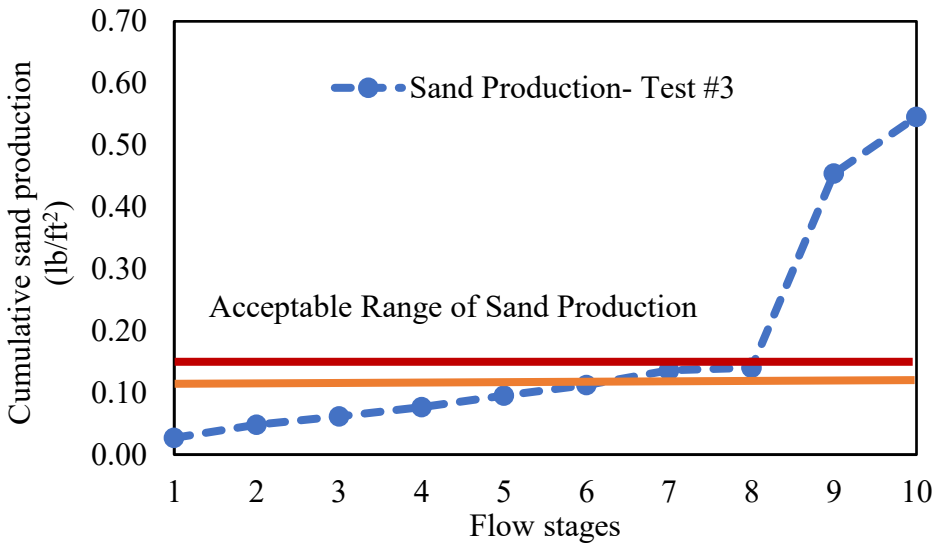

Figure 4.6 Cumulative sand production and the comparison to the acceptable range of sand production- Test #3, large cell SRT.

Test #3 is conducted with heightened precision in monitoring various parameters. Notably, the axial load is diligently fixed to the set point every 2 minutes using the hydraulic pump, ensuring stability during the experiment. Additionally, meticulous attention is given to maintaining constant brine and oil tank levels at each stage by adding the requisite amounts of brine and oil. These measures serve to enhance the accuracy and rigor of the test and facilitate a more comprehensive evaluation of the sand pack behavior.

4.3.4 Test #4

To maintain uniformity and consistency within the sand pack, two samples are extracted during the packing process, and their Particle Size Distributions (PSDs) are analyzed. This step is crucial in ensuring that the PSD remains identical throughout the height of the sand pack. Following the packing approach implemented in Tests #2 and #3, the desired initial absolute permeability of 2000 mD is successfully achieved.

Nonetheless, it is noteworthy that Test #4 demonstrates distinct sanding and fines production characteristics compared to the tests. **Figure 4.7** presents a comprehensive overview of the sand production observed in Test #4. Notably, the results indicate an acceptable range of sand production falling within 0.12 to 0.15 lb/ft^2. These findings imply that Test #4 achieves more

favorable outcomes in terms of sand production compared to Tests #2 and #3, warranting further examination and investigation to ascertain the factors contributing to the observed differences.

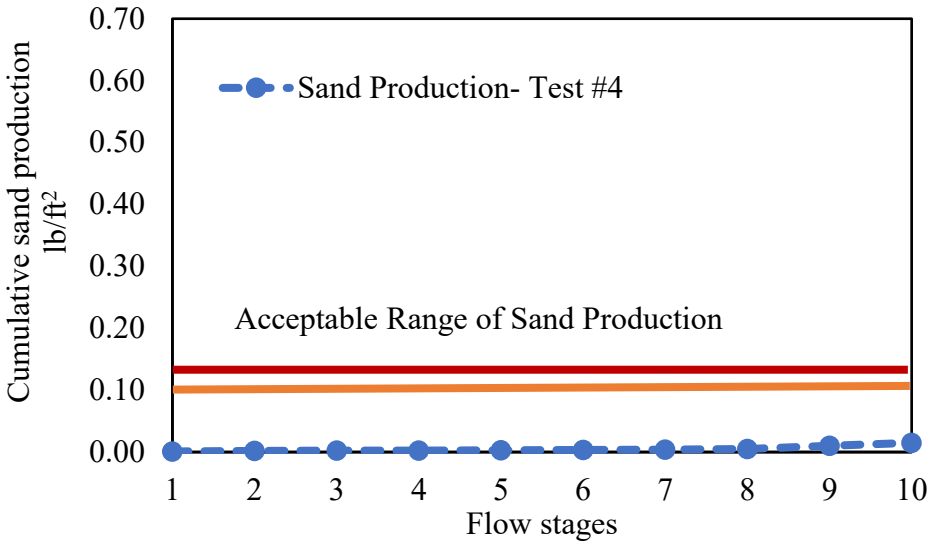

Figure 4.7 Cumulative sand production and the comparison to the acceptable range of sand production- Test #4, large cell SRT.

The observed results can be attributed to several potential factors, which warrant careful consideration and analysis:

- The application of axial load and subsequent unloading during the test may have introduced disruptions within the sand pack, influencing the test outcomes.
- During the saturation stage, the implementation of high flow rates may have led to fines migration and alterations in the matrix structure of the sand pack. The pumps employed in the test are better suited for handling high flow rates, rendering them less accurate when operating at low flow rates, which are essential for a precise saturation of the sand pack without inducing changes.
- The fluctuating flow rate, arising from variations in discharge pressure, presents challenges in maintaining a consistent flow rate throughout each stage of the tests. This fluctuation can contribute to inconsistencies in the experimental results and necessitates careful monitoring and control during the test's duration.

Given these potential reasons, it becomes evident that ensuring meticulous attention to the experimental procedures and control parameters is imperative. This attention is necessary to guarantee the reliability and accuracy of the test results. Addressing these factors may aid in

enhancing the validity of the findings and contribute to a more robust understanding of the sand pack characteristics and its response to varying conditions.

4.3.5 Results and Discussions

A comparative analysis of the four extensive test results reveals a lack of replication among them, indicating the unreliability of the current setup and methodology. **Figure 4.8** presents a visual representation of the injected flow rates in Stages 1 to 10 for all large cell SRT tests, highlighting fluctuations of plus or minus 500 cc/hr in certain stages. Consequently, achieving a constant flow rate throughout the tests proves to be a challenging endeavor. The cumulative injected liquid pore volumes for Tests #1, 2, 3, and 4 are recorded as 16, 15.2, 13.7, and 15.6, respectively.

The absence of replication among these tests underscores the need for a more robust and standardized experimental approach to ensure reliable and consistent results. The observed fluctuations in flow rates raise concerns about the stability and accuracy of the experimental setup, as they significantly impact the overall dynamics of the testing procedure. These findings warrant meticulous scrutiny of the experimental conditions and call for potential refinements in the methodology to attain a more reliable and repeatable experimental framework.

To attain meaningful and conclusive results, the establishment of stringent control measures to address flow rate fluctuations and maintain a consistent flow regime is essential. Furthermore, a comprehensive assessment of the experimental setup, including the calibration of equipment, monitoring of axial loads, and adherence to standardized protocols, is imperative to enhance the reproducibility and validity of the tests. Only through such efforts can the experimental outcomes be rendered reliable, contributing significantly to the advancement of knowledge in the field.

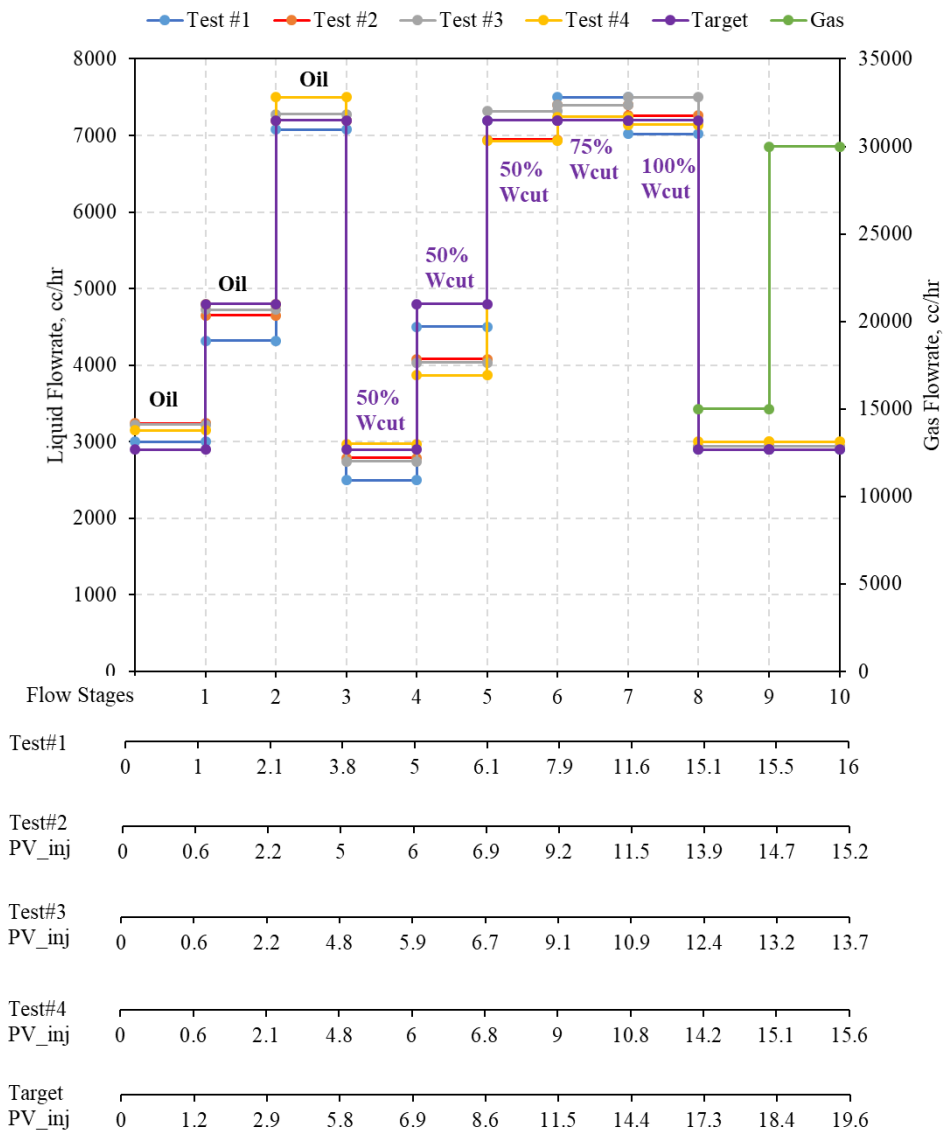

Figure 4.8 Applied flow rates comparison of each stage of Test#1, 2, 3, 4 plus the target flow rates. The amount of injected liquid is shown based on pore volume.

Figure 4.9 provides a comparison of the pressure drop in the near-screen zone for all four large-cell SRT tests. Test #1 exhibits the highest pressure drop throughout the test, primarily attributed to the low porosity of the sand pack utilized in this specific test. In contrast, the other three tests demonstrate lower and relatively comparable pressure drops, with Test #2 and Test #3 exhibiting particularly close values.

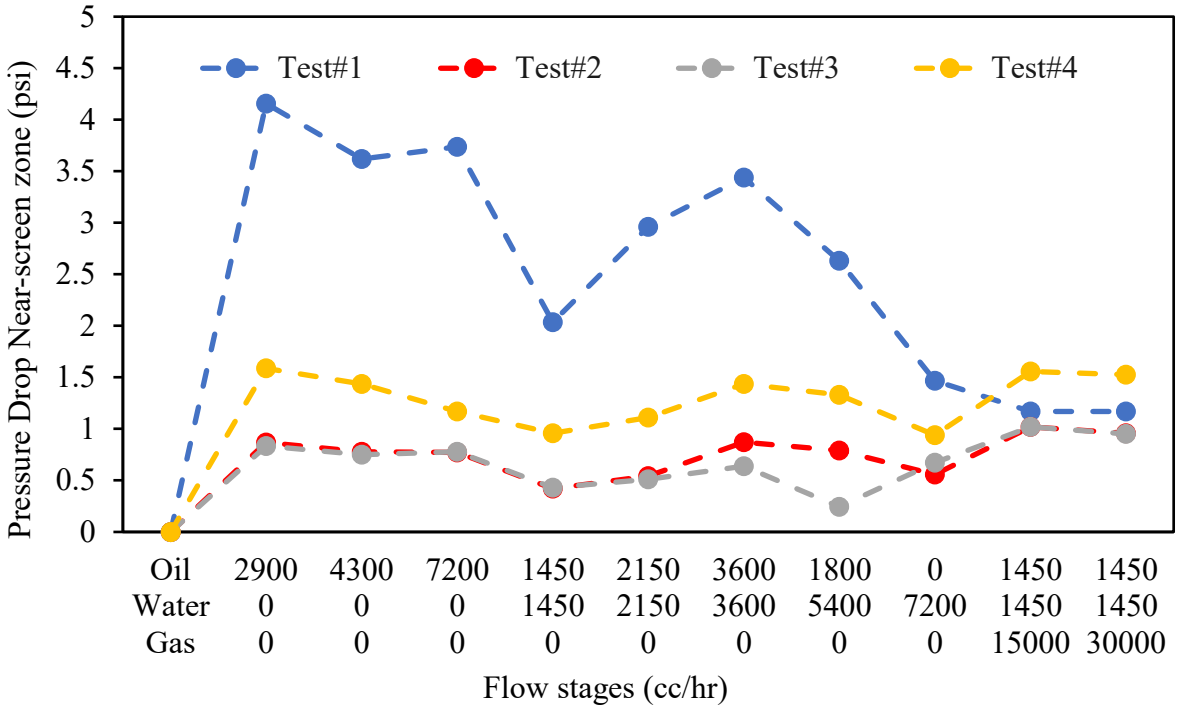

Figure 4.9 Pressure drop comparison near screen zone (2 inches) through Stages 1 to 10 for Tests # 1, 2, 3, and 4.

Focusing on sand production reported in lb/ft^2 of the screen coupon, these four large-cell SRT tests are evaluated against the acceptable range of 0.12 - 0.15 lb/ft^2. **Figure 4.10** indicates that Test #4 most closely aligns with the target test in terms of sand production, while the other three tests manifest unacceptable sand production levels during gas injection in Stages 9 and 10.

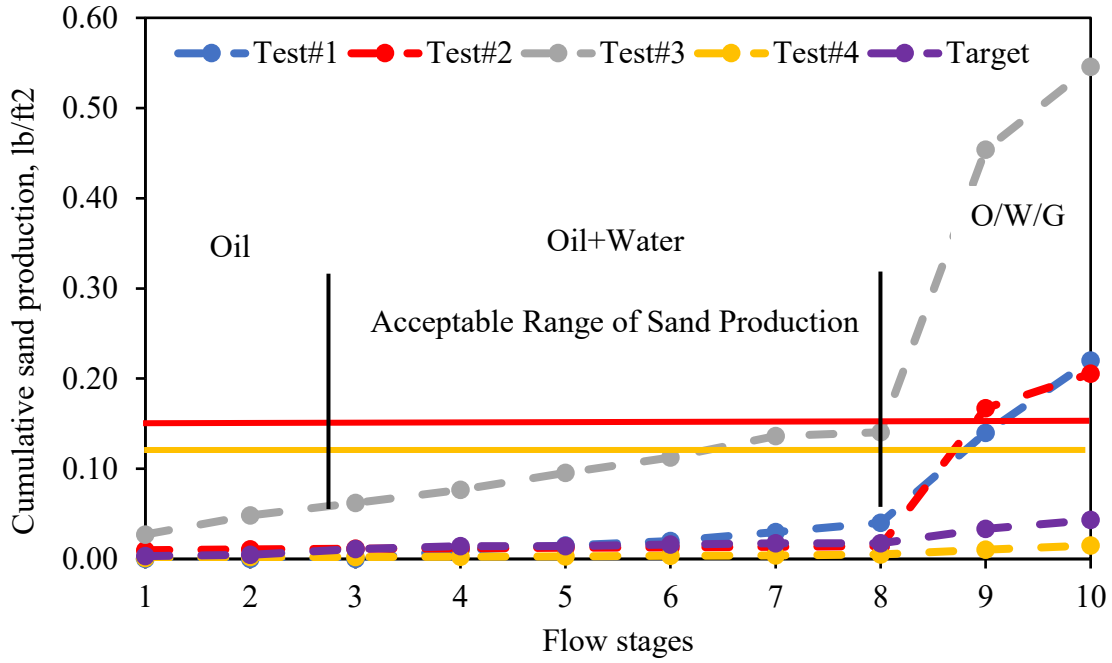

Figure 4.10 Cumulative sand production comparison through Stages 1 to 10 for Test #1, 2, 3, and 4 and the expected target sand production.

Examining produced fines concentration, **Figure 4.11** illustrates the fines concentration observed during each stage across all the large-cell SRT tests. Notably, Test #3 exhibits the highest fines concentration, followed by Test #1, Test #4, and, finally, Test #2.

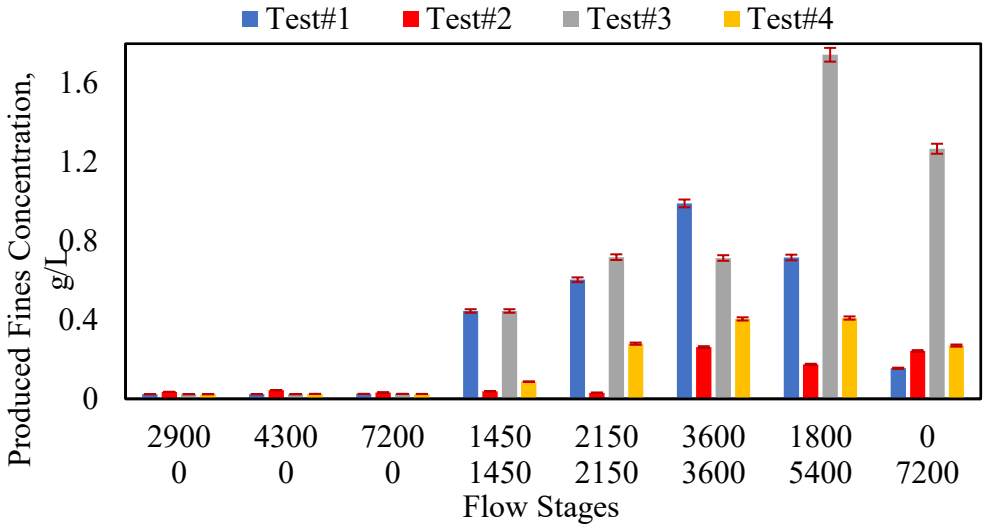

Figure 4.11 Produced fines concentration through Stages 1 to 8 for Test #1, 2, 3, and 4.

The divergent results obtained from these four tests underscore the need for enhancements to achieve repeatable and consistent outcomes. Consequently, several changes are proposed for the forthcoming two tests:

- Installation of a pressure gauge on the top interval of the sand pack to monitor pressure levels.
- Replacement of the axial load's pressure gauge with a pressure gauge featuring a shorter range to measure the desired 60 psi more accurately.
- Comprehensive recording and documentation of test details, including axial load, pump set points, test duration, liquid tank levels, and sand pack pressure.
- Substitution of the large compartment with a small-scale cell to improve sand pack homogeneity and facilitate ease of packing.
- Modification of the methodology and flow test design to achieve a retained permeability of less than 1 in the near-screen zone, thereby representing SAGD conditions.
- Investigation of the effects of changing salinity from high to low levels.
- Installation of a smaller aperture to prevent substantial sanding and enable the study of fines migration.

By implementing these proposed changes, the experimental setup aims to attain more consistent and reliable results, facilitating a deeper understanding of the sand pack behavior and its response to varying conditions.

4.4 Small Cell SRT (Hydrodynamic Effect, Multi-Phase Flow, Salinity Change Effect)

The small SRT setup retains most of the extensive setup facilities, with the notable difference being the reduction in the size of the sand pack cell. The smaller cell adopts a cylindrical aluminum structure measuring 30.5 cm in height and 6.2 cm in width. The cell is filled with sand, reaching a height of approximately 15.5 cm. Subsequently, a mesh is placed on top of the sand, followed by the addition of clean gravel, ensuring a consistent linear flow toward the sand pack.

4.4.1 Test #5

Test #5 marks the initial experimentation conducted using the newly introduced small-cell SRT setup. The primary features are explained below:

4.4.1.1 Packing

The sand mixture is formulated to possess the same composition as employed in other tests. Subsequently, it is meticulously packed in six distinct layers, with the addition of 7000 ppm brine during the mixing process. The two lowermost layers, situated near the screen, are packed to achieve a porosity of 38%, followed by a gradual decrease in porosity to 37% for the two intermediate layers. The final two uppermost layers are packed with a porosity of 36%. The overall average porosity stands at 37%, which serves as a representative value for typical Athabasca oil sand reservoirs.

Table 4.2 Sand pack specification for small-cell SRT, Test #5.

Sand pack specifications	
Diameter, cm	6.2
h, cm	15.5
Bulk Volume, cc	481
Pore Volume, cc	181
Grains Specific Gravity	2.65
Added water, wt%	10%

4.4.1.2 Pressure Transducers

To ensure accurate differential pressure readings, three pressure transducers have undergone calibration. For the low range, calibration was performed using a manometer with a precision of 0.014 psi. Conversely, for the higher range, a FRUKE calibrator was utilized. The inclusion of a manometer for the low ranges notably improves the precision of differential pressure readings at the lower flow rates, which are crucial for calculating permeability.

The subsequent **Figure 4.12** provides a visual representation of the sand pack's top, middle, and bottom sections within the cell. The overall length of the cell spans 30.5 cm, with the sand pack occupying a length of 15.5 cm. The remaining portion of the cell is filled with clean gravel and topped by the upper platen to complete the setup.

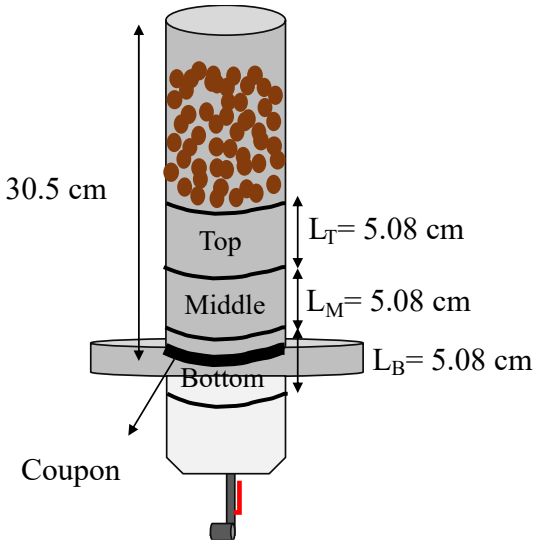

Figure 4.12 Schematic of the small cell including different intervals of top, middle, and bottom.

4.4.1.3 Axial load

The application of the axial load to the upper platen on top of the cell serves the purpose of preventing fluidization. To maintain a consistent axial load, a manual hydraulic pump is employed. However, observation reveals that hydraulic oil is being released and leaked during the test, resulting in a gradual decrease in the axial load to zero psi.

To address this issue, a needle valve is strategically installed along the hydraulic oil pathway. Once the axial load is set at 60 psi, the needle valve is closed, effectively mitigating the problem of load and unload stress. This measure ensures that the sand pack does not undergo unintended stresses caused by repetitive adjustments to the axial load during the test and provide a more stable and controlled experimental environment.

4.4.1.4 Flow Test Design Test#5

Figure 4.13 presents a comprehensive overview of various measured and calculated parameters in Test #5, alongside their corresponding target values. Thirteen stages are displayed, including total fluid flow rate, cumulative injected pore volume, injection time, water cut, and brine salinity. The target values for water cut are achieved with a minor 2% deviation in Test #5. The flow rates depicted on the plot represent the set values after adjusting the flow rate in each stage, and although fluctuations occur in most stages, for simplicity, we have omitted their depiction.

Stage A, designed for saturation, aims to have a 50 cc/hr flow rate of 7000 ppm brine from bottom to top. However, in Test #5, this objective is not fully met due to the pump's working range or capacity limitation. The minimum pumpable amount from bottom to top with this pump capacity is 360 cc/hr.

Stage B, known as K_{abs}, involves injecting 7000-ppm brine from the top of the sand pack at three different flow rates: 150, 180, and 210 cc/hr, each for a duration of 10 minutes to determine the absolute permeability. In Stage C (displacement stage), the target flow rate is 200 cc/hr for single-phase oil, whereas Test #5 exhibits an actual oil flow rate of 300 cc/hr.

Across the ten stages starting from Stage 1, the flow rates generally stay within ± 10% of the designed flow rate, except for Stage 5, where it decreases further to -12.8%. Nevertheless, the overall error range remains acceptable for these stages. Notably, Stage A demonstrates the highest flow rate error in Test #5, as the flow rate is approximately six times higher than the intended rate. Additionally, Stage C shows a flow rate error of +50%.

Regarding salinity, Test #5 maintains a salinity of 7000 ppm from Stage A to Stage 8, which subsequently decreases to 400 ppm in Stages 9 and 10. These latter stages reflect a scenario observed in a SAGD process, wherein low salinity steam condensate is produced alongside high salinity formation water and oil.

The total injected pore volume is approximately 190, and the test duration spans 53.16 hours for Test #5.

While Stage B involves three different flow rates applied to the sand pack, **Figure 4.13** displays only the most significant value. Stage 8, however, experienced multiple flow rates towards the end to calculate permeability, with only the dominant, sustained flow rate being illustrated in the figure.

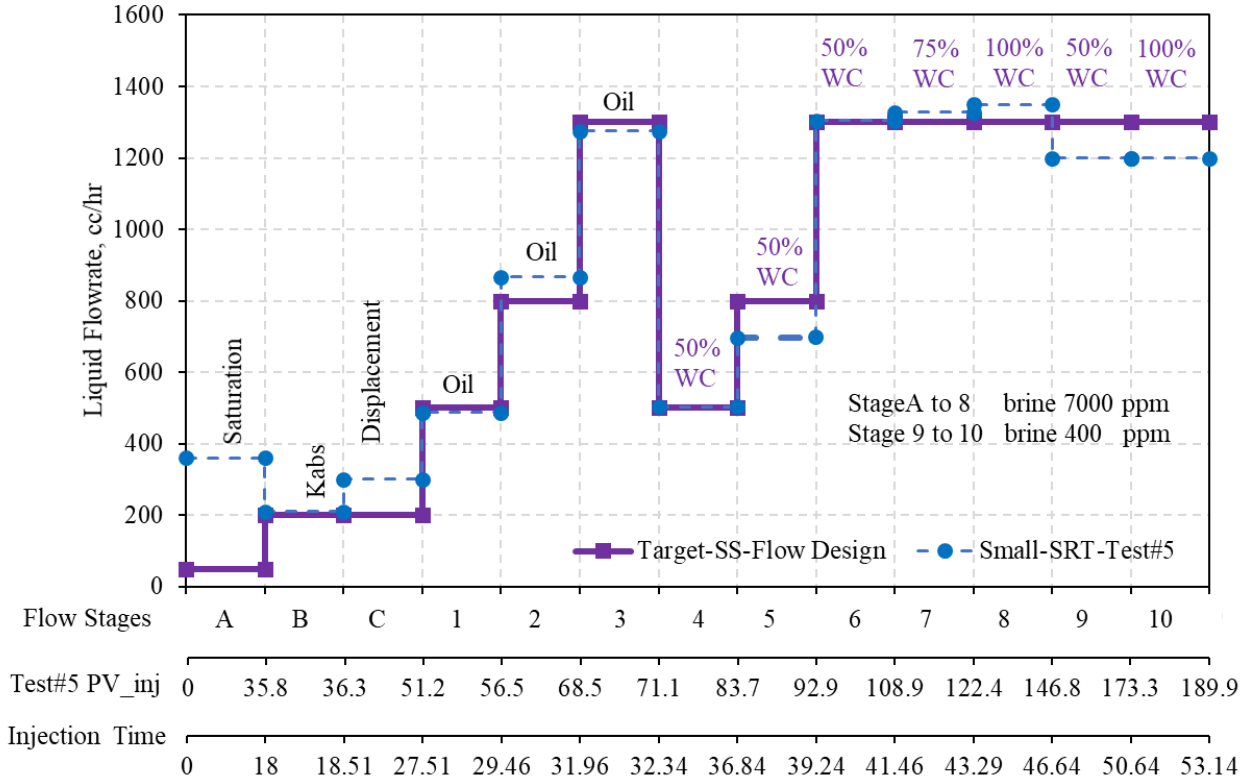

Figure 4.13 The target experiment design versus the applied flow rates in Test #5.

4.4.1.5 Differential Pressures Test #5

Figure 4.14 presents the pressure profile recorded by three differential pressure transducers at three positions (top, middle, and bottom) of the sand pack. The profile spans from the beginning of Stage B (K_{abs} measurement stage) to the completion of Stage 10. The initial three gray lines represent 150, 180, and 210 cc/hr 7000 ppm brine injections in Stage B, each lasting for 30 minutes. Stage C, the displacement stage, takes approximately 9 hours to ensure that S_{wirr} (irreducible water saturation) is reached. During this stage, the entire sand pack's differential pressure rises with oil injection to displace the brine, followed by a rapid decrease before reaching a plateau, indicating irreducible water saturation.

In Stages 1, 2, and 3, where single-phase oil is injected, the differential pressure (DP) increases with the flow rate. Towards the end of Stage 2, the DP of the middle section becomes lower than that of the top section, while the top section shows a minimal increase in DP during this period.

Moving to Stage 4, the injection of two-phase flow rates further increases DP in all sections. However, the gap between the middle and top sections widens. The reason for this phenomenon requires further investigation.

In Stage 5, with a constant 50% water cut and increased flow rate, the top and middle DP values increase, while the bottom section's DP decreases. Stage 6 exhibits higher DP in the top, middle, and bottom sections, respectively. This pattern remains consistent through Stages 7 and 8, but the DP values for all three areas decrease as the flow rate remains constant while the water cut increases from 50% to 100%. The lower DP indicates higher permeability, suggesting that increasing the water cut leads to increased production of fines, resulting in higher permeability.

Stage 9 introduces a 50% low salinity (400 ppm) brine to the sand pack, causing an abrupt increase in DP for all three sections. However, due to the pressure transducer's limitations, this rise in DP is not recorded for the middle and bottom sections. Subsequently, the DP value in the top area gradually decreases, while the middle and bottom regions experience an increase. This might be due to the fines production from the top section and their migration and plugging in the middle and bottom regions.

Finally, in Stage 10, while other parameters remain constant, increasing the water cut leads to a further decrease in DP in the top section, indicating higher fine production and permeability. However, no recorded data is available for the middle and bottom sections during this stage.

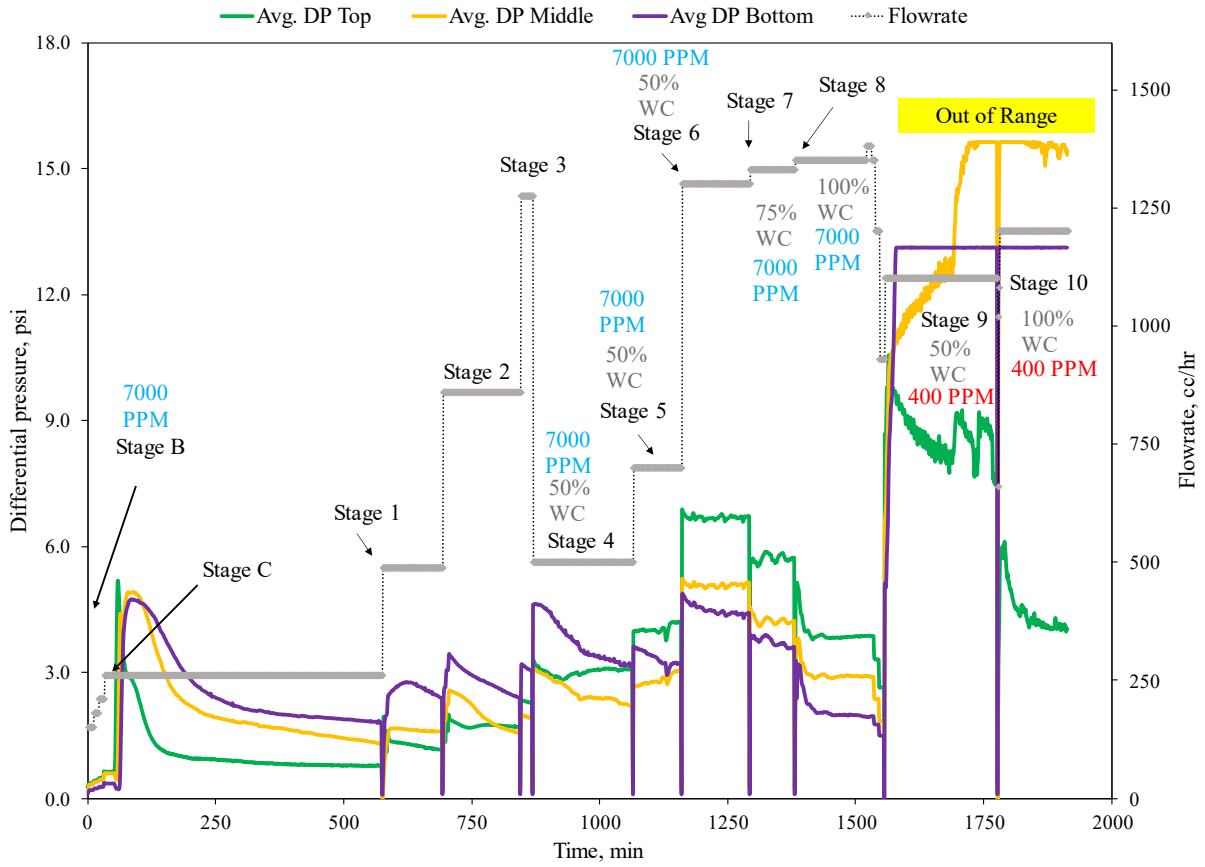

Figure 4.14 Recorded differential pressure and the injected flow rates through Stages B to 10, Test #5.

4.4.1.6 Fines Concentration Test #5

Figure 4.15 illustrates the collected produced fine particle data at five-minute intervals from the sampling valve during each stage. Since the fine particles concentration during Stages 4 to 6 is negligible, the plot starts from Stage 6 and continues until the end of the test.

Throughout the stages, the flow rate remains constant with a variation of ±10%. From Stage 6 to 8, as the water cut increases from 50% to 100%, a peak appears at the beginning of Stage 8, indicating the onset of fines migration. Subsequently, the fines concentration decreases and stabilizes. This pattern is also observed at the start of Stages 9 and 10.

At Stage 9, there is a change in salinity from 7000 to 400 ppm, accompanied by a decrease in water cut compared to Stage 8. This leads to a significant rise in fine concentration, evident by three peaks in Stage 9 that gradually diminish over time, taking more than an hour to stabilize.

In Stage 10, the increase in water cut results in a prominent peak at the beginning. The concentration then stabilizes before experiencing fluctuations later, possibly caused by flow rate instability.

In summary, increasing the water cut (carrier phase) leads to a peak in produced fine concentration at the beginning of each stage, likely due to the mobilization of previously unattached fines. Additionally, the change in salinity from high to low affects the migration and production of fines. These observations contribute to a better understanding of the fines migration and production in the sand pack under varying test conditions.

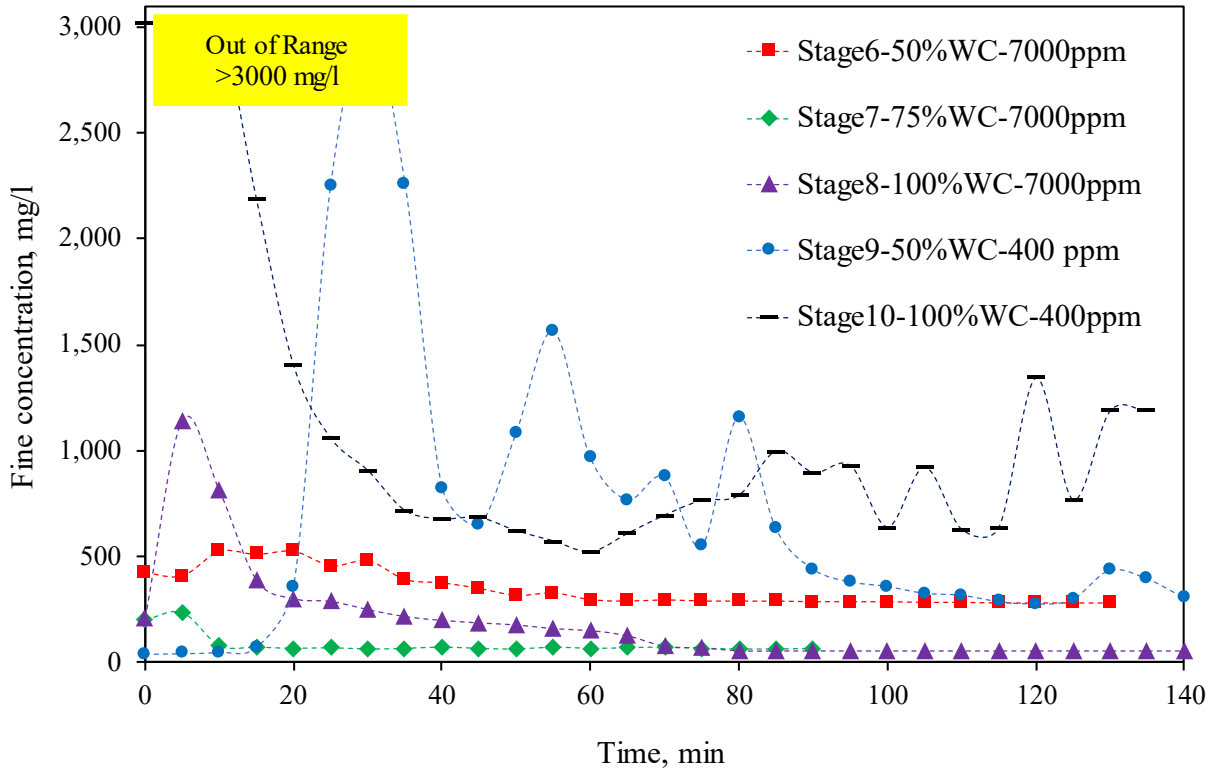

Figure 4.15 The fines concentration through Stages 6 to 10, Test #5.

4.4.2 Test #6

Test #6 is designed with various improvements to simulate the SAGD conditions more effectively. Specifically, it aims to replicate the scenario where high saline formation water becomes mixed and produced alongside the oil and condensed steam. The subsequent section provides a comprehensive description of the flow test design implemented in Test #6.

4.4.2.1 Flow Test Design Test #6

Figure 4.16 presents a comparison between the applied small SRT liquid flow rates and the designed liquid flow design. Notably, considerable disparities are observed during the saturation stage (Stage A), where the applied flow rate exceeds the planned rate by more than eightfold. Similarly, in Stages B and C, the differences amount to approximately 1.5 and 2 times, respectively, compared to the intended values. However, for the subsequent stages, the deviations are minimal, staying below 10%. These discrepancies in the flow rates can be attributed to the pump's capacity, which is limited to 25 liters per hour and not well-suited for low flow rates, such as those in Stages A to C.

Furthermore, the figure depicts the saturation of the sand pack with high salinity brine during Stage A, followed by Stage B with the same salinity. However, from Stage 4 onwards, the salinity decreases to a lower value and remains constant until the test's completion. It is noteworthy that the figure only shows Stages A to 5, whereas originally, Test #2 was planned to cover Stages A to 8. The reason for this alteration is the pressure transducer's range, which spans from 0 to 50 psi. Consequently, during Stage 4, as the salinity changes from high to low, the differential pressure rises significantly and exceeds the transducer's range. As a result, Test #2 was concluded after Stage 5.

The plot features three horizontal axes. The first axis represents the stages, the second axis (Test #6 PV_inj) displays the cumulative amount of injected pore volume at the end of each stage, and the third axis indicates the cumulative time spent on each stage. This test comprises five stages, spanning approximately 40 hours, during which 107 pore volume of liquid is injected.

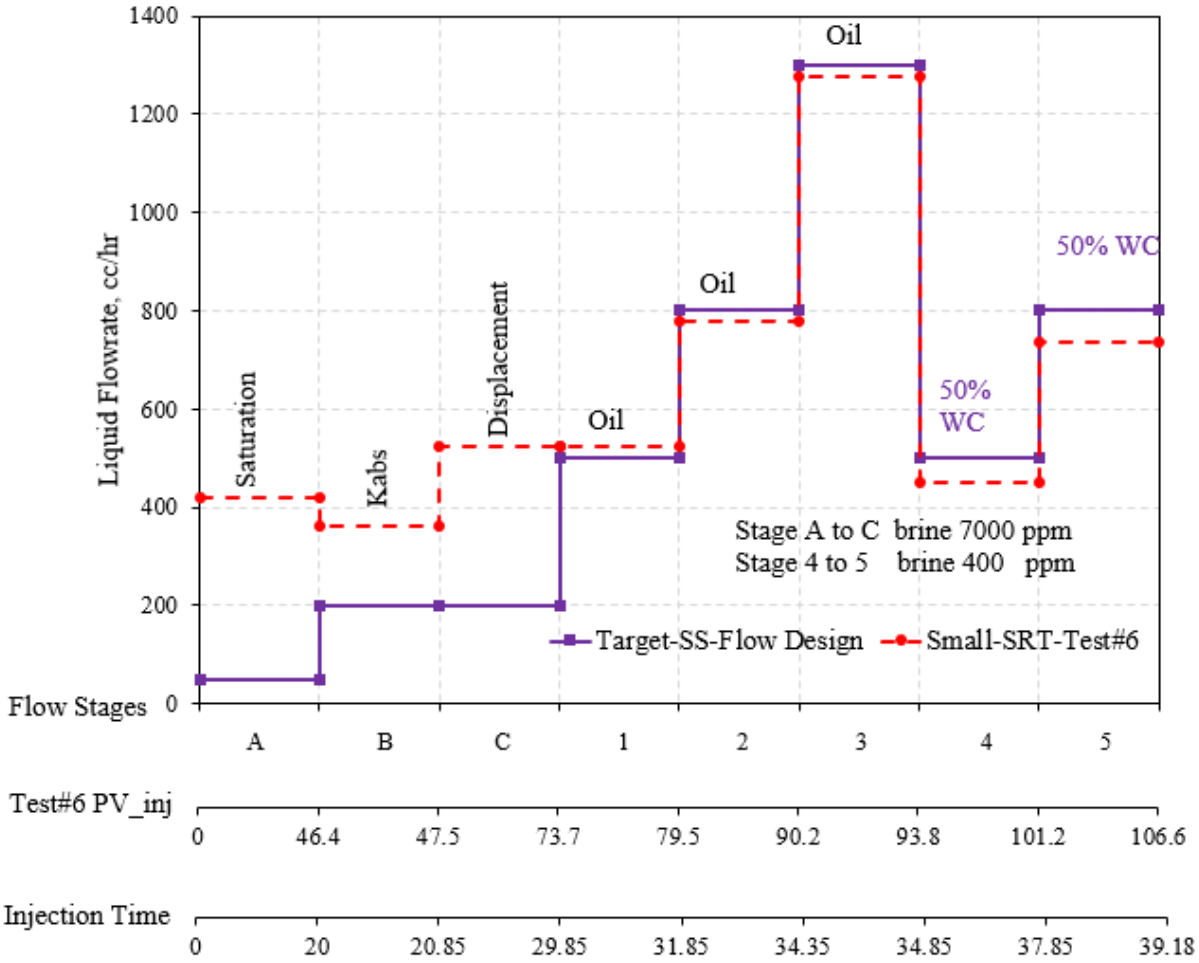

Figure 4.16 The target experiment design versus the applied flow rates in Test #6.

4.4.2.2 Differential Pressures Test #6

The differential pressure measurements near the screen zone exhibit a continuous and substantial increase, with the pressure gauge on top of the sample indicating a high pressure of 150 psi during Stage 5. This stage involves the injection of a 50% water cut, 400 ppm brine, and oil into the sand pack at a total flow rate of 13 cc/min. **Figure 4.17** displays the differential pressure values across the top, middle, and bottom sections of the sand pack, along with the applied flow rates, water cut, and salinity for each stage.

The initial absolute permeability measurement is conducted in Stage B, where brine is injected into the sand pack at five different flow rates. This process aims to determine the initial absolute permeability using Darcy's law. The results indicate a stepwise rise in differential pressure with an increase in flow rate; higher flow rates lead to greater differential pressure. Additionally, the

bottom, middle, and top sections exhibit the highest differential pressures, respectively. Elevated differential pressure may indicate lower permeability, with the middle section displaying the most permeability and the bottom section showing the lowest permeability within the sand pack.

When oil is injected to displace brine in Stage C, the differential pressure experiences an initial sharp rise across all three sections, followed by a gradual decrease before stabilizing at 600 minutes. The sharp peak in differential pressure probably marks the point at which the oil path finds its way out of the sand pack, after which the oil continues to displace more brine until it stabilizes and reaches irreducible water saturation. Stage C stabilizes at a higher differential pressure than Stage B, suggesting that the new liquid (oil) is more viscous than the previous (brine) fluid, thereby causing higher differential pressure.

During Stage 1, the lowest single-phase oil injection results in higher differential pressure than Stage C due to the higher flow rate. Stage 2, with a further increase in flow rate, results in higher differential pressure in the middle and bottom sections, while the differential pressure in the top section decreases to half of that observed in Stage 1. This observation needs further study to reveal the root causes. However, it might be explained by fines migration from the top section, which subsequently becoming trapped in the middle and bottom sections, leading to higher differential pressures in these regions.

At Stage 3, with a further rise in oil flow rates, the differential pressure increases across all three sections. Stage 4 involves the injection of a two-phase flow with a 50% water cut, 400 ppm brine, and the lowest flow rate of oil and brine, followed by a subsequent increase in flow rate while maintaining other parameters constant in Stage 5. A significant increase in differential pressure across all three sections is observed in Stage 4 due to the change in salinity from high to low, which destabilizes the sand pack, displaces existing fines, and reduces permeability. In Stage 5, the differential pressure increases further, with the bottom sections showing the most significant increase, exceeding the pressure transducers' range of 50 psi. However, the top and middle sections exhibit a gradual decrease in differential pressure after experiencing a peak at the beginning of Stage 5, indicating fines movement and an increase in permeability in these sections. Test #6 was stopped in the middle of Stage 5 after 20 hours due to the high pressure. The pressure transducers are limited to measuring a maximum differential pressure of 15 psi, rendering further continuation of the test futile.

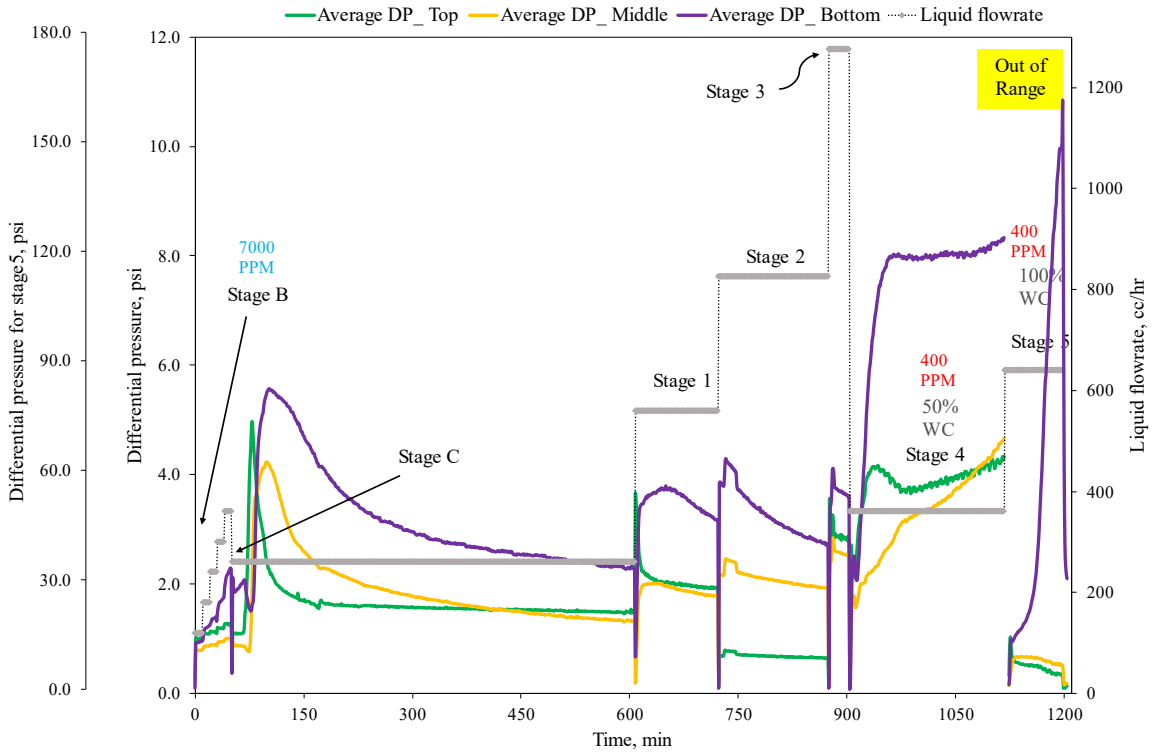

Figure 4.17 Recorded differential pressure and the injected flow rates through Stages B to 5, Test #6.

4.4.2.3 Fines Concentration Test #6

Figure 4.18 presents the produced fines concentration in mg/l during Stages 4 and 5 of Test #6. The mentioned value exhibits a gradual increase during Stage 4, reaching a peak that persists for approximately 50 minutes before gradually declining and eventually stabilizing at a plateau.

Comparing **Figure 4.17** (The DP) with the subsequent plot (**Figure 4.18**), it is evident that the peak amount of differential pressure (DP) coincides with the peak of produced fines concentration. This alignment indicates that when the two-phase fluid front reaches the outlet, the maximum concentration of produced fines is achieved, which then gradually diminishes alongside the reduction in DP. The produced fines concentration rises significantly, exceeding the full measurement range of the Turbidimeter device (1000 NTU), rendering it unmeasurable until the conclusion of the test.

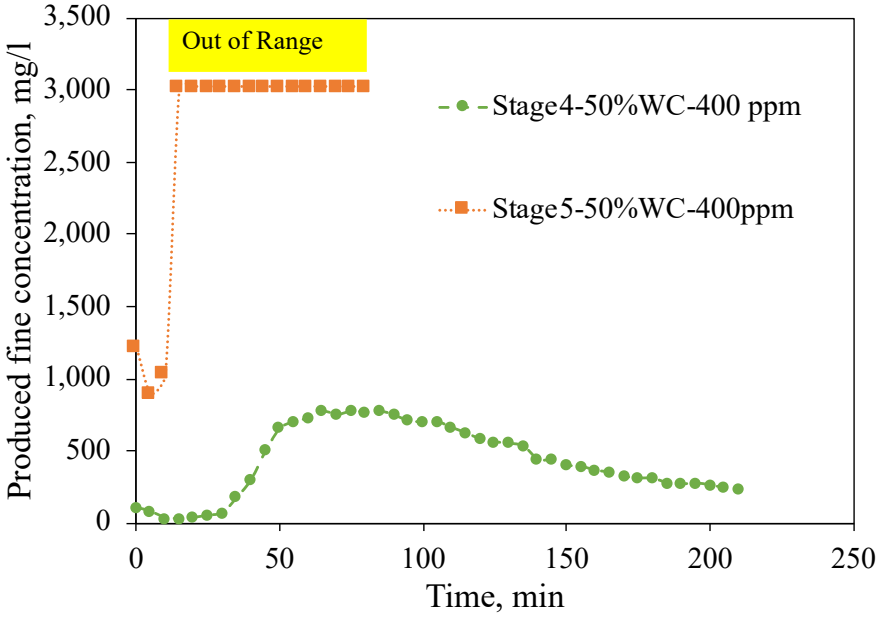

Figure 4.18 The fines concentration through Stages 4 to 5, Test #6.

Post-mortem results reveal an increase in the fines content of the sand pack after the test. Several potential reasons are considered for this discrepancy:

- The packing method utilized during the test is rigorous, leading to the crushing of some pointy grains and generating more fines in the sand pack.
- The saturation process, initiated from the bottom to the top of the sand pack, could result in detached, smaller particles moving towards the top section when flowing with brine for the first time. The pump's inability to deliver at a suitable rate may contribute to this phenomenon.
- The gravel used in the test might be contaminated from a previous experiment, or the application of axial load could crush the pointy parts of the gravel, generating additional fine particles.

4.4.3 Lessons Learned and Conclusions

- Small SRT cell provides the benefit of using the lower capacity but high accuracy pumps of ISCO pump. ISCO pump delivers the desired low flow rate of 2 cc/min during the saturation and does not compromise the sand pack. Furthermore, the flow rate is constant and independent of head and discharge pressure.

- The pressure transducers are limited to up to 15 psi measurements. The sample 6 inches high is replaced by 4 inches high to reduce the source of fines production and prevent plugging.
- The slotted liner coupon of 0.010” with 42 SPC should be replaced by a stainless steel one with 0.012” and 54 SPC. The next size is chosen as the 0.012” stainless steel coupon is unavailable in the lab (0.013” and 54 SPC).
- The methodology and flow test design for the following two tests are changed to better replicate the SAGD well condition.
- A higher accuracy is achieved when applying the same flow rates for Stage B (Saturation) and Stage D (retained permeability measurement). Chapter 6 thoroughly explains the last two tests, Test #7 (mentioned as Test #1 in Chapter 6) and Test #8 (reported as Test #2 in Chapter 6).

4.5 Summary

In this chapter, six SRTs were employed to assess the testing methodology's effectiveness and repeatability. The SRTs comprise two distinct cells: a larger cell and a smaller scale cell. While four tests were conducted using the larger cell, the obtained results indicated a retained permeability greater than 1, which deviates from the conditions observed in an actual SAGD process.

To enhance the accuracy of the outcomes, each test underwent refinements concerning the homogenization of the sand pack, maintenance of a constant flow rate, and application of axial loads. Despite these improvements, the results remained inconclusive. Consequently, the adoption of the smaller scale cell for SRTs proved essential in mitigating flow and packing errors.

Through the implementation of two tests in the smaller cell, conditions closely resembling those in an actual SAGD operation were successfully achieved. These conditions included a retained permeability of less than one, alongside consistent flow rates and axial loads. As a result of these advancements, the final two tests were designed and executed, and their specific details can be found in Chapter 6.

5 Calibration and Improvements

5.2 Introduction

This chapter presents the enhancements made to the Sand Retention Test (SRT) setup, aiming to achieve improved precision and reproducibility of results. By addressing limitations identified in the previous configuration, the current SRT facility provides a more robust platform for studying sand retention and production phenomena in porous media. Calibration procedures and meticulous testing have fine-tuned the setup, reducing uncertainties and errors in key parameters, and increasing the confidence in obtained results. These improvements lay the foundation for comprehensive studies, facilitating a deeper understanding of fluid flow behavior and sand retention mechanisms in subsurface reservoirs.

5.3 Previous SRT Setup

The previous SRT setup comprised a metal cell with dimensions of 17.1 cm in diameter and 47 cm in height, capable of holding 13 kg of sand. Brine and oil injection were performed using a pair of hydraulically actuated diaphragm triplex metering pumps, specifically the LEWA ecodos® ESC 0006-13 model. These pumps had a flow rate capacity of twenty-five liters per hour at a pressure of 50 psi. To regulate the flow rate, a variable frequency drive was connected to the pumps. Additionally, two reservoirs with a capacity of forty liters each were employed for storing brine and oil. Precise injection flow rates were determined using two weight balances, the ULINE Deluxe Counting Scale H-5822, with a precision of ±1g. The weight loss observed in the reservoirs was then converted into corresponding injection flow rates (Wang, 2019). A loading frame was designed to apply 60 psi on top of the sand pack, preventing fluidization.

5.4 Current SRT Facility

A total of eight tests have been conducted to achieve reliable and repeatable results. With each test, the accuracy of the results became more evident. The subsequent sections describe the quality improvements made to the tests and, consequently, the results.

5.4.1 Permeability Measurement

Accurate measurement and recording of relevant parameters are crucial for determining the permeability of the porous medium using Darcy's equation. These parameters include the

differential pressure at the inlet and outlet, the injection flow rate, fluid viscosity, sand pack length, and the surface area of the porous medium perpendicular to the injection direction.

5.4.1.1 Syringe Pump

To enhance accuracy, syringe pumps were introduced to replace the reciprocating pumps commonly used in laboratory experiments. Syringe pumps offer advantages, including high accuracy, repeatability, and the ability to deliver fluids at extremely low flow rates. This change increased the flow rate precision to within 0.3% of the set point.

The previous pumps' limitations, such as fluctuating flow rates, dependency on fluid levels in the tank, and shock to the sand pack, were addressed by using Three ISCO pumps. One pump is designated for brine, another for oil, and the third as a backup, effectively resolving the issues.

5.4.1.2 Manometer & Pressure Transducer Calibration

Pressure transducers play a critical role in measuring permeability. The use of DPharp EJX110A pressure transducers by Yokogawa was prevalent in both previous and current studies. However, the range of these pressure transducers is 0-15 psi, with an accuracy of ± 0.00375 psi.

In the current study, the FLUKE pressure calibrator was employed to calibrate the pressure transducers, reducing the reading error margin from 0.0375 psi to 0.15 psi. This addressed the issue of high error in pressure reading, especially at low flow rates, ensuring more accurate permeability measurements. The pressure transducers undergo calibration through a manometer with a precision of 0.001 psi, specifically for low pressure ranges spanning from 0 to 0.15 psi.

5.4.1.3 Multiple Points

To enhance accuracy, the current study utilized at least three points to measure the permeability of the sand pack, determining the slope of the linear line passing through these points. This approach offset errors in differential pressure and flow rate measurements during permeability determination. Moreover, the flow rates employed for assessing the retained permeability remained consistent with those used for determining the initial permeability.

5.4.1.4 Axial load

To maintain sand pack stability during testing and prevent fluidization, an axial load was applied in the SRT test. A hydraulic pump and pressure gauge were used to apply and monitor the axial

load. However, the previous practice of releasing and reapplying the hydraulic oil pressure every five minutes caused shocks to the sand pack, affecting sand and fines production, and preventing the study of other influential factors. To resolve this issue, a needle valve was introduced to stabilize the hydraulic pressure throughout the test, effectively eliminating the shocks and ensuring consistent results.

5.5 Methodology

The existing Standard Operating Procedure (SOP) for performing the SRT underwent improvements, ensuring repeatability with minimal deviations in results. Post-mortem analysis of sand pack samples was optimized by ensuring complete dryness before analysis. Specific time intervals were designated for the washing process, and a turbidimeter was employed to measure cloudiness, enabling continuous washing until the desired clarity was achieved.

5.5.1 Post-mortem Analysis

Following the completion of each test, the post-mortem analysis of the sand pack provides valuable insights into the residual fines present within the porous medium. This analysis elucidates the distribution of fines across different layers and identifies the most affected layer during fines migration and plugging processes. Considering this analysis, certain enhancements are being considered to further optimize the post-mortem investigation.

5.5.2 Dry Samples

During post-mortem experiments, the sand pack samples are subjected to drying in an oven. To ensure accurate results, specific time intervals are strictly adhered to achieve complete dryness of the samples. The significance of this drying process lies in its ability to prevent the co-washing of residual liquids alongside the fine particles during subsequent washing procedures. To address this concern, each sample is meticulously weighed and labeled before being placed in the oven. Regular weight checks are conducted every 6 hours, and a sample is deemed dry when its weight remains consistent between consecutive measurements.

5.5.3 Fix Time Wash and Using Turbidimeter

Establishing a standard operating procedure (SOP) that ensures repeatability and minimizes deviations in test results is crucial. In this regard, precise timing and the utilization of measuring devices play vital roles in maintaining consistency throughout the experiment. During the washing

process, specific fixed time intervals of five minutes and 12 minutes are employed for the thorough mixing of water and sand samples, as well as the actual washing process.

Furthermore, a turbidimeter (HACH 2100P) with a 2% full-scale accuracy is employed to measure the cloudiness of distilled water after it has passed through the sieve and sand mixture. This instrument aids in determining the optimal washing duration, ensuring that the washing continues if the turbidity value exceeds the predefined threshold of 10 NTU, as per the study's criteria.

5.6 Experimental Error and Uncertainty Analysis

The uncertainty analysis in this study is crucial for determining the accuracy and reliability of measured parameters. F (X_1, ..., X_n) represents a function dependent on independent variables X_1, ..., X_n, and its associated standard uncertainty, U (F), is determined using the equation:

$$U^2(F) = \sum_{i=1}^{n} \left[\left(\frac{\partial F}{\partial X_i} \right)^2 u^2(X_i) \right] \quad (4)$$

Here, $u(X_i)$ represents the standard uncertainty of variable X_i, which is a combination of the variance ($s^2(X_i)$) resulting from N measurements of X_i and the standard uncertainty ($u_e^2(X_i)$) due to the measurement system:

$$u^2(X_i) = \frac{s^2(X_i)}{N} + u_e^2(X_i) \quad (5)$$

The variance_ square of the standard deviation_ ($s^2(X_i)$) is calculated using the formula (6). Where X_i represents the value of each N measurement, and X_i represents the mean value of the N measurements (Bodaghia et al., 2014).

$$s^2(X_i) = \frac{1}{N-1} \sum_{j=1}^{n} \left(X_{ij} - \bar{X}_i \right)^2 \quad (6)$$

Using the Darcy equation and equation (5), the combined standard uncertainty of permeability, U(k), can be determined as:

$$U^2(k) = \left(\frac{\partial k}{\partial Q} \right)^2 u^2(Q) + \left(\frac{\partial k}{\partial \mu} \right)^2 u^2(\mu) + \left(\frac{\partial k}{\partial L} \right)^2 u^2(L) \quad (7)$$

$$+ \left(\frac{\partial k}{\partial P} \right)^2 u^2(P) + \left(\frac{\partial k}{\partial A} \right)^2 u^2(A)$$

For variables obtained through single measurements, their variances do not exist, and thus the standard uncertainty is solely determined by the uncertainty arising from the measurement system. Therefore, equation (6) can be rewritten as:

$$u^2(X_i) = u_e^2(X_i) \tag{8}$$

To calculate the uncertainty in permeability, each term in equation (7) must be determined. We utilize a syringe pump with a flow rate accuracy of 0.3% of the reading value. Pressure readings are calibrated using a manometer with an accuracy of 0.001 psi. Length and diameter measurements are conducted using a caliper with an accuracy of 0.01 cm. Viscosity measurement is performed using a Brookfield viscometer with an accuracy of 0.02 cp. Differentiating k concerning each parameter while keeping the others constant yields the following partial derivatives:

$\left(\frac{\partial k}{\partial Q}\right) = \frac{\mu L}{A\Delta P}$, $\left(\frac{\partial k}{\partial \mu}\right) = \frac{QL}{A\Delta P}$, $\left(\frac{\partial k}{\partial L}\right) = \frac{Q\mu}{A\Delta P}$, $\left(\frac{\partial k}{\partial \Delta P}\right) = -\frac{Q\mu L}{A(\Delta P)^2}$, and $\left(\frac{\partial k}{\partial D}\right) = -\frac{2*4*Q\mu L}{\pi\Delta P(D)^3}$. So,

$$\begin{aligned} U^2(k) = {} & \left(\frac{\mu L}{A\Delta P}\right)^2 * \left(\frac{0.3}{100}Q\right)^2 + \left(\frac{QL}{A\Delta P}\right)^2 * (0.02)^2 + \left(\frac{Q\mu}{A\Delta P}\right)^2 * (0.01)^2 \\ & + \left(-\frac{Q\mu L}{A(\Delta P)^2}\right)^2 * \left(\frac{0.1}{100}\Delta P\right)^2 + \left(-\frac{2*4*Q\mu L}{\pi\Delta P(D)^3}\right)^2 * (0.01)^2 \end{aligned} \tag{9}$$

Dividing both sides by k^2 gives

$$\left(\frac{U(k)}{k}\right)^2 = \left(\frac{0.3}{100}\right)^2 + \left(\frac{0.02}{\mu}\right)^2 + \left(\frac{0.01}{L}\right)^2 + \left(\frac{0.1}{100}\right)^2 + \left(\frac{2*0.01}{D}\right)^2 \tag{10}$$

$\frac{U(k)}{k}$ shows the relative error of the measured permeability. For our permeability measurement experiments, we use an oil sample with a viscosity of 8 cp, a sand pack with a length of 10.64 cm, and a diameter of 6.27 cm. So, the relative error is $\frac{U(k)}{k} = 0.024$. In other words, the accuracy of permeability measurement is approximately 2.4% of the reading value. For example, if the calculated permeability value is 880 mD, the measurement accuracy is 21 mD.

5.7 Summary

This chapter focuses on the calibration and improvements made to the Sand Retention Test (SRT) setup to enhance the accuracy and repeatability of results. The previous SRT setup involved a

metal cell with specific dimensions capable of holding 13 kg of sand. Hydraulically actuated diaphragm triplex metering pumps were used for injecting brine and oil, with variable frequency drives to regulate flow rates. However, the previous setup had limitations, such as the inability to inject low and constant flow rates, resulting in fluctuations and inaccuracies in permeability measurements.

To address these issues, the SRT facility underwent several improvements. The reciprocating pumps were replaced with syringe pumps, offering higher accuracy and repeatability, particularly at low flow rates. The pressure transducers were calibrated using a FLUKE pressure calibrator and a manometer to reduce reading errors. Multiple points were used to measure permeability, offsetting possible errors in pressure and flow rate measurements. Axial loads were stabilized using a needle valve to prevent shocks to the sand pack during testing.

The methodology for performing SRTs was also refined. Post-mortem analysis of sand pack samples was optimized, ensuring samples were completely dry before analysis. Fixed-time wash and the use of a turbidimeter aided in maintaining consistency during the washing process. Additionally, the chapter delves into the analysis of experimental error and uncertainty, employing mathematical equations to determine the uncertainty associated with measured parameters.

Overall, these calibration and improvement efforts have significantly enhanced the accuracy and repeatability of the SRT setup, providing more reliable results for the permeability measurement of porous media. The improved SRT facility and methodology lay the foundation for further research and exploration in this field.

6 Test Results and Discussions

2.1 Introduction

SRT is a technique to evaluate a mechanical screen's performance and helps select the optimum size for the actual thermal/SAGD wells. The optimum size is defined from the balance between acceptable sand production, well deliverability/flow performance, fines production, and minimal pore plugging.

However, the results are accurate when the actual SAGD conditions are applied to the test. The focus here is the fines migration; therefore, a sample of discharge liquid is taken during tests, and the amount of released fine particles is measured using a turbidimeter.

Besides this, after the tests, the sand pack's wet sieving analysis reveals the residual fines content in each section of the sand pack.

Overall, this chapter shows and discusses the results of the measured PSDs, recorded differential pressure, applied flow rates, the produced fines concentration, initial and final fines content, and initial and retained permeabilities for Test #7 and Test #8 (mentioned as Test #1 and Test #2).

Test #1 is regarded as the base test, which incorporates the effect of single/two-phase flow, flow rate, and water cut, whereas Test #2, which shows the result of varying and decreasing the injected brine salinity in SRT and reveals the impact on the near-screen permeability and screen performance.

2.2 Test #1 (Hydrodynamic Effect)

2.2.1 Initial Brine Absolute Permeability Measurement

Test #1 investigates the permeability variation of the sand pack (far and near-screen intervals) under only the multi-phase hydrodynamic effect of the fines migration process.

Figure 6.1 shows the differential pressures for the top and bottom intervals of the sand pack at three different low flow rates of 2.5, 3.5, and 5.5 cc/min. The slope of high R-squared linear fits resulted in an initial absolute permeability of 885± 21 mD for the sand pack using Darcy's law formula.

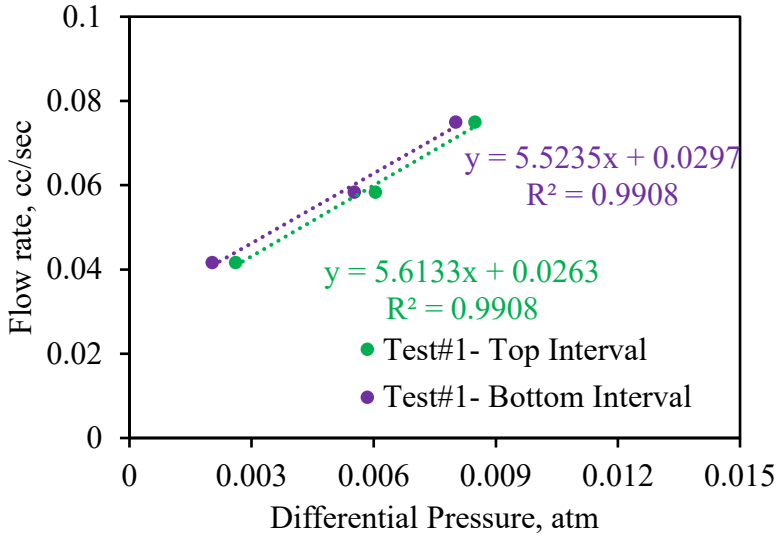

Figure 6.1 The flow rate versus differential pressure for top and bottom intervals of the sand pack- Test #1.

2.2.2 Single-Phase Oil Flow (Stages 1-3)

The differential pressure variations with increased flow rate for the single-phase oil flow (Stages 1-3) are shown in **Figure 6.2**; no significant sand and fines production was observed during these stages. The initial sharp increase in differential pressures is due to a change in flow rate, and the gradual decrease until stabilization can be attributed to the reduction in residual water saturation at higher oil flow rates. Pressure drops for the bottom interval incorporates the additional pressure drops imposed by the slotted liner coupon.

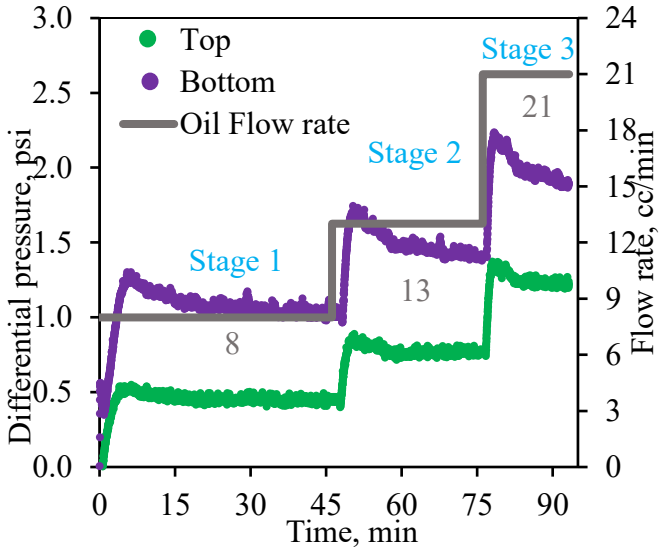

Figure 6.2 Differential pressure of three stages of single-phase flow injection with different flow rates- Test #1.

2.2.3 Two-phase Flow (Stages 4-8)

Figure 6.3 and 6.6 shows the differential pressure and the produced fines concentration of Stages 4 through 8, in which the effect of water cut, and flow rate is investigated. Note that all stages keep the brine salinity constant at 7000 ppm. Consistent criteria were considered to stop flow for each step when pressure differentials stabilized within the accuracy range of pressure transducers, and the measured turbidimeter values were negligible.

In all stages, no sand production was observed. Stage 4, with a low flow rate and 50% water cut, did not produce a noticeable fines concentration, and the two-phase flow was stabilized quickly. However, for Stages 5 and 6 with the same water cut but higher flow rates, the produced fines concentration peaked and gradually decreased consistently with pressure drops, indicating fines migration within the sand pack.

The gradual decrease in pressure drops implies that the net effect of the fine particles release mechanism is more significant than retention mechanisms such as straining and bridging. Although the concentration of the fine at higher water cuts is decreasing, the produced fines mass rates remain nearly constant. The pressure drops did not vary significantly for these stages and stabilized rapidly. The lower pressure drops compared to Stage 6 are primarily due to a decrease in oil saturation.

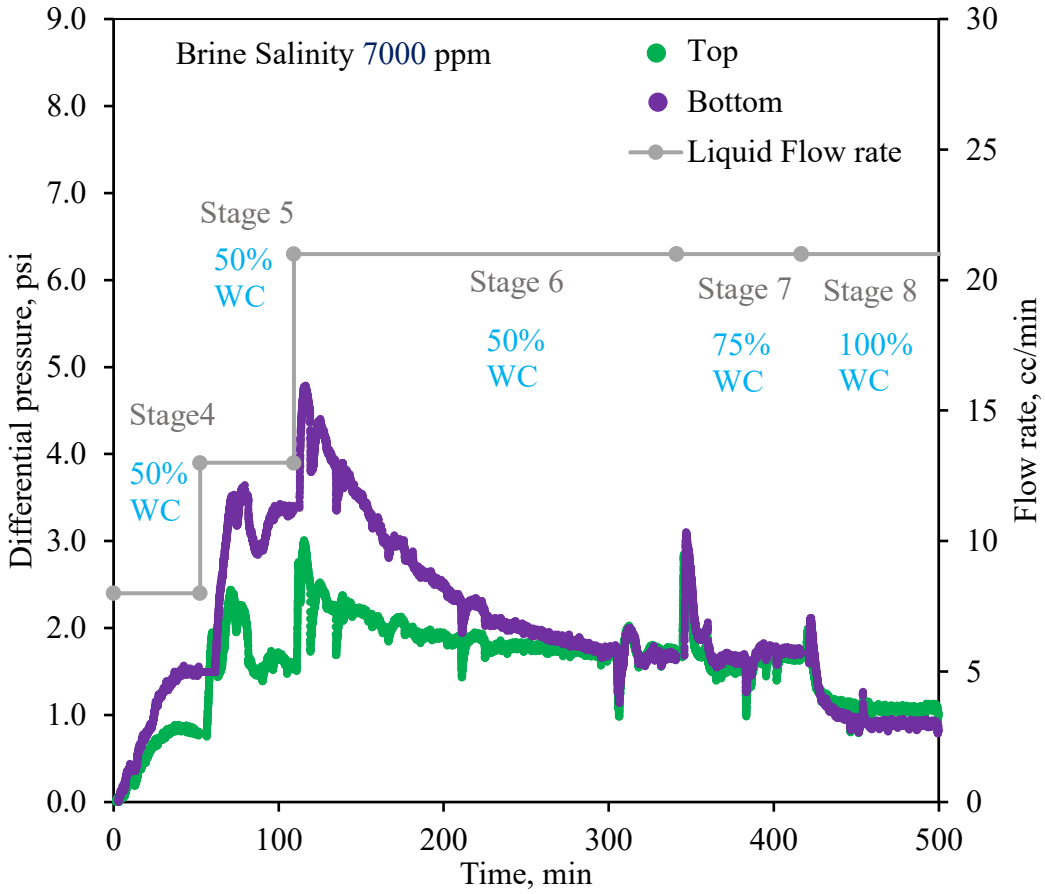

Figure 6.3 Recorded differential pressure, applied flow rates, and water cut through Stages 4 to D, Test #1.

2.2.4 Retained Permeability Measurement

At the end of Stage 8, the effective permeability of the sand pack for the top and bottom intervals was determined at three different flow rates in an equivalent way to the initial absolute permeability determination. **Figure 6.4** shows the differential pressures and brine injected flow rates versus time, and the corresponding linear fits for the top and bottom layers of the sand pack are shown in **Figure 6.5**.

The calculations using Darcy's formula showed effective permeabilities of 560 mD and 520 mD for the top and bottom intervals, respectively. Assuming a range of 0.48 to 0.52 for the brine relative permeability at residual oil saturation (Wang et al., 2020), the final absolute permeability of the bottom interval was 1000 -1,080 mD. Eventually, the retained permeability as the ratio of final and initial absolute permeability was 1.13-1.22% for the bottom interval, indicating permeability improvement of the sand pack under the multi-phase hydrodynamic effect of the fines migration process.

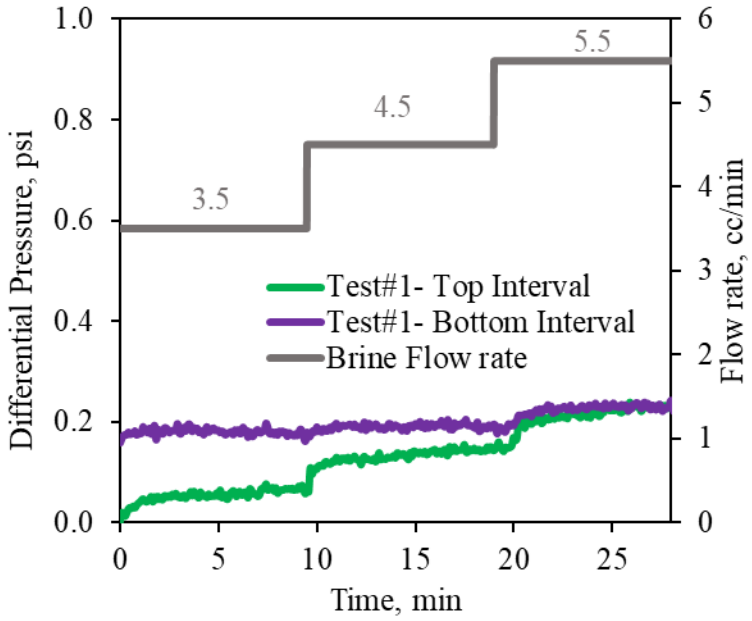

Figure 6.4 Recorded differential pressure at three flow rates at Stage D, Test#1.

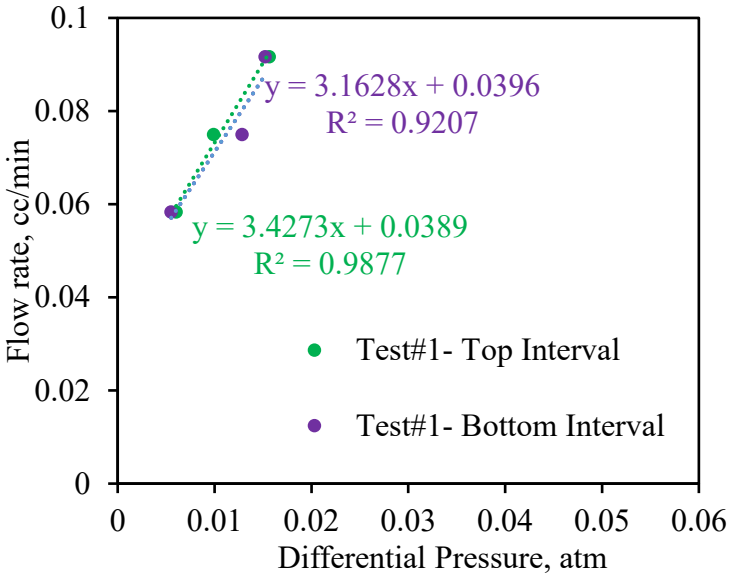

Figure 6.5 Top and bottom layer trend line formula at Stage D, Test #1.

2.2.5 Produced and Retained Fines Analysis

2.2.5.1 Produced Fines Concentration

The following figure shows produced fines concentration variations for Stages 4 through 8. The discharge fluid's fines concentration was negligible through Stages 1 to 3. Therefore, **Figure 6.6** represents the values above for Stages 4 to 8.

However, for Stages 5 and 6 with the same water cut but higher flow rates, the produced fines concentration peaked and gradually decreased consistently with pressure drops, indicating fines migration within the sand pack. The gradual decrease in pressure drops implies that the net effect of the fine particles release mechanism is more significant than retention mechanisms such as straining and bridging. An increase in the water cut from 50% to 75% and 100% at Stages 7 and 8 showed a slight rise in produced fines concentration due to an additional low amount release of fines within the sample.

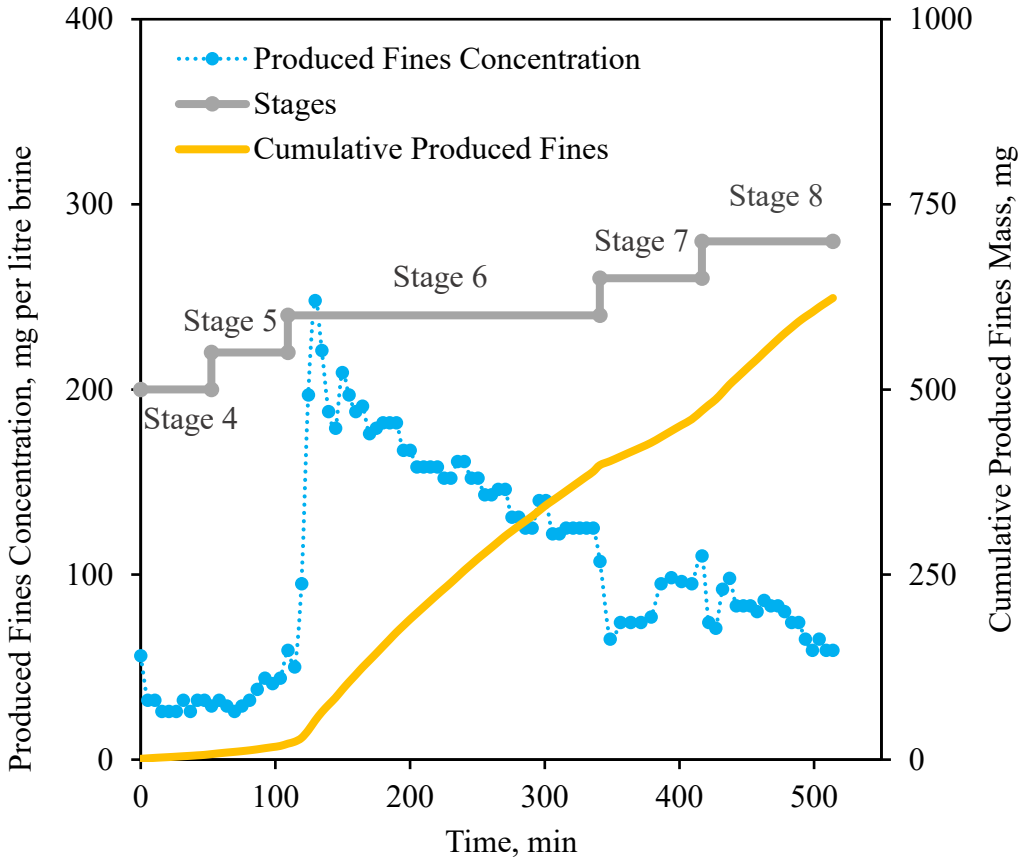

Figure 6.6 Measured instant and cumulative fines concentration during Stages 4 to 8, Test #1.

2.2.5.2 Initial and Final Fines Content

After the test, to evaluate the profile of fines content variation in the sand pack, the whole sand of each layer is taken and dried. Then the dried sand samples are weighed and washed on Sieve 325 to remove fine particles less than 44 microns. The difference in weight of dried and washed sand samples determines each layer's mass and fines content. **Figure 6.7** shows the layers' initial and final (retained) fines content. The results show that all layers do not lose noticeable fines content; however, the near-screen layer loses slightly more fines which is affected by high flow velocities toward the screen.

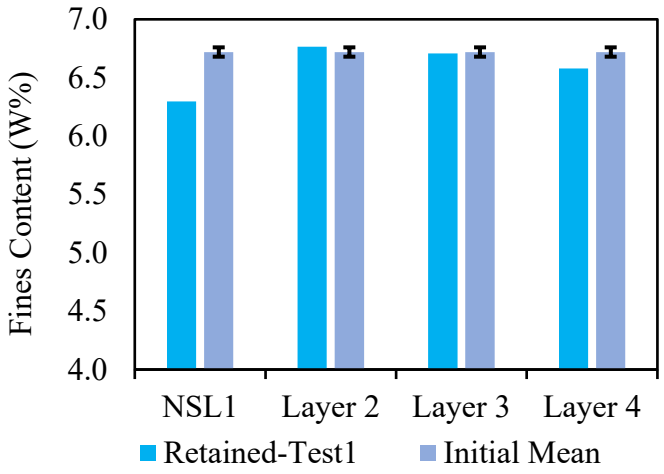

Figure 6.7 Comparison between initial and final fines content percentage, Test #1.

2.3 Test #2 (Salinity Change Effect)

2.3.1 Initial Brine Absolute Permeability Measurement

Test #2 was performed to investigate the effect of the decline in salinity on the fines migration process and the affected permeability of the sand pack. Therefore, in contrast to Test #1, the initial brine salinity of 7,000 ppm was decreased to 4,000 ppm, 1,000 ppm, and 400 ppm at Stages 5, 6, and 7-8, respectively. The flow rates and water cuts were kept like those at each stage for Test #1 to compare the results.

Figures 6.8 and 6.9 show the differential pressure variations and the linear trendlines of flow rate versus differential pressure used to determine the initial absolute brine permeability for the top and bottom intervals of the sand pack. A slight difference in absolute permeabilities of 960 ± 23 mD

for the top interval and 1,040 ± 25 mD for the bottom interval confirmed a uniform sand pack before the main flow stages.

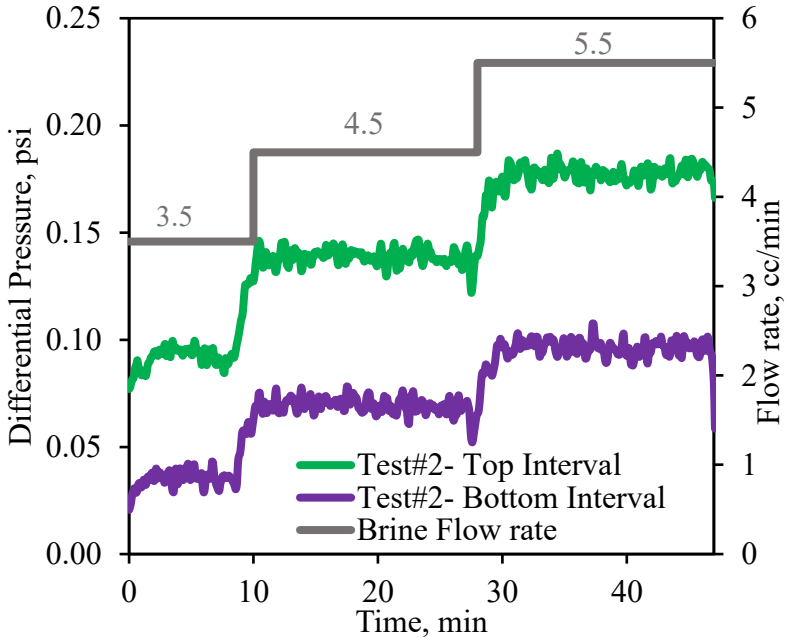

Figure 6.8 Differential pressure of three stages of single-phase flow injection with different flow rates- Test #1.

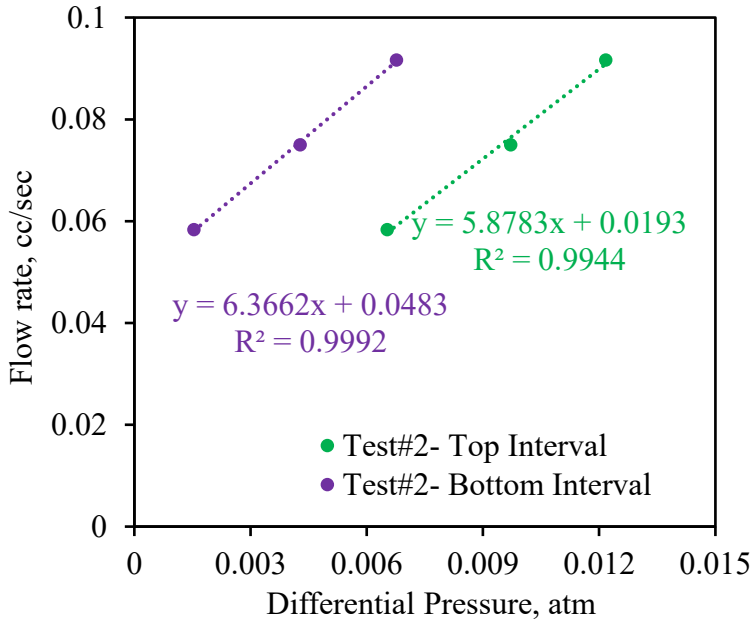

Figure 6.9 The differential pressure versus flow rate for top and bottom intervals of the sand pack- Test #2.

2.3.2 Single-Phase Oil Flow (Stages 1-3)

The differential pressure variations for the single-phase oil flow (Stages 1-3) are shown in **Figure 6.10**; a similar trend and no sand and produced fines concentration to Test #1 was observed.

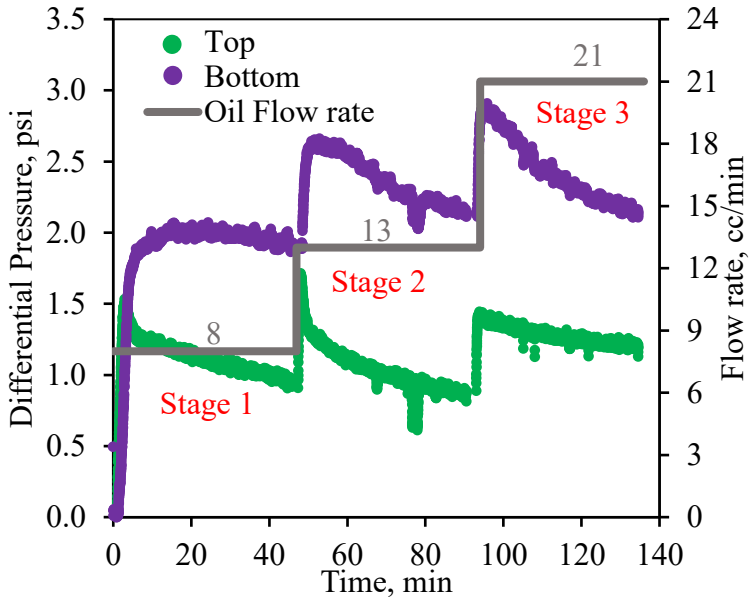

Figure 6.10 Differential pressure of three stages of single-phase flow injection with different flow rates- Test 2.

2.3.3 Two-phase Flow (Stages 4-8)

Figure 6.11depicts the differential pressure variations for Stages 4-8 in which the brine salinity decreased under two-phase flow conditions. As mentioned earlier for Test #1, similar criteria were considered to stop flow in every stage. As seen from the differential pressure trends and produced fines concentration behavior (**Figure 6.14**), changing the salinity triggered a high-level fines migration process within the sand pack. The effect was significant for lower salinity of 400 ppm where the produced fines concentration values were out of the turbidimeter range for a long time. The differential pressure curves show an initial increase followed by a gradual decrease indicating simultaneous retention and detachment of the released fine particles at pore throats. In early times the retention mechanism was dominant due to the high concentration of mobile fine particles.

In contrast, the net effect of detachment or breaking some loose bridges is dominant at late times. In Stage 8, like Test #1, increasing the water cut to 100% resulted in the release of fine particles with 400 ppm brine in other parts of the sand pack previously occupied with oil. However, because of the low concentration of mobile fines compared with Stage 7, the net effect of the retention

mechanism was not significant for this stage, and pressure differential curves show a decreasing trend from the beginning.

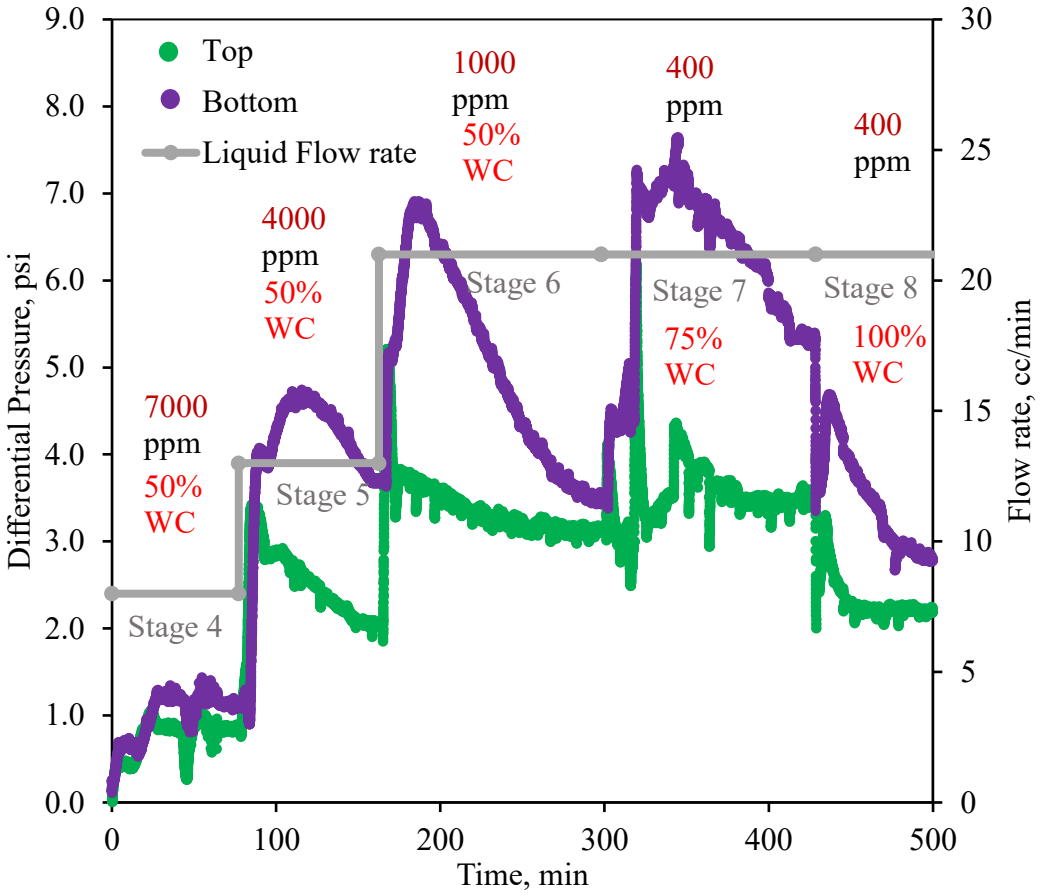

Figure 6.11 Recorded differential pressure, applied flow rates, and water cut through Stages 4 to D, Test #2.

2.3.4 Retained Permeability Measurement

Stage D is performed the same as Test #1; results are shown in **Figures 6.12** and **6.13**, respectively. The linear trendlines of flow rate versus differential pressure to determine the final absolute permeability of the sand pack at the end of Stage 8 are shown in **Figure 6.13**. Brine effective permeabilities of 280 mD and 320 mD were obtained for the top and bottom intervals, respectively. Applying similar relative permeability ranges to Test #1 resulted in retained permeability of 0.59-0.64% for the bottom interval near the screen, showing an almost 40% decrease in the initial absolute permeability of the sand pack under the chemical effect of the fines migration process.

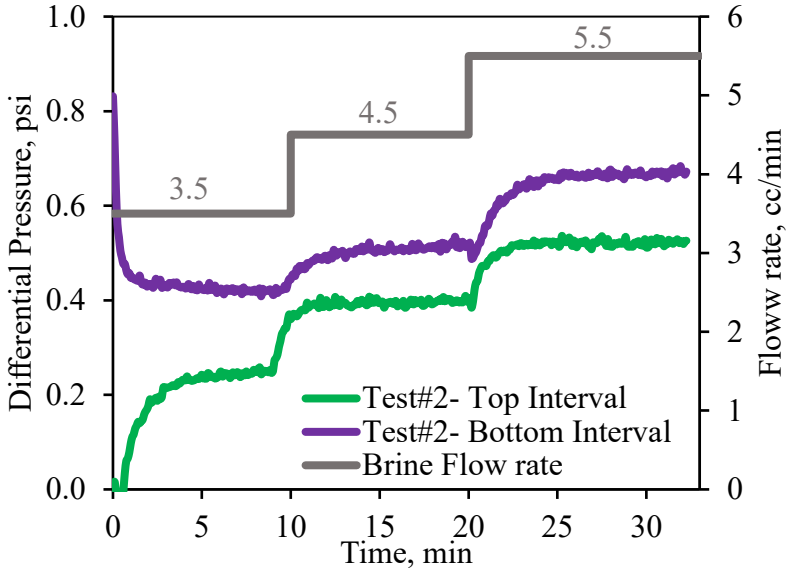

Figure 6.12 Recorded differential pressure at three flow rates at Stage D, Test#2.

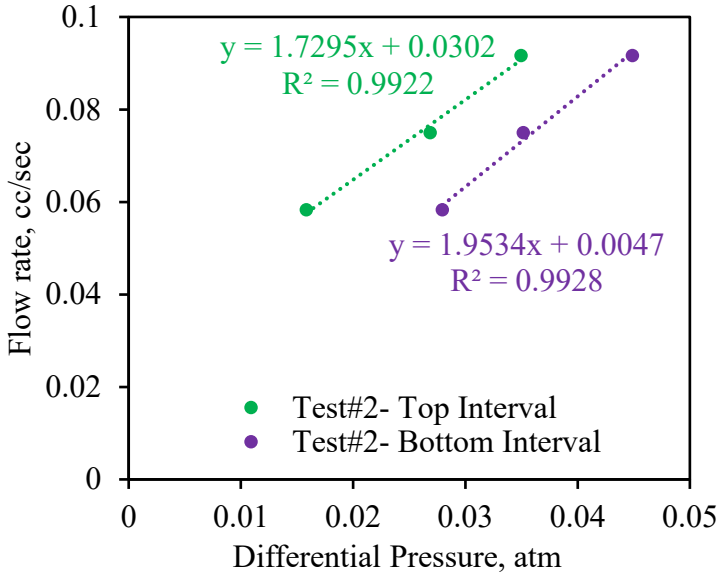

Figure 6.13 Top and bottom layer trend line formula at Stage D, Test #1.

2.3.5 Produced and Retained Fines Analysis

This section provides the fines production results for Test #2. The results incorporate the concentration of the fines in discharged fluids measured every five minutes. The cumulative mass of collected fines from the sand trap after the finish of each stage is another result. The result compares the initial fines content and the retained (residual) fines content of the sand pack after Test #2. The produced fines concentration is presented in the following section.

2.3.5.1 Produced Fines Concentration

Figure 6.14 illustrates the discharge fluids fines concentration throughout Test #2. This figure presents the impact of decreasing salinity on the amount of suspended fine particles in discharge fluids. As the salinity of Stage 4 is the same as the formation water salinity (the saturation phase salinity), the changes from Stages 1, 2, and 3 are insignificant. By decreasing the salinity to 4000 ppm in Stage 5, a moderate rise in the produced fines concentration is observed, significantly increasing by reducing the salinity further to 1000 ppm. At Stage 7, when the salinity reduces to 400 ppm, the above amount hits the maximum of the turbidimeter, and it stays constant for almost one hour. After that, in Stage 8, the 400-ppm salinity brine is injected again, and the water cut increased to 100%; the value then hit the maximum and decreased and became stable.

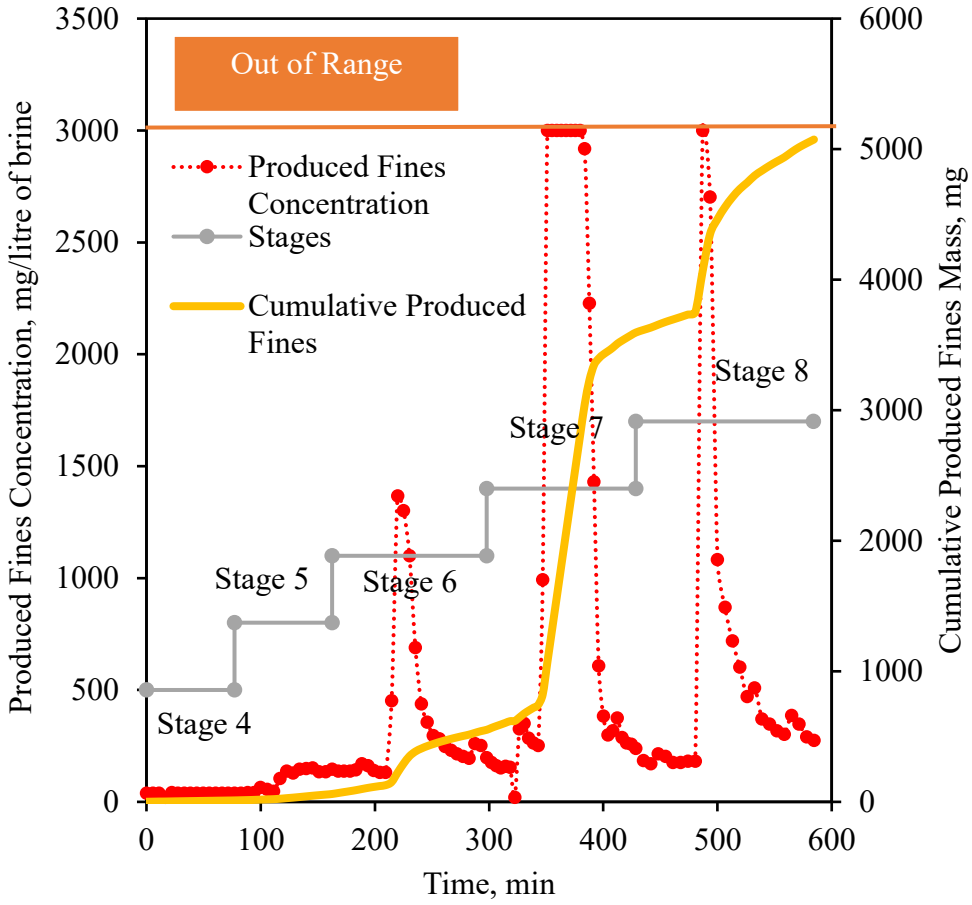

Figure 6.14 Measured instant and cumulative fines concentration during Stages 4 to 8, Test #2.

2.3.5.2 Collected Fines of Sand Trap

Alongside cumulative produced fines mass calculated from measured produced fines concentration, the mass of produced fines collected in the sand trap for each stage was also measured. **Figure 6.15 (a)** shows the collected fines from the sand trap after each stage. The screen coupon is 54 SPC and 0.013 in. wide. **Figure 6.15 (b)** demonstrates the results in a pie chart. As it is seen, the high mass percentage of fines collected in Stage 7 is consistent with pressure differential variation in the fines migration process.

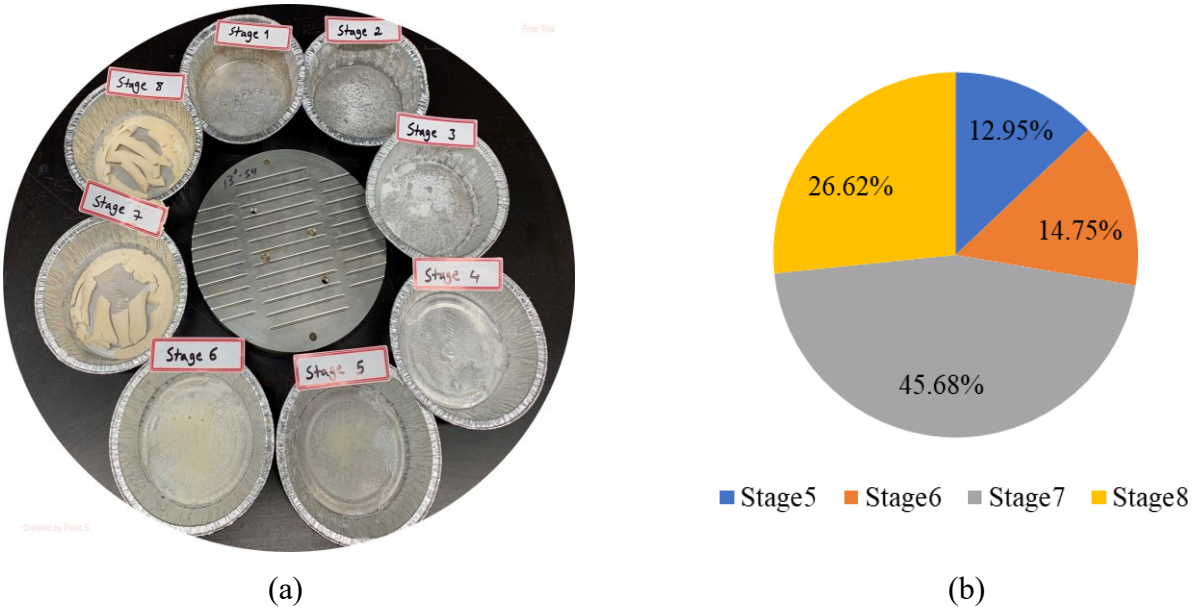

(a) (b)

Figure 6.15 Collected fines from sand trap after completion of each stage, Test #2 (a) The fines mass, and (b) Pie chart and the share percentage.

2.3.5.3 Initial and Final Fines Content

Figure 6.16 shows the fines content profile for the sand pack after the test, which was obtained in a similar procedure as described for Test #1. The results show that all layers have lost fines under the fines migration process; however, the effect on the layers near the sand screen is significant. The first layer near the screen has lower fines than the second layer due to the retention of migrated fine particles near the screen. The results are consistent with differential pressures for the top and bottom intervals of the sand pack. The top interval showed lower differential pressures due to the low-level effect of the fines migration process. The sand screen affects the bottom interval causing higher fine content variations. Note that the effect of fines migration on pressure differentials or

permeability is local and significant in thin pore throats where the most pressure drops occur by retention of fines particles. Therefore, although the first layer has lost fines compared with its initial fines content, the retention of fines particles is responsible for the higher differential pressure drops for this interval.

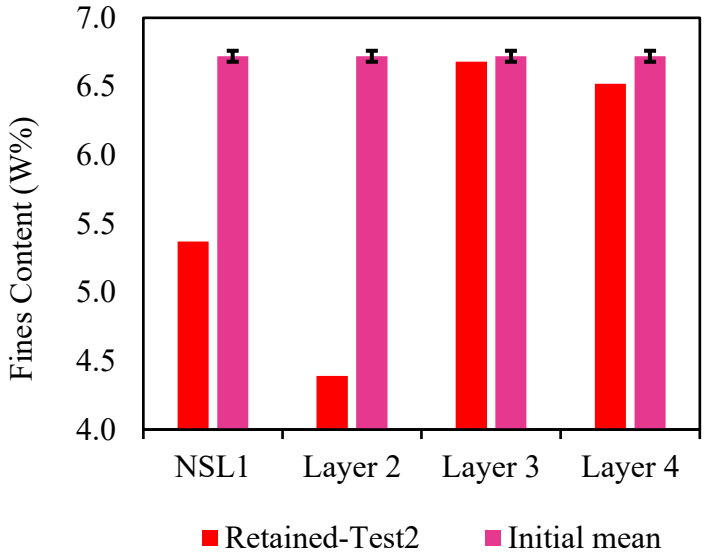

Figure 6.16 Comparison between initial and final fines content percentage, Test #2.

6.2 Summary

This chapter focuses on two pivotal tests designed to closely emulate the conditions encountered in a near-producer well during actual Steam-Assisted Gravity Drainage (SAGD) operations. While both tests aimed to replicate the SAGD scenario, they differed in their flow designs. The first test adhered to a conventional flow setup, similar to previously conducted Sand Retention Tests (SRTs). This served as a baseline reference, enabling researchers to assess the accuracy of existing methodologies and evaluate previous results. By employing well-established conditions, this first test functioned as a control to gauge the impact of introducing novel elements in the second test.

In contrast, the second test introduced a novel aspect by incorporating salinity changes during the flow process. This innovative design aimed to simulate the dynamic salinity conditions found in actual SAGD operations. In near-producer wells, the salinity of the formation water gradually declines due to dilution and production along with condensed steam. By replicating this variation

in salinity, the second test sought to investigate the influence of changing salinity levels on flow behavior and sand retention capabilities.

The comparison of the test results revealed the crucial role played by salinity in multi-phase flow SRTs. Notably, the second test, which incorporated salinity variations, demonstrated a retained permeability of less than one, closely resembling conditions observed in real-world SAGD scenarios. Conversely, the first test, which lacked salinity changes, yielded a retained permeability of more than one, indicating a departure from SAGD conditions.

The findings underscored the significance of considering salinity variations in SRT flow test procedures to achieve a more accurate simulation of actual SAGD operations. Neglecting the effect of salinity could lead to misleading outcomes and limit the applicability of the results to real-world conditions. By incorporating salinity variations in SRTs, researchers can enhance the accuracy and relevance of their findings, leading to a deeper understanding of sand retention behavior and contributing to the optimization of SAGD operations.

7 Conclusion and Recommendations

7.2 Conclusion

This thesis presents a comprehensive investigation of fines migration, plugging, and retained permeability in multi-phase Sand Retention Tests (SRTs) under Steam-Assisted Gravity Drainage (SAGD) conditions. A typical McMurray formation sand mixture was replicated and synthetic sands and oil with similar viscosity to bitumen were utilized. Eight SRTs were conducted out of which, two of them were successful to simulate the near-wellbore zone in SAGD operations. The focus of this research was primarily on examining the influence of varying and decreasing salinity on fines migration and retained permeability.

The results of the SRT experiments reveal significant insights into the impact of salinity levels, flow rates, water cuts, and multi-phase flow conditions on fines migration behavior. It was observed that single-phase oil flow had minimal effect on fines migration within the sand pack, with fine particles moving with the carrier fluid at higher flow rates, leading to a slight increase in fines concentration at the outlet.

In constant salinity flow test, higher flow rates and water cuts substantially induced fines migration within the sand pack, resulting in noticeable pressure drops. The differential pressure behaviors indicated that fine particles were retained and detached simultaneously due to hydrodynamic effect. However, the detachment mechanism partially offsets the initial retention mechanism at later stages. This observation suggested that the permeability near screen zone is improved unlike the actual near-wellbore SAGD permeability.

Unlike the constant salinity flow, which cause the higher permeability around the slotted liner coupon, the varying and decreasing brine salinity test impaired the permeability in the near-screen zone. Reducing salinity levels intensified fines migration within the sand pack, causing higher-pressure differentials. The differential pressure behaviors indicated that fine particles were simultaneously retained and detached due to the chemical effects of fines migration. However, the retention mechanisms surpassed the detachments and cause the permeability impairment in near-screen zone.

Interestingly, the study revealed that pressure differentials under the chemical effects of fines migration in multi-phase flow did not stabilize at a peak but rather started to decline. This decline

could be attributed to the disruption of particle bridges caused by pressure disturbances generated under multi-phase flow conditions.

To ensure accurate and controlled flow rates during the experiments and isolate the impact of salinity reduction on fines migration, several improvements were made to the SRT setup. Calibration of the pressure transducers and the use of a manometer significantly improved the accuracy of pressure readings. Replacing reciprocating pumps with syringe pumps mitigated flow rate fluctuations and sanding issues. Moreover, applying a fixed axial load stabilized the sand pack, preventing unintentional changes to the test results.

7.3 Assumptions and Limitations

Despite the valuable insights gained from this research, it is crucial to consider certain limitations that may affect the interpretation of the findings. Firstly, the linear flow representation of the SRT differs from the radial flow in real SAGD producer wells. This difference in flow patterns may introduce variations in fines migration behavior, potentially impacting the generalizability of the results to real-world SAGD operations.

Secondly, the absence of matching temperature and pressure conditions in the experimental setup to those encountered in actual SAGD operations may limit the direct applicability of the findings. Temperature and pressure are known to influence fines migration dynamics, and their omission from the test conditions could affect the observed outcomes.

Additionally, the reported permeabilities are accompanied by a measurement uncertainty of plus minus 2.4%, which introduces a certain level of variability in the reported values. Researchers and practitioners should consider this uncertainty when interpreting and applying the results in practical applications.

Moreover, the use of synthetic materials, including synthetic oil and sand mixtures, may introduce discrepancies compared to real-world oil sands. While the use of synthetic materials allows for controlled experimental conditions, it is essential to acknowledge the potential impact on the accuracy and representativeness of the results obtained.

7.4 Recommendations for future research

To further enhance the testing procedure and increase the accuracy of the results, several recommendations are proposed for future research:

- Conduct the SRT under conditions that closely resemble actual SAGD producer wells, incorporating elevated temperature and pressure to ensure greater realism in the experiments.
- Utilize actual oil sands instead of synthetic sand and replace synthetic oil with bitumen from the target formation. This approach can enhance the representativeness of the results and improve their applicability to real-world SAGD processes.
- Investigate the effects of scaling and asphaltene deposition on-screen performance and develop effective strategies to prevent and mitigate these issues. Understanding the impact of these phenomena is crucial for optimizing sand control in SAGD operations.
- Perform SRTs with sand pack saturation from both directions of bottom to top and top to bottom and compare the post-mortem analysis to investigate whether fines are mobilized and redistributed during the saturation phase. This additional investigation can provide valuable insights into the dynamics of fines migration during the saturation process.

By addressing these recommendations, future research can further advance our understanding of fines migration dynamics in SAGD operations and contribute to the development of more efficient and effective sand control strategies. These advancements will be crucial for maximizing oil recovery and optimizing production in SAGD reservoirs.

References

Abram, M., & Cain, G. (2014). Particle-Size Analysis for the Pike 1 Project, McMurray Formation. *Journal of Canadian Petroleum Technology, 53(06*), 339-354.

Anderson, M. (2017). SAGD sand control: large scale testing results. *SPE Canada Heavy Oil Conference* (p. D011S002R004). SPE.

Ansari, S., Yusuf, Y., Kinsale, L., Sabbagh, R., & Nobes, D. S. (2018). Visualization of fines migration in the flow entering apertures through the near-wellbore porous media. *SPE Thermal Integrity and Design Symposium* (p. D033S007R005). SPE.

Bennion, D. B., Gupta, S., Gittins, S., & Hollies, D. (2009). Protocols for slotted liner design for optimum SAGD operation. *Journal of Canadian Petroleum Technology*, *48*(11), 21-26.

Bergendahl, J., Grasso, D. (2000). Prediction of colloid detachment in a model porous media: hydrodynamics. *Chemical Engineering Science*, *55*(9), 1523–1532.

Bergaya, F., & Lagaly, G. (2013). Handbook of clay science.

Bradford, S. A., & Orizaba, S. (2013). Colloid interaction energies for physically and chemically heterogeneous porous media. *Langmuir*, *29*(11), 3668–3676.

Bratli, R. K., & Risnes, R. (1981). Stability and failure of sand arches. *Society of Petroleum Engineers Journal, 21(02)*, 236-248.

Butler, R. M., Mcnab, G. S., Lo, H. Y. (1981). Theoretical studies on the gravity drainage of heavy oil during in-situ steam heating. *The Canadian Journal of Chemical Engineering*, *59*(4), 455–460.

Chapman, D. L. (1913). A contribution to the theory of electrocapillarity, *Philosophical Magazine*, *Vol. 25, No. 6*, pp. 475–481.

Coberly, C. J. (1937). Selection of screen openings for unconsolidated sands. *Drilling and Production Practice*.

Cowie, B. R., James, B., Mayer, B. (2015). Distribution of total dissolved solids in McMurray formation water in the Athabasca oil sands region, Alberta, Canada: Implications for regional hydrogeology and resource development. *AAPG Bulletin*, *99*(1), 77–90.

Derjaguin, B. V., and Landau, L. (1941). Theory of the stability of strongly charged lyophobic sols and the adhesion of strongly charged particles in solutions of electrolyte, *Acta Physicochimica (URSS), Vol. 14*, pp. 633–662.

Derksen, J. J., Larsen, R. A. (2011). Drag and lift forces on random assemblies of wall-attached spheres in low-Reynolds-number shear flow. *Journal of Fluid Mechanics*, *673*, 548–573.

E. Fjaer. (2008). Petroleum Related Rock-Mechanics Compress. 2nd edition, *Developments in Petroleum Science 53, Elsevier.*

Egbogah, E. O. (1984). An effective mechanism for fines movement control in petroleum reservoirs. *Annual Technical Meeting, PETSOC ATM 1984*, 269–282.

Elimelech, M., Gregory, J., Jia, X. (2013). Particle deposition and aggregation: measurement, modelling, and simulation. *Butterworth-Heinemann*.

Fattahpour, V., Azadbakht, S., Mahmoudi, M., Guo, Y., Nouri, A., Leitch, M. (2016). Effect of near wellbore effective stress on the performance of slotted liner completions in SAGD operations. *Society of Petroleum Engineers - SPE Thermal Well Integrity and Design Symposium 2016*, 142–153.

Fermaniuk, B. (2013). Sand control in steam-assisted gravity (SAGD) wellbores. Graduate Studies.

Freitas, A. M., Sharma, M. M. (2001). Detachment of particles from surfaces: an AFM study. *Journal of Colloid and Interface Science*, *233*(1), 73–82.

Gabriel, G. A., Inamdar, G. R. (1983). Experimental investigation of fines migration in porous media. *Society of Petroleum Engineers of AIME, (Paper) SPE*.

Ge, J., Zhang, X., Le-Hussain, F. (2022). Fines migration and mineral reactions as a mechanism for CO2 residual trapping during CO2 sequestration. *Energy*, *239*, 122233.

Gouy, G. (1910). Sur la constitution de la charge electrique a lasurface d'un electrolyte, *Anniue Physique (Paris), Serie 4, Vol. 9*, pp. 457– 468.

Gruesbeck, C., Collins, R. E. (1982). Entrainment and deposition of fine particles in porous media. *Society of Petroleum Engineers Journal*, *22*(6), 847–856.

Gunter, W. D., Zhou, Z., & Perkins, E. H. (1994). Modelling formation damage caused by kaolinite from 25 to 300 C in the oil sand reservoirs of Alberta. *SPE Advanced Technology Series, 2(02)*, 206-213.

Haftani, M., Kotb, O., Nguyen, P. H., Wang, C., Salimi, M., Nouri, A. (2020a). A Novel sand control testing facility to evaluate the impact of radial flow regime on screen performance and its verification. *Journal of Petroleum Science and Engineering*, *195*, 107903.

Haftani, M., Kotb, O., Nguyen, P. H., Wang, C., Salimi, M., Nouri, A. (2020b). A Novel sand control testing facility to evaluate the impact of radial flow regime on screen performance and its verification. *Journal of Petroleum Science and Engineering*, *195*.

Haftani, M., Wang, C., David Montero Pallares, J., of Alberta, U., Mahmoudi, M., Fattahpour, V. (2019). An Investigation into the effect of brine salinity on fines migration in SAGD operations. *SPE-195370-ms*.

Hall Jr, C. D., & Harrisberger, W. H. (1970). Stability of sand arches: a key to sand control. *Journal of Petroleum Technology, 22(07)*, 821-829.

Huang, F., Dong, C., You, Z., Shang, X. (2021). Detachment of coal fines deposited in proppant packs induced by single-phase water flow: Theoretical and experimental analyses. *International Journal of Coal Geology*, *239*.

Junmano1, T., Soon1, L. B., Amornprabharwat1, A., Kittisupalauk1, S., and Rangsan Bhengbhun. (n.d.). Sand arch. Sand production management: The critical challenge in Zawtika gas production.

Kaminsky, H. A. W. (2009). Characterization of an Athabasca oil sand ore and process streams. *Library and Archives Canada.*

Kotb, O., Haftani, M., Nouri, A. (2021). An investigation into current sand control testing practices for steam assisted gravity drainage production wells. *Eng*, *2*(4), 435–453.

Lim, S. S. S., Elochukwu, H., Nandong, J., Bennour, Z., & Hamid, M. A. (2023). A review on the mechanisms of low salinity water/surfactant/nanoparticles and the potential synergistic application for c-EOR. *Petroleum Research*.

Mahmoudi Eshkaftaki, M. (2017). New sand control design criteria and evaluation testing for steam assisted gravity drainage (SAGD) wellbores. *PhD Thesis*.

Mahmoudi, M., Fattahpour, V., Nouri, A., Leitch, M. (2016). An experimental investigation of the effect of pH and salinity on sand control performance for heavy oil thermal production. *Society of Petroleum Engineers - SPE Canada Heavy Oil Technical Conference*.

Miri, R. (2022.). Near-wellbore permeability damage by fines migration in steam assisted gravity drainage wells. *PhD Thesis. University of Alberta.*

Miri, R., Haftani, M., Salimi, M., Nouri, A. (2022). Novel laboratory methodology for fines migration testing for SAGD wells. *Journal of Petroleum Science and Engineering*, *217,*110859.

Miri, R., Salimi, M., Lange, C. F., Nouri, A. (2023). Permeability decline by fines migration near sand control screens in steam assisted gravity drainage: A numerical assessment. *Fuel*, *334*(P1), 126578.

Mitchell, James K. Soga, Kenichi. (2005). Fundamentals of Soil Behavior (3rd Edition) - *6.8 Elements of Double-Layer Theory*. John Wiley & Sons.

Montero, J. D., Chissonde, S., Kotb, O., Wang, C., Roostaei, M., Nouri, A., Mahmoudi, M., Fattahpour, V. (2018). A critical review of sand control evaluation testing for SAGD applications. *Society of Petroleum Engineers - SPE Canada Heavy Oil Technical Conference, CHOC.*

Montero Pallares, J. D., Wang, C., Nouri, A., Haftani, M., Mahmoudi, M., Fattahpour, V. (2019). Assessment of existing design criteria for wire-wrapped screens in thermal wells. *53rd US Rock Mechanics/Geomechanics Symposium*.

Montero, J. (2019). Design Criteria and Performance Evaluation of Wire-Wrapped Screens for Steam Assisted Gravity Drainage (SAGD) Wellbores (Master thesis at the University of Alberta.

Morita, N., Whitfill, D. L., Fedde, O. P., & Lovik, T. H. (1989). Parametric study of sand-production prediction: analytical approach. *SPE Production Engineering, 4(01),* 25-33.

Muecke, T. W. (1979). Formation fines and factors controlling their movement in porous media. *Journal of petroleum technology, 31(02)*, 144-150.

Nasr, T. N., & Ayodele, O. R. (2005, December). Thermal techniques for the recovery of heavy oil and bitumen. In *SPE international improved oil recovery conference in Asia Pacific* (pp. SPE-97488). SPE.

Patchett, M., & Lozowy, A. J. (2012). Reframing the Canadian oil sands. Imaginations: *Journal of Cross-Cultural Image Studies*, 3(2), 140-169.

Rahman, M. S., Rahman, S. S., Arshad, A. (1994). Control of fines migration: A key problem in petroleum production industry. *Proceedings - SPE International Symposium on Formation Damage Control*, 233–247.

Rahmati, H., Jafarpour, M., Azadbakht, S., Nouri, A., Vaziri, H., Chan, D., Xiao, Y. (2013). Review of sand production prediction models. *Journal of Petroleum Engineering*,

Romanova, U. G., Ma, T. (2013). An investigation of the plugging mechanisms in a slotted liner from the steam assisted gravity operations. *SPE - European Formation Damage Conference, Proceedings, EFDC*, *1*, 285–292.

Romanova, U. G., Ma, T., Piwowar, M., Strom, R., Stepic, J. (2015). Thermal formation damage and relative permeability of oil sands of the Lower Cretaceous formations in western Canada. *Society of Petroleum Engineers - SPE Canada Heavy Oil Technical Conferenc,* 1474–1488.

Roostaei, M., Soroush, M., Mohammadtabar, F., Mohammadtabar, M., Hosseini, S. A., Mahmoudi, M., Sadrzadeh, M., Ghalambor, A., Fattahpour, V. (2021). Design for reliability: Experimental and numerical simulation of cased and perforated completions with standalone screen. *SPE Drilling and Completion*, *36*(3), 680–706.

Russell, T., Chequer, L., Borazjani, S., You, Z., Zeinijahromi, A., Bedrikovetsky, P. (2018). Formation damage by fines migration: Mathematical and laboratory modeling, field cases. In *Formation Damage during Improved Oil Recovery: Fundamentals and Applications* (pp. 69–175). Elsevier.

Russell, T., Pham, D., Neishaboor, M. T., Badalyan, A., Behr, A., Genolet, L., Kowollik, P., Zeinijahromi, A., Bedrikovetsky, P. (2017). Effects of kaolinite in rocks on fines migration. *Journal of Natural Gas Science and Engineering*, *45*, 243–255.

Santarelli, F. J., Brown, E. T. (1989). Failure of three sedimentary rocks in triaxial and hollow cylinder compression tests. In *International Journal of Rock Mechanics and Mining Sciences & Geomechanics Abstracts* (Vol. 26, No. 5, pp. 401-413).

Sarkar, A. K., Sharma, M. M. (1990). Fines migration in two-phase flow. *Journal of Petroleum Technology*, *42*(05), 646–652.

Shafiei, A., Dusseault, M. B., Memarian, H. O. S. S. E. I. N., & Sadeh, B. S. (2007). Production technology selection for Iranian naturally fractured heavy oil reservoirs. In *PETSOC Canadian International Petroleum Conference*.

Sharma, M. M., Chamoun, H., Sarma, D. S. H. S. R., & Schechter, R. S. (1992). Factors controlling the hydrodynamic detachment of particles from surfaces. *Journal of Colloid and Interface Science*, *149*(1), 121–134.

Sharma, M. M., Filoco, P. R. (2000). Effect of brine salinity and crude-oil properties on oil recovery and residual saturations. *SPE Journal*, *5*(03), 293–300.

Sharma, M. M., Yortsos, Y. C. (1987). Fines migration in porous media. *AIChE Journal*, *33*(10), 1654–1662.

Torkzaban, S., Bradford, S. A., Walker, S. L. (2007). Resolving the coupled effects of hydrodynamics and DLVO forces on colloid attachment in porous media. *Langmuir*, *23*(19), 9652–9660.

Vaidya, R. N., Fogler, H. S. (1992). Fines migration and formation damage: influence of pH and ion exchange. *SPE Production Engineering*, *7*(04), 325–330.

VanNess, K., Rasmuson, A., Ron, C. A., & Johnson, W. P. (2019). A unified force and torque balance for colloid transport: Predicting attachment and mobilization under favorable and unfavorable conditions. *Langmuir*, *35*(27), 9061–9070.

Verwey, E. J. W., and Overbeek, J. Th. G. (1948). Theory of the Stability of Lyophobic Colloids, *Elsevier*.

Wang, C. (2021). Experimental and numerical study into the performance assessment of stand-alone screens in steam assisted gravity drainage operations. *PhD thesis, University of Alberta.*

Wang, C., Haftani, M., Pallares, J. D. M., Nouri, A. (2020). An improved set of design criteria for slotted liners in steam assisted gravity drainage operation. *Energies*, *13*(21).

Wang, C., Montero Pallares, J. D., Haftani, M., Nouri, A. (2020). Developing a methodology to characterize formation damage (pore plugging) due to fines migration in sand control tests. *Journal of Petroleum Science and Engineering*, *186*.

Wang, J., Wan, R. G., Settari, A., Walters, D. (2005). Prediction of volumetric sand production and wellbore stability analysis of a well at different completion schemes. *American Rock Mechanics Association - 40th US Rock Mechanics Symposium, ALASKA ROCKS 2005: Rock Mechanics for Energy, Mineral and Infrastructure Development in the Northern Regions*.

Yang, Y., Yuan, W., Hou, J., & You, Z. (2022). Review on physical and chemical factors affecting fines migration in porous media. *Water Research, 214*, 118172.

Yuan, H., & Shapiro, A. A. (2011). Induced migration of fines during waterflooding in communicating layer-cake reservoirs. *Journal of Petroleum Science and Engineering, 78(3-4),* 618–626.

Zeinijahromi, A., Farajzadeh, R., Bruining, J., & Bedrikovetsky, P. (2016). Effect of fines migration on oil-water relative permeability during two-phase flow in porous media. *Fuel*, *176*, 222–236.